Aalto University
School of Chemical
Technology

School of Chemical Technology
Degree Programme of Chemical Technology

Irene Lönnqvist

PHASE EQUILIBRIA AND MODELLING OF POLYMER SYSTEMS

Master's thesis for the degree of Master of Science in Technology submitted for inspection, Espoo, 1 August, 2016.

Supervisor **Professor Ville Alopaeus**

Instructor **D.Sc.(Tech.) Petri Uusi-Kyyny**
PhD Mohammad Al-haj Ali

Aalto University
School of Chemical
Technology

Aalto University, P.O. BOX 11000, 00076
AALTO
www.aalto.fi

Abstract of master's thesis

Author	Irene Lönnqvist
Title of thesis	Phase Equilibria and Modelling of Polymer Systems
Department	Department of Biotechnology and Chemical technology
Professorship	Processes and products
Code of professorship	Kem-42
Thesis supervisor	Professor Ville Alopaeus
Thesis advisor(s) / Thesis examiner(s)	Petri Uusi-Kyyny, Mohammad Al-haj Ali
Date	01.08.2016
Number of pages	82+32
Language	English

Abstract

The production of linear low density polyethylene is carried out typically by solution polymerization. In solution polymerization it is important to keep the solution in a desired phase. Polymer systems go through a liquid-liquid split at certain conditions. The liquid-liquid split, also called as cloud point and lower critical solution temperature, is unfavorable in solution polymerization due to inefficient polymerization and mass transfer difficulties. Therefore in this study the aim was to found the phase boundaries for the polymer solutions which are processed in industry.

In this study the lower critical solution temperature of several polymer systems were studied. The lower critical solution temperature indicates that the cloud point is found by heating at high temperatures. In this work also some bubble points (vapor-liquid and vapor-liquid-liquid splits) of the polymer systems were measured. The cloud and bubble points were measured for five different polymers in a multicomponent solutions. The polymer systems in this work consisted of polymer, ethylene monomer, 1-octene co-monomer and a four component solvent mixture. In this study it was studied the effect of nitrogen and component compositions to the cloud and bubble points. Moreover a simple polynomial model was created for modeling the polymer composition effect to the cloud points.

The cloud and bubble points were measured with small variable volume cell, and the points were measured at constant temperature and composition by varying the pressure in the cell. The detection of the phase transitions were done by visually. It was found In this work that nitrogen acts as a strong antisolvent in the polymer system. The nitrogen addition shifted the cloud point line significantly to higher pressures and lower temperatures, and therefore lowered the solubility of the polymer. Moreover, when nitrogen was added, a clear shift of the bubble points was detected to higher pressures. Also the polymer, monomer and co-monomer amounts in the system effected to the cloud points. The cloud point line shifted to lower pressures and higher temperatures when more polymer, monomer and co-monomer were added. The polymer, monomer and co-monomer amounts though did not influenced significantly to the location of the bubble point lines.

Keywords Linear low density polyethylene, solution polymerization, cloud point, lower critical solution temperature, liquid-liquid split, bubble point, modelling, polyethylene process, variable volume cell.

Aalto-yliopisto
Kemian tekniikan korkeakoulu

Aalto-yliopisto, PL 11000, 00076
AALTO
www.aalto.fi

Diplomityön tiivistelmä

Tekijä Irene Lönnqvist

Työn nimi Polymeeri systeemien faasitasapainot ja mallinnus

Laitos Biotekniikan ja kemian tekniikan laitos

Professuuri Prosessit ja tuotteet **Professuurikoodi** kem-42

Työn valvoja Professori Ville Alopaeus

Työn ohjaaja(t)/Työn tarkastaja(t) TkT Petri Uusi-Kyyny, FT Mohammad Al-Haj Ali

Päivämäärä 01.08.2016 **Sivumäärä** 82+32 **Kieli** Englanti

Tiivistelmä

Lineaarisen pienitiheyspolymeerin valmistus toteutetaan tyypillisesti liuospolymerisoinnilla. Liuospolymeroinnissa on tärkeää pitää liuos halutussa faasissa. Polymeeri systeemit tekevät neste-neste erotuksen tietyissä olosuhteissa. Neste-neste erotus, tai toiselta nimeltään samepiste tai alempi kriittinen lämpötila, on epätoivottu liuospolymerisoinnissa tehottoman polymerisoinnin ja liuoksen aineensiirto vaikeuksien takia. Tämän työn tarkoituksena täten oli löytää faasirajat polymeeri systeemeille, joita prosessoidaan teollisuudessa.

Tässä työssä alemmat kriittiset liuoslämpötilat mitattiin useille eri polymeerisysteemeille. Alempi kriittinen liuoslämpötila tarkoittaa sitä, että samepiste on havaittavissa lämmittäessä korkeissa lämpötiloissa. Tässä työssä mitattiin lisäksi joitakin polymeeri systeemien kuplapisteitä (höyry-neste, höyry-neste-neste erotuksia). Polymeerisysteemit tässä työssä koostuivat polyeteenistä, etyleenimonomeeristä, 1-octeeni co-monomeeristä sekä neljä komponenttisesta liuotin seoksesta. Työssä tutkittiin typen ja komponenttimäärien vaikutusta same- ja kuplapisteisiin. Tässä työssä luotiin myös yksinkertainen polynomimalli, jotta voitiin arvioida samepisteiden riippuvuus systeemin komponentti määristä.

Same- ja kuplapisteet mitattiin pienellä muuttuva tilavuuksisella kennolla, ja pisteet mitattiin vakio lämpötilassa ja koostumuksessa muuttamalla kennon painetta. Faasimuutokset havaittiin visuaalisesti. Tässä työssä havaittiin, että typpi toimii vahvana anti-liuottimena polymeerisysteemeissä. Typpi siirsi samepisteitä selkeästi korkeampaan paineeseen ja alempaan lämpötilaan, ja täten heikensi polymeerin liukoisuutta. Lisäksi typpilisäys siirsi myös kuplapisteitä korkeampaan paineeseen. Lisäksi komponenttimäärät systeemissä vaikuttivat samepisteisiin. Kasvattaessa polymeerin, monomeerin ja co-monomeerin määrää systeemissä samepisteet siirtyivät alempaan paineeseen ja korkeampaan lämpötilaan. Polymeeri, monomeeri ja co-monomeeri määrät tosin eivät vaikuttaneet merkittävästi kuplapisteiden sijaintiin.

Avainsanat Lineaarinen pientiheyspolyeteeni, liuospolymerisointi, samepiste, alempi kriittinen liuoslämpötila, neste-neste erotus, kuplapiste, mallinnus, polyeteeniprosessi, Muuttuva tilavuuksinen kenno.

Foreword

The experiments presented in this work and the writing of this thesis was done at the department of Biotechnology and Chemical Engineering of Aalto University, and was funded by Borealis Polymers Oy.

I would like to thank the Chemical Engineering research group at Aalto University. In particular, I want to show gratitude to my advisor Petri Uusi-Kyyny and supervisor Ville Alopaeus for their guidance and advises I have received during this work. Technician Heikki Viianranta also deserves my thanks for maintaining the measurement equipment always in a fastest possible way.

I am also very grateful to Borealis Polymers Oy for funding this work, and therefore making possible to do my master's thesis on an interesting topic. Especial thanks belong to my advisor at Borealis Polymers, Mohammad Al-Haj Ali who gave me valuable comments and advises during this work.

Finally I want to thank my mother, boyfriend and friends for their mental support and interest on the progress of this thesis.

Espoo, August 2016

Irene Lönnqvist

Table of Contents

Abbreviations

COR	Chain of rotators
FV	Free volume
GC	group-contribution
HPPE	High pressure polyethylene
HPS	High pressure separator
EOS	Equation of state
LCEP	Lower critical end point
LCST	Lower critical solution temperature
LPS	Low pressure separator
LDPE	Low density polyethylene
LL	Liquid-liquid
LLDPE	Linear low density polyethylene
LLE	Liquid-liquid equilibrium
PC-SAFT	Perturbed-chain statistical association fluid theory
PHSC	Perturbed hard-sphere-chain
RTD	Resistance temperature detector
SAFT	Statistical association fluid theory
SL	Solid-liquid
SRK	Soave-Redlich-Kwong
SWP	Sako-Wu-Prausnitz
UCEP	Upper critical end point
UCST	Upper critical solution temperature
VLE	Vapor-liquid equilibrium
VL	Vapor-liquid

1. Introduction

Polyethylene is considered as one of the most important polymer materials, and annually over 60 million tons of polyethylene is produced (Anon 1, 2016). Three main forms of polyethylene exists: high density polyethylene (HDPE), linear low density polyethylene (LLDPE) and low density polyethylene (LDPE) (Anon 1, 2016). Polyethylene is utilized mostly for packaging, such as films, bags, seals and bottles (Bergstra, 2004). It is also used for piping and tubing due to the chemical resistance and strength of the material. Moreover automobile industry is one significant polyethylene user (Bergstra, 2004).

The knowledge of the phase boundaries of different polymer systems is important. The understanding of the phase equilibria enables safe and efficient ways to produce polyethylene (Folie *et al.*, 1995). In this work the phase equilibria of five different unknown LLDPE types were studied. LLDPE is typically manufactured by solution copolymerization of ethylene and 1-alkene in a hydrocarbon solvent (Nagy *et al.*, 2006). In this reaction it is important to keep the solution in a desired phase region by adding enough pressure. Therefore in this work, the liquid-liquid (LL) split (called also lower critical solution temperature (LCST) or cloud point) of these five polymer systems were determined at different temperatures.

The objective in this work was to investigate how these phase boundaries change when a small amount of nitrogen was added. Also the polymer, monomer and co-monomer amounts in the systems were changed and a simplified model was created. With the model it was possible to interpolate or extrapolate the cloud points for different component weight fractions. This work is also a continuation to the Thesis work of Tom Cameron (Cameron, 2016). In this work the measurements were conducted with the same polymers and apparatus. Though the other components in the systems and their compositions were different in this work.

The literature part of this work is divided to three sections. The second chapter describes different routes to produce polyethylene. The production of HDPE, LDPE and LLDPE are briefly described. Both catalytic and free radical polymerization

reactions are presented. Moreover, the phase equilibria of polymer systems is presented, and the importance of understanding these phase boundaries in the polyethylene process.

The third chapter describes the polymer phase equilibria measurement techniques found in literature. It was found that typically the cloud points are detected either by purely visually or by utilizing some kind of light scattering technology. The phase boundary measurements can be done at constant temperature by changing the pressure by altering the volume of the cell or at constant pressure by altering the temperature of the system.

Many models have been created for predicting the polymer system phase equilibria. This is due to the difficulty and cost of conducting phase equilibria measurements. Chapter four describes some of these models. The development of these models from the first Flory-Huggins model to the currently interesting SAFT model is presented. In this work only a polynomial model, implemented in Excel, was developed due to the time limit and unknown polymers. However these measurement results could be utilized also for more sophisticated modeling.

Chapter five consists of the experimental part of this work. The measurement apparatus utilized in this work is described there. The apparatus used in this work was a variable volume cell built at Aalto University and designed by professor Richon. In this work the phase transitions were detected by visually and the measurements were done at constant temperature by changing the pressure. Also the pressure sensor calibration and the test procedure are illustrated in the experimental part. The effect of the nitrogen addition and the component amounts to the cloud and bubble points are illustrated by graphs.

It is shown that the nitrogen addition shifts the cloud points to higher pressures and lower temperatures. Also by changing the polymer, co-monomer and monomer amounts in the system, a clear change appeared. When more polymer, co-monomer and monomer were added, the cloud point line moved to lower pressures and higher temperatures. These findings are also in line with the experimental results for LLDPE published by de Loos *et al.*, 1996 and Nagy *et al.*, 2006. Finally the operation of the polynomial model was illustrated with several graphs.

Literature part

2. Polyethylene process and phase equilibria

2.1 Background of the polyethylene process

The first patent on producing polyethylene from ethylene was accepted in 1937 (Brydson, J, 1999). After that the LDPE production was commercialized (Bergstra, 2004). Then commercialized LDPE process was a radical polymerization, and this reaction forms a highly branched polyethylene (Bergstra, 2004). Commercially all polyethylene was manufactured through this high pressure process until mid-1950s.

In 1950s two other processes were developed for manufacturing polyethylene (Brydson, 1999). These processes utilized catalysts, and the processes were named as the Phillips process (metal oxide catalyst) and the Ziegler process (aluminium alkyl or similar) (Bergstra, 2004). The Phillips catalyst was developed by the Phillips Petroleum Company in 1950. The Ziegler catalyst was found in 1953 at University of Mülheim (Bergstra, 2004). By using these two processes it was possible to produce polyethylene at lower temperatures and pressures (Brydson, 1999). Moreover the molecular structure could be modified. Therefore the material has higher density and is harder than the polymer material prepared with high pressure LDPE processes (Brydson, 1999).

It was also found that the Ziegler catalyst can be used for producing both HDPE and LLDPE polymers (Bergstra, 2004). The first commercialized LLDPE production plant started in Frankfurt in the late 1950s (Bergstra, 2004). Properties of LLDPE are in the between of the high pressure and low pressure polyethylene properties (Brydson, 1999). In the late 1970s there was an increasing interest on developing LLDPE. In the beginning LLDPE had strong markets especially for film manufacturing (Brydson, 1999).

Later in 1990s there was also much interest in developing a new polyethylene process that utilized metallocene catalyst (Brydson, 1999). Metallocene catalysts was found in the 1950s (Bergstra, 2004). Though the breakthrough of metallocene catalyst came later (Bergstra, 2004). Polymers produced with metallocene catalyst have narrower molecular weight distribution than polymers produced with Ziegler catalyst.

2.2 Industrial polyethylene processes

LLDPE and HDPE polymerization processes utilize typically a Ziegler or inorganic catalyst. HDPE processes utilizes only a pure ethylene feed which acts as a monomer. LLDPE production needs also a co-monomer feed along with the ethylene feed. Both HDPE and LLDPE products can be manufactured by slurry, gas or solution phase processes. Contrarily to the HDPE and LLDPE processes, LDPE is produced by free radical polymerization. With the free radical polymerization the polymer chain has different sizes of branches in the chain. The LLDPE also has branches in the chain. Though the branch sizes in LLDPE can be varied by changing the co-monomer type (Anon 1, 2016)

LDPE is produced by free-radical bulk polymerization in supercritical ethylene (Folie *et al.*, 1995). In this polymerization different size of branches in the polymer chain are formed with no added co-monomers (Mecking, 2001). This LDPE reaction takes place at high pressures (1000-3000 bar) and relatively high temperatures (180-300 °C) (Folie *et al.*, 1995). High-pressure polyethylene (HPPE) reaction where LDPE is produced occurs in excess amount of monomer (Folie *et al.*, 1995; Liu *et al*., 1980). The monomer conversion is quite low (10-30 wt % depending on the type of the reactor) when the reactor residence time is short (30-90 s). Therefore the excess unreacted ethylene is separated from the polyethylene product and recycled back to the reactor with the fresh monomer. The fresh monomer addition is first pre-pressurized before combining it with the recycled monomer. After this, the combined monomer stream is pressurized to the reactor pressure (Folie *et al.*, 1996). Simplified process flow diagram is represented in Figure 1.

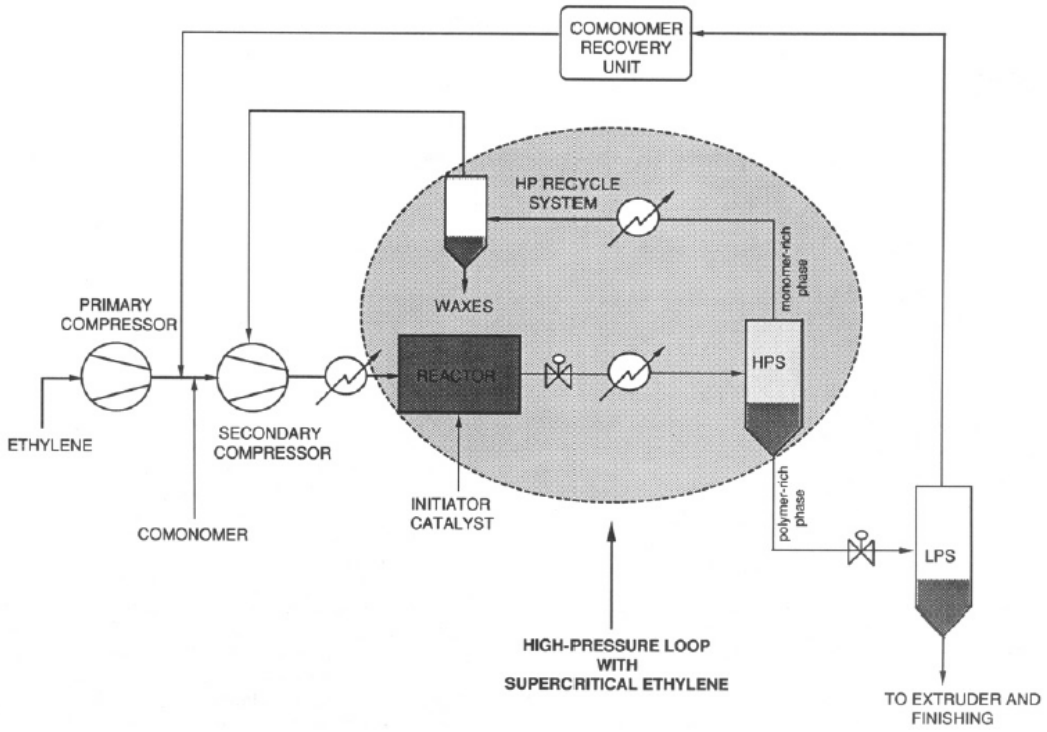

Figure 1. Flow diagram of the HPPE process. (Folie *et al.,* 1996)

The HPPE polymerization process typically takes place in a well-stirred single-stage, multistage autoclave or a tubular reactor (Folie *et al.*, 1996). The high pressure operation enables better control of the polymer molar weight distribution, and moreover it is possible to avoid a formation of a very viscous polymer-rich phase, by compressing the ethylene into the solution (Krenz, *et al.*, 2007; Nagy *et al.*, 2007). Polymerization is initiated by free-radical initiators such as benzyol peroxide, azodi-isobutyronitrile or oxygen (Brydson, 1999). The reaction temperature is controlled, depending on the type of reactor, either by altering the addition of initiator or by cooling the reactor wall (Folie et al., 1996). The molecular weight of the polymer can be controlled by changing the reactor temperature and pressure or additionally with a chain-terminating agent. The ethylene can act both as a solvent and reactant in this polymerization reaction (Folie *et al.*, 1996).

After the polymerization reaction the pressure of the reactor outlet stream is lowered by using a pressure reduction valve to lower the pressure to 150-250 bar (Folie *et al.*, 1996). This is done so that the separation of the product polymer from the unreacted ethylene and the inert solvent can occur by liquid-liquid , vapor-liquid (VL) and finally solid-liquid (SV) separation. (Folie *et al.*, 1996; Krenz, et al., 2007).

The first separation (LL) occurs in the so called high-pressure separator (HPS) column (Folie *et al.*, 1996). The upper outlet stream of the HPS column, containing mostly the monomer, is cooled and recycled back to the reactor. The lower outlet polymer-rich stream is led to a second separation column (VL), called a low-pressure separator (LPS). The LPS operates at near atmospheric pressure. The upper outlet stream of the LPS is recycled back to the reactor. The lower polymer product stream can, for example be stripped in a vacuum devolatilizing extruder (SV) to remove the residual ethylene (Folie *et al.*, 1996). The residual ethylene is separated to avoid explosion risks (Liu *et al.,* 1980). After extrusion the polymer is pelletized, dried and stored in silos that are under continuous stream of warm air (Folie *et al.*, 1996).

LLDPE can be produced through solution polymerization (Krenz, *et al.*, 2007; de Loos *et al.* 1996). In this type of polymerization, ethylene reacts in an inert hydrocarbon solvent with a catalyst to form polyethylene. In industrial processes the inert solvent are typically alkanes and isomers from butane to octane (C4-C8) (Nagy *et al.*, 2007). Hexane isomers such as n-hexane, isohexane, cyclo-hexane are the most common types of inert solvents utilized for producing different varieties of LLDPE (Nagy *et al.*, 2007). In the LLDPE reaction also a co-monomer such as 1-octene is present (de Loos *et al.,* 1996). The polymer product properties can be changed by altering the ethylene and co-monomer ratios (Anon 1, 2016). It is important in this reaction that the solution stays homogeneous through the polymerization so that the polymer product has the desired properties and also for kinetic reasons. The reaction temperature has to be chosen between the crystallization temperature of the polymer in solution and liquid-liquid separation temperature (de Loos *et al.,* 1996).

LLDPE can be produced also with metallocene catalysts (Anon 1, 2016). The polymer product is more homogenous by utilizing this type of catalyst. Also the molecular mass and the configuration of the molecule can be controlled better. Typically the metallocene catalyst processes utilizes a slurry or solution phase process (Anon 1, 2016).

HDPE can be produced by utilizing two types of catalysts; Ziegler-Natta or inorganic Phillips-type catalysts. The polymerization can be performed either in

slurry, gas or solution phase reactors. The slurry phase reaction can be performed either in continuous stirred tank reactor or in a loop reactor. The gas phase reaction occurs in a fluid bed reactor. (Anon 1, 2016).

In the HDPE Ziegler process the catalyst is either first prepared, then fed to the reactor or the catalyst is prepared *in situ* by feeding the components directly to the reactor. Usually the catalyst consists of titanium tetrachloride and triethylaluminium. The polymer properties can be altered in this reaction by varying the Al-Ti ratio in the catalyst. The properties can be changed also by adding various amounts of hydrogen and changing the temperature. The added hydrogen acts in this case as a chain transfer agent. The polymerization is performed in absence of oxygen and water due to their ability to deactivate the catalyst. The reaction temperature is kept below 100 °C and the formed polymer has a density of around 945 kg/m$^{3.}$ (Brydson, 1999)

In the HDPE Phillip catalyst process the temperature is maintained at 130-160 °C and at pressure of 14-35 bar (Brydson, 1999). The ethylene is dissolved to an inert hydrocarbon solvent such as cyclohexane. The solvent dissolves the polymer as the reaction proceeds and it also acts as heat transfer agent. The catalyst typically contains chromium oxides that are attached on a silica-alumina support, and the catalyst is activated by heating it to 250 °C (Brydson, 1999; Bergstra, 2004). The density of the polymer is approximately 960 kg/m^3. One option is also to carry out the reaction at lower temperatures (90-100°C) (Brydson, 1999). Then the temperature is below crystalline melt point of the polymer and therefore the polymer is poorly soluble into the solvent. Therefore the polymer forms around the catalyst particle and becomes a slurry granule type of a formation. (Brydson, 1999)

2.3 Phase equilibria of polymer solutions

The LL split (or cloud point) is more common in polymer systems than in low molecular weight component mixtures (Kontogeorgis *et al.*, 1995). The LL separation is due to the expansion of the solvent when temperature is increased (de Loos et al., 1996). Phase separation in polymer systems can appear in two ways. These are by cooling at low temperatures, called the upper critical solution temperature (UCST) and by heating at high temperatures, called the lower critical

solution temperature (LCST) (Kontogeorgis *et al.*, 1995). UCST naming indicates that the system is miscible at temperatures above this UCST curve (Anon 2, 2016). LCST again means that the polymer solution is miscible at lower temperatures than the LCST curve. Figure 2 presents phase equilibrium behavior for common polymer system.

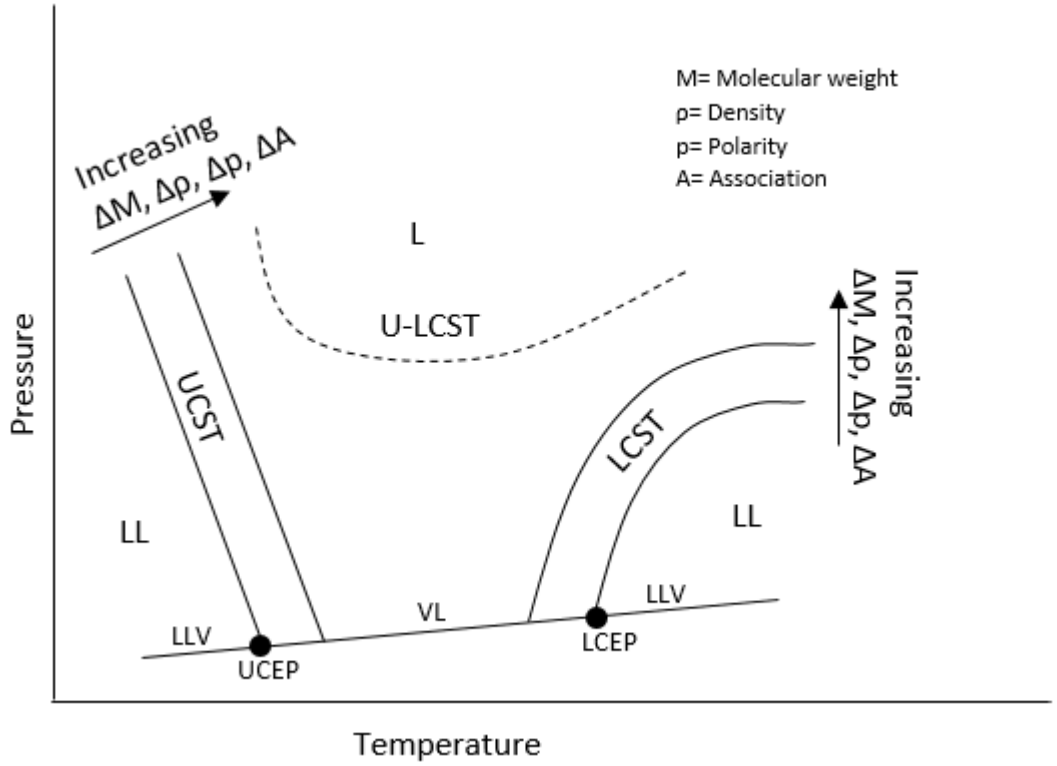

Figure 2. Typical phase behavior of an amorphous and monodisperse polymer. The effect of increasing asymmetry to LSCT and UCST curves which are approaching eatch others (Folie *et al*, 1995).

The phase behavior depends on the free volume and energetic contributions of the system components (Chen *et al.,* 1992a). Here the so called free volume refers to the large difference between the size and chain length of the polymer and solvent molecules (Patterson, 1969). The free volume means that the solvent is much more expanded than the dense polymer. The mixing of solvent and polymer can be considered as a condensation of gas (solvent) into a polymer medium and therefore the overall volume change is negative for this mixture (Patterson, 1969).

The reason for UCST phase separation is the unfavorable energy effect, and for LCST phase separation the unfavorable entropy effect (Kontogeorgis *et al.*, 1995). Moreover at LCST conditions negative excess volumes and negative enthalpies of mixing have been measured. Therefore the LCST is due to the difference of free-volume percentages between polymer and solvent. This free volume difference becomes important at high temperatures near the solvents gas-liquid critical temperature (Kontogeorgis *et al.*, 1995). LCST and UCST points are measured as cloud points that are close to the solvent vapor pressure, or in other words near the bubble point of the solution (Chen *et al.,* 1992a).

Many systems can have both UCST and LCST as the two lines approaches each other, and this line is typically called as U-LCST as demonstrated in Figure 2 (Kontogeorgis *et al.*, 1995; Folie *et al.,* 1995). The U-LCST line forms when the molecular asymmetry between the polymer and solvent increases (Folie *et al.,* 1995). The molecular asymmetry can be due to a difference of molar weights of the components. Alternatively it can be due to the difference of the density for nonpolar systems, difference in polarity for polar non-associating systems and difference in self-association and cross-association for polar associating systems. Between, the upper critical end point (UCEP) and the lower critical end point (LCEP), is the mixture vapor-liquid (VL) curve. In addition two three phase curves liquid-liquid-vapor (LLV) are present below UCEP and above LCEP (Folie *et al.,* 1995).

The knowledge of the phase equilibria of polymer systems is important typically in two situations which are in the reactor and in the separation column (Liu *et al.*, 1980). When considering only a polyethylene + ethylene system, at high pressures ethylene is soluble to the polyethylene phase and only one phase appears. If either the pressure is decreased or the temperature is increased at this point the polymer mixture might become cloudy and this pressure-temperature-composition point is called as cloud point. The cloud point data is important for the reactor operation to ensure that polymerization occurs in a desired phase (Liu *et al.*, 1980). The cloud point curve can be formed by determining the cloud-point pressures at constant temperature by varying the polymer composition (Jog *et al.*, 2002).

Phase behavior of polyethylene in hydrocarbon solutions depends on the molecular weight distribution and branching of the polymer. Thus these molecular properties can be controlled by changing the polymerization conditions (Krenz, *et al.*, 2007). Moreover the solvent type and molecular weight of the polymer influences to the phase equilibrium of the solution (de Loos *et al.*, 1996). De Loos *et al.* investigated these LLDPE + solvent phase equilibriums for different types of LLDPE and solvents. They showed that the cloud point temperature increased in isobaric conditions when the alkane chain length increased. Also by increasing the weight fraction of the polymer in the solution, the cloud point temperature increased at isobaric conditions. For higher density polymers the cloud point temperature was lower than for low density polymers. The same phenomena was detected also for high molecular weight polymers where the density was kept almost constant for all the samples (de Loos et al., 1996).

The amount of ethylene also influences to the cloud point location (de Loos et al., 1996). When increasing the ethylene amount in the system the cloud point temperature decreases in isobaric conditions. This antisolvent ability was also proved by Chen *et al.* 1992a. They found that ethylene lowers the solubility of polymer and co-monomer when added to systems of poly(ethylene-propylene) + 1-butene and poly(ethylene-propylene) + 1-hexane (Chen *et al*., 1992a). Therefore even small changes in the polymer solutions properties affect the temperature and pressure boundaries were the polymerization can occur (de Loos et al., 1996).

Uncontrolled phase transition can cause numerous problems in the reactor (Folie *et al.*, 1996). In tubular reactors undesired phase transition can cause film formation to the inner wall of the tube. This is due to the cooling of the reactor by through-wall heat transfer. This film formation impacts the heat transfer efficiency and therefore on-line purification is required (Folie *et al.*, 1995). Moreover the polymer molecular weight distribution is difficult to control if a two-phase liquid system appears (Nagy *et al.*, 2007). Furthermore the heavy components would concentrate to one of the phases and create a highly viscous solution and therefore create poor flow properties. This second polymer rich phase can, on the other hand, cause hot spots in the reaction solution and start dangerous runaway reactions (Folie *et al.*, 1996). However in some cases though it is desirable to perform the polymerization in the two-phase region (Folie *et al.*, 1996). In free

radical polymerization, the reaction in two-phase region narrows the molecular weight distribution and reduces long-chain branches in the molecule (Folie *et al.*, 1996).

In the flash separation unit understanding of the phase equilibria is important. In the flash unit the unreacted ethylene, solvent and other residual co-monomers leave as vapor to the upper stream (Chen *et al.*, 2002). The lower liquid stream contains polymer and solvent and small amounts of monomer and residual co-monomers. If the incoming stream to the flash unit contains low molecular weight polymer molecules they might leave to the upper stream and recycle back to the reactor. The polymer properties such as melt index can change due to this fractionation. This phenomena can be favorable or unfavorable. Still in both cases it is important to know the degree of fractionation at certain temperatures and pressures and therefore in this case the VLE (vapor-liquid equilibrium) data of the polymer solution is valuable (Chen *et al.*, 2002).

It is important to understand the effect of the polymer molar weight, microstructure and chemical composition to the phase behavior of the specific polymer system due to the large diversity of polyethylene types (Folie *et al*., 1996). In the reactor the understanding of the phase boundaries are important and the phase compositions are essential in the liquid-vapor separator unit. Moreover when designing a liquid-liquid separator the knowledge on the liquid-liquid equilibria (LLE) for the solvent-polymer system is needed (Chen *et al.,* 2005). The energy consumption can be reduced by utilizing a liquid-liquid separator due to the diminished need of vaporization. The use of a supercritical fluid (for example ethane, propane or nitrogen) in the polymerization processes is usually beneficial if the polymer-solvent separation is done by liquid-liquid split (Haruki *et al.*, 2008; Nagy *et al.*, 2006). This is due to the shift of LCST curve to lower temperatures. This leads to lower energy consumptions in the process and moreover the degradation of the polymer product can be avoided (ter Horst *et al.*, 2002). Figure 3 represents the desired phase conditions for each process unit.

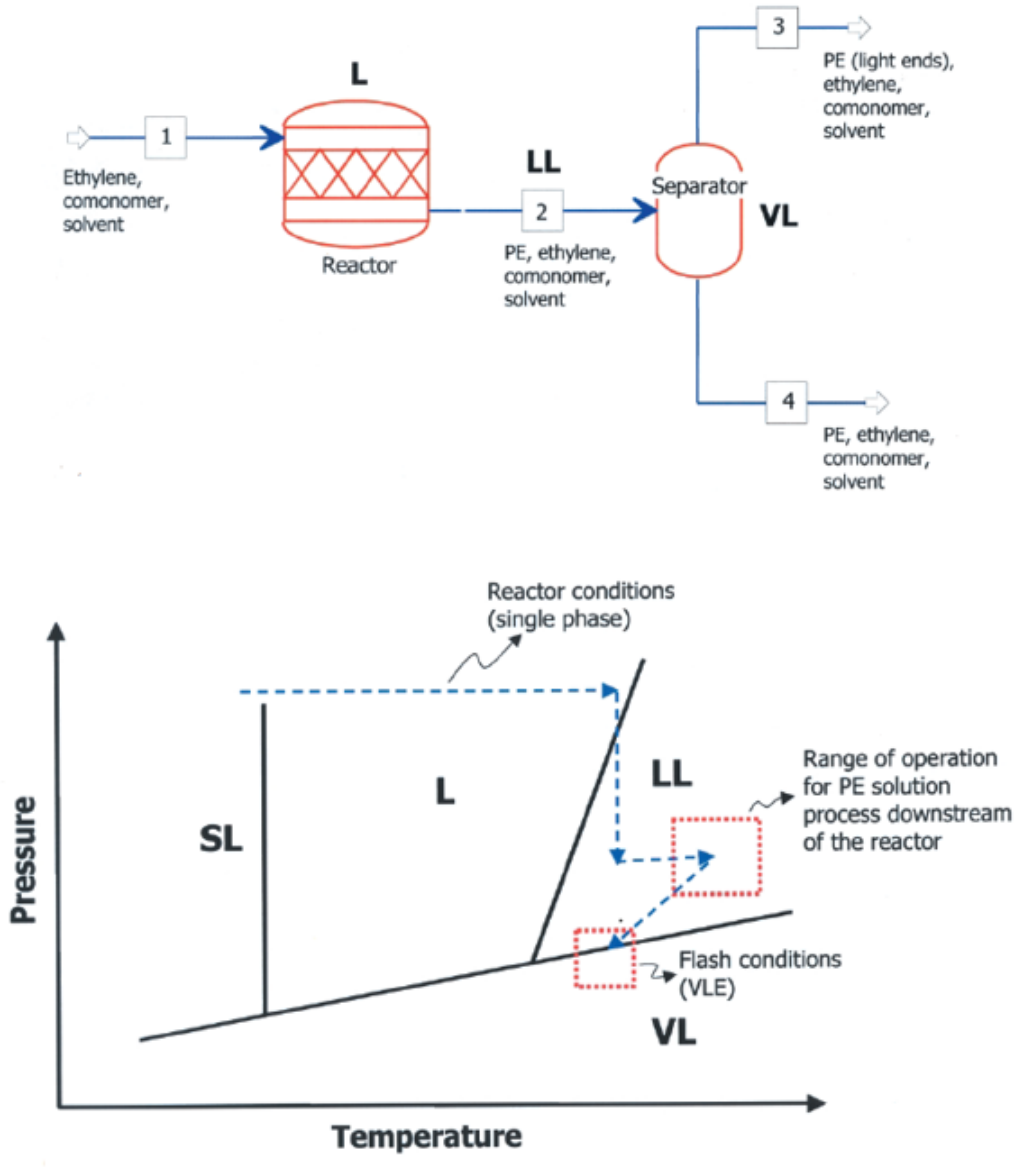

Figure 3 Polymerization process and the desired phase condition for each unit (Chen *et al.*, 2002).

3. Measurement techniques

The phase equilibrium behavior of polymer solutions such as cloud point curves are typically measured with small high-pressure variable-volume optical batch cells (Folie *et al.*, 1995). In the cells the pressure can be varied and the phase transition can be observed at constant composition and temperature. The cloud points are typically specified by light scattering or visually through sapphire windows (Folie *et al.*, 1995). The following chapters describe some measurement techniques found in literature for determining different polymer system phase equilibria.

3.1 Visual determination method

Nagy *et al.* 2006 measured the cloud point curve of LCST for LLDPE (Nagy *et al.*, 2006). The measurements were conducted on binary LLDPE + n-hexane and ternary LLDPE + n-hexane + ethylene systems. The experiment was performed with so-called Cailletet apparatus. The same apparatus was used in another research conducted by de Loos *et al.1986*; a more detailed description of the apparatus is presented in the publication. Moreover later Nagy *et al.* 2007 measured the binary LLDPE + isohexane phase equilibria with the same Cailletet apparatus. Figure 4 shows the construction of the apparatus.

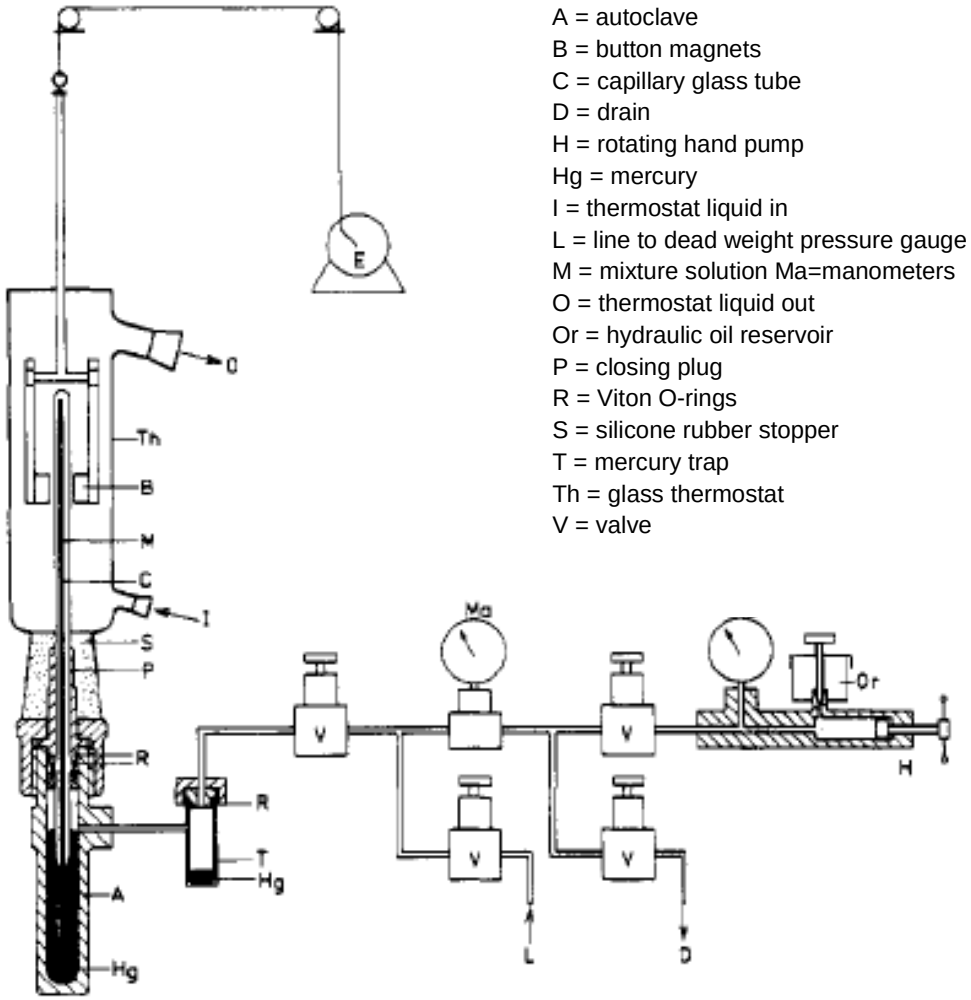

Figure 4 The Cailletet apparatus (de Loos *et al.*, 1986).

In this apparatus the maximum pressure was 200 bar and the maximum temperature was 200 °C (de Loos *et al.*, 1986). The determination of the phase transition was conducted by visual observation. The mixture M was placed in the capillary Pyrex glass tube that had one side sealed. The open side of the capillary was immersed in mercury so that the measurement mixture was in the sealed end of the capillary. The mercury in the capillary and autoclave acted as a pressure intermediate between the sample and the hydraulic oil. The mixture solution could be stirred using a small soft-iron rod stirrer. Two up and down moving magnets B moved the stirrer (de Loos *et al.*, 1986).

The temperature of the capillary was kept constant by a thermostat with circulating oil. The temperature was measured with a platinum resistance thermometer. The

pressure was added hydraulically by a screw pump H and the pressure was measured with a dead-weight pressure gauge. (de Loos *et al.*, 1986)

The experiment was conducted so that, first the pressure and temperature was set to the two-phase fluid region (de Loos et al., 1986). Then the pressure was changed until one of the phases vanished. Previous measurement method was repeated at other temperatures (de Loos et al., 1986). By this method the bubble-point curve (L_2+V)→L_2, cloud point curve L_2 →(L_1+L_2) and three phase curve L_2 L_1V could all be determined (Nagy et al., 2006).

In addition Chen *et al.* 1992a; 1992b measured binary and ternary phase equilibria of polymer systems with another type of apparatus. They performed the measurements with optical variable-volume cell for poly(ethylene-propylene) with ethylene, and additionally in ternary case with different solvents (Chen *et al.,* 1992a; Chen *et al.,* 1992b). More recently Haruki *et al.*, 2008 measured the phase behavior of supercritical ethylene + hexane + polyethylene with similar type of optical variable volume apparatus.

The pressure was controlled by moving the piston and the cloud points were determined visually with a borescope and a video screen (Chen *et al.*, 1992b). The maximum pressure used with this equipment was 550 bar at 200 °C (Chen *et al.*, 1992b). The mixing cell was placed in a temperature controlled oven. A simplified diagram of the apparatus is represented in Figure 5.

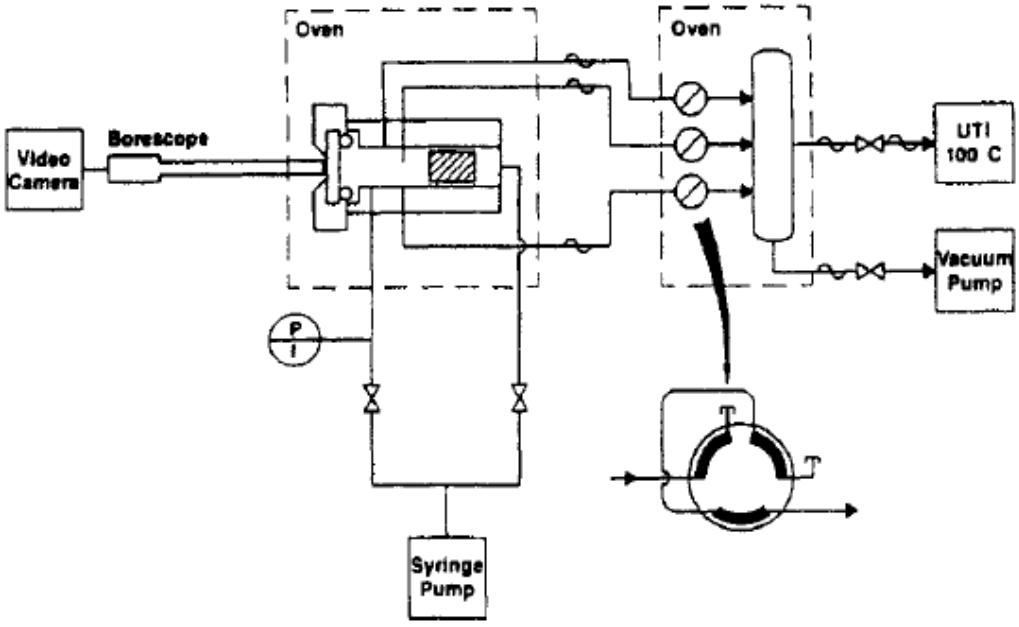

Figure 5 The optical variable-volume cell (Chen et al., 1992b).

The mixture composition was determined from known amounts of the components (by weighting) or material balance based volumetric-gravimetric sampling (adding through syringe pump) (Chen *et al.*, 1992a; Chen *et al.*, 1992b). The volumetric-gravimetric sampling is schematically presented in Figure 6. The syringe pump addition was used when the solvent was highly volatile. Additionally analytical methods such as gas chromatography or mass spectrometry were used for analyzing the solution compositions. Before conducting the measurements the polymer solution was let to swell up to 2 days in the mixing cell depending on the solvent and the molecular weight of the solvent (Chen *et al.*, 1992a; Chen *et al.*, 1992b).

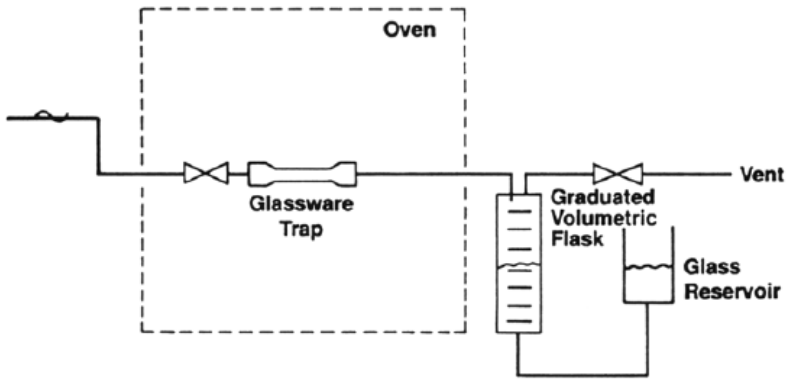

Figure 6. Diagram of the analytical sampling section (Chen *et al.*, 1992b).

In another study, de Loos *et al.* 1983 measured the polyethylene and ethylene binary system phase equilibria at high pressures with an optical high-pressure cell. The cell was designed to obtain pressures up to 4000 bar and temperatures of 175 °C. The apparatus contained a sapphire window and a magnetic stirrer (de Loos *et al.*, 1983). The apparatus is shown in figure 7.

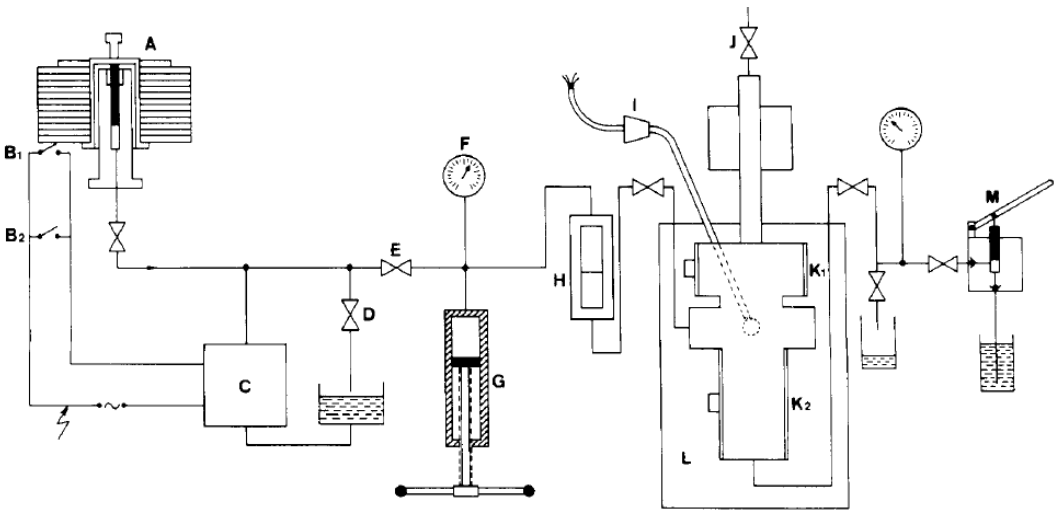

Figure 7. A=pressure balance for pressure measurements, B_1=automatic pressure control switch, B_2=manual pressure control switch, C=high-pressure bench, G=rotating pump, H=Hydraulic oil-water separator, I=platinum resistance thermometer, $K_{1,2}$=electronic heating mantles, L= thermostated air bath M=hand pump (de Loos *et al.*, 1983).

In this apparatus the cell was heated with two electric heating mantles and controlled with electronic regulators. The heating mantles were placed with the measurement cell in a thermostated air bath for better temperature stability. The pressure could be generated in two ways. One way was by using a hand pump (up to 500 bar) and the second way was by operating a high-pressure bench which was connected to the cell through a hydraulic oil-water separator. Small changes to the pressure could be generated with a rotating pump. In this study the pressure could be generated through water medium and the measurement solution was separated from the water with mercury. The high-pressure bench could be operated both manually and automatically. (de Loos *et al.*, 1983)

3.2 Light scattering technology

Light-scattering techniques utilizes radiation. He-Ne laser is pointed to the solution and the scattered light intensity is measured. This is done continuously as the pressure of the system is changed and the wanted phase change is observed. At systems cloud point the intensity of the light changes rapidly as the clear solution changes to non-transparent. (Folie *et al.*, 1996).

Szydlowski *et al.* 1992 measured the phase equilibrium points for acetone + polystyrene solution with apparatuses which utilized light scattering technology. They constructed three different measurement equipment and one of those is described in more detail below. The two other equipments, not described in this work, were intended for the close critical point measurements, and more expensive deuterated polymer/solvent solution measurements. (Szydlowski *et al.*, 1992)

The equipment measured the intensity change between transmitted and scattered light with 5 mW HeNe laser (Szydlowski *et al.*, 1992). The laser was pointed through the solution in the cell and two sapphire windows. The intensity change of scattered light and transmitted light occurred when a phase transition appeared. The phase transition was due to the change of temperature at constant pressure or the change of pressure at constant temperature. At cloud point the intensity of scattered light increased and transmitted light decreased (Szydlowski *et al.*, 1992). The construction of the cell system is presented in Figure 8.

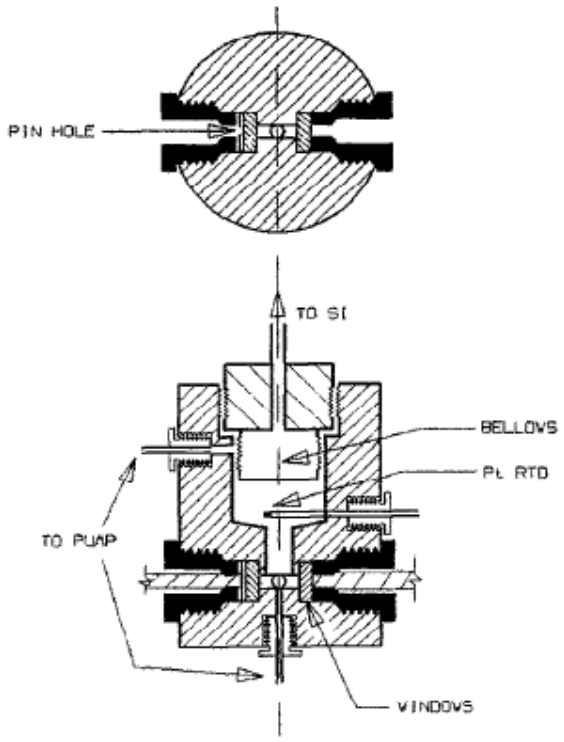

Figure 8. The measurement cell with mixing loop (Szydlowski *et al.*, 1992)

The sample was placed in a cylindrical high-pressure sapphire-windowed stainless steel cell and the cell was immersed in an oil bath. The temperature of the thermostat was computer controlled. The computer detected the temperature in the cell near the light beam with a low heat capacity platinum resistance temperature detector (RTD) or alternatively with a thermocouple temperature sensor. The pressure was changed using a computer control. The volume of the cell was changed by changing the amount of hydraulic oil in the stainless steel bellows located at the top of the cell. (Szydlowski *et al.*, 1992)

The optical cell was placed in the sample/mixing loop which included a magnetically working slide pump. The loop system functioned across the desired pressure range and moreover even for viscous solutions. The loop though had to be completely filled with the solution in order to work properly. The pumping in the loop promoted the thermal equilibrium with the bath and ensured that the solution stayed thoroughly mixed. A valve was also installed in the loop so that the solvent or the solution could be added to the mixing cell. Therefore this apparatus could be used to investigate different solvent-polymer ratios by only one charge of

polymer. One valve was intended for waste and vacuum line operation. (Szydlowski *et al.*, 1992)

Melchior *et al.*, 1991 measured phase behavior of polymer-solvent systems with a high-pressure variable volume cell. The measured polymers were polyethylene, poly(ethylene-co-methyl acrylate) and poly(methyl acrylate). The polymers were mixed with propane and chlorodifluoromethane. A schematic picture of the measurement cell is shown in Figure 9. Two different cells could be used alternatively (Meilchen *et al.*, 1991). For pressures lower than 1000 bar a 316 stainless steel cell was used and for pressures over 1000 bar a high nickel content cell was available. The pressure was generated with a movable piston which could be moved with high-pressurized water. The pressure of the polymer system was determined from the high pressurized water that moved the piston. Mostly this measurement procedure differed in how the cloud points were determined. Melchior et al. utilized both visual and laser determination. The 10 mW laser was directed to the cell and reflected to a mirror. In this study the cloud point was defined as a point when 90 % decrease of the transmitted laser light intensity was observed (Meilchen *et al.*, 1991).

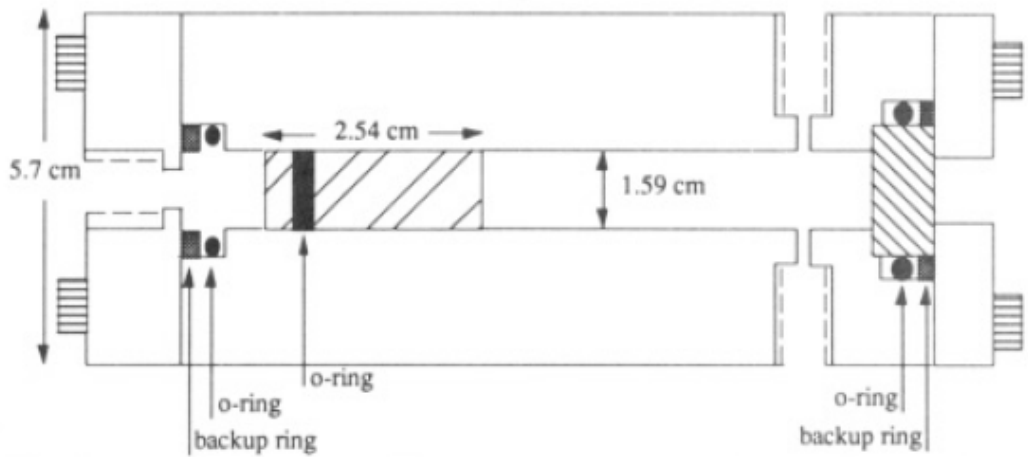

Figure 9 Variable-volume high pressure cell. (Meilchen *et al.*, 1991)

4. Phase equilibria models of polymer systems

4.1 Development of the polymer system models

It is experimentally difficult to measure the phase equilibria of polymer solutions over a wide range of temperatures, pressures and molecular weight distributions (Liu *et al.*, 1980). Due to this it is useful in most cases to obtain a physical model so that interpolating and extrapolating is possible with limited experimental data (Liu *et al.*, 1980). Also the phase behavior prediction models are needed in process simulators (Khare *et al.,* 2002). The modeling of the polymer systems is typically done either with free energy models or equation of state models (Pedrosa *et al.*, 2006). In addition Song *et al.* divides models describing the LLE in to four categories that are incompressible-lattice models, compressible-lattice models, generalized van der Waals partition function theories and off-lattice (continuous-space) models of chain fluids (Song *et al.*, 1993).

The lattice models such as Flory-Huggins (from 1940s) and Sanchez-Lacombe (from 1970s) were the first models for describing the polymer solutions behavior (Chen *et al.*, 2005). Previously modeling have been concentrated to simple fluid polymer systems (Tumakaka *et al*., 2005). However today polymers have many different applications and therefore the variety of polymer types and polymerization techniques has increased (Pedrosa *et al.*, 2006). Therefore there is an increasing need for models that are applicable to complex systems. These complex systems can contain different polymers or copolymers and specific interactions such as hydrogen bonding and polar interactions (Tumakaka *et al.*, 2005). Still the modeling of these polymer phase equilibrium systems has some challenges (Pedrosa *et al.*, 2006).

Today the development of models that are based on theoretical statistical mechanics such as SAFT and PHSC models are more popular (Chen *et al.*, 2005). Many publications has been made on these continuous-space EOS for polymer solutions (Song *et al.*, 1993). Moreover the interest of model development goes toward models that can account additional characteristics for example copolymer composition and polydispersity (Chen *et al.*, 2005). Therefore typically the first

choice for thermodynamic models in the process industries are Polymer NRTL and PC-SAFT. Secondary choices typically are Sanchez-Lacombe, SAFT and UNIFAC-FV (Chen *et al.*, 2005).

4.2 Activity coefficient models

Activity coefficient or so called free energy models such as Flory-Huggins, NRTL, UNIFAC and UNIFAC-FV can be used to model different polymer systems (Pedrosa *et al.*, 2006). The Flory-Huggins lattice model is the most utilized activity coefficient model (Pedrosa *et al.*, 2006). Lattice models in general are quite strong for modeling polymer systems, rather than systems containing smaller molecules (Madden *et al.*, 1990). Lattice models are based on a theory where the fluids are mixtures of molecules and holes that are bonded to sites on a lattice (Khare *et al.*, 2002).

The Flory-Huggins model was created by Flory based on the work by Huggins (Flory *et al.,* 1944). It is one of the widely used incompressible lattice models due to its simplicity (Folie *et al.*, 1996; Pedrosa *et al.*, 2006; Song *et al.*, 1993). The model is derived from the lattice fluid theory and it predicts numerous common polymer systems relatively well (Pedrosa *et al.*, 2006). Still the model has some flaws especially when the polymer is in supercritical fluid at high-pressure (Folie *et al.*, 1996; Liu *et al.*, 1980). Malony *et al.* 1976 calculated the solubility of ethylene in LDPE for process separator design using the Flory-Huggins model. They stated that the error might be even 50 % or more when presenting the pressure as a function of ethylene concentration if the pressure is above 200 bar (Maloney *et al.*, 1976). Moreover the model assumes that there is no excess volume of mixing and therefore it is only exploitable for incompressible fluids.

In addition the Flory-Huggins X-parameter is a strong function of temperature and composition (Kontogeorgis *et al.*, 1995). Therefore the parameter is specific for each system. Another limitation is that the model does not take into account the free volume difference between the polymer and the solvent. Therefore the LCST phase behavior prediction fails (Folie *et al.*, 1996; Kontogeorgis *et al.*, 1995). In addition Madden *et al.* stated that the Flory-Huggins theory fails in low polymer volume fractions (Madden *et al.*, 1990).

Another activity coefficient model UNIFAC is utilized for modeling polymer systems (Kontogeorgis *et al.*, 1995). UNIFAC is a predictive group-contribution (GC) model and it has different variations. Kontogeorgis *et al.* investigated four activity coefficient models for predicting the LLE behavior of binary polymer solution (Kontogeorgis *et al.*, 1995). Original UNIFAC (Fredenslund *et al.*, 1989), new-UNIFAC (Hansen *et al.,* 1992), modified Flory-Huggins (Kontogeorgis *et al.*, 1995) and entropic free volume (entropic-FV) (Elbro *et al.*, 1990) models were used. In this study the Flory-Huggins and the entropic-FV were the only two models that could predict both LCST (also near critical temperature of the solvent) and UCST behavior. Especially the entropic-FV model proved to predict polymer solution behavior qualitatively well. With all of these models the binary solutions activity coefficient can be calculated with a combinatorial (or combined combinatorial/free volume) and a residual (energetic) term as in equation (1) (Kontogeorgis *et al.,* 1995):

$$\ln\gamma_i = \ln\gamma_i^{comb} + \ln\gamma_i^{res} \tag{1}$$

These four models (Original UNIFAC, new-UNIFAC, modified Flory-Huggins, entropic-FV) mostly differ in the form of the combinatorial or residual term, or alternatively by the type of the parameter table they utilize. In this study the modified Flory-Huggins model has the same combinatorial term as in the original Flory-Huggins. However the residual term is taken from a linear temperature dependent parameter table. Therefore in the modified Flory-Huggins model the combinatorial term was based on volume fractions as in equation (2). (Kontogeorgis *et al.*, 1995)

$$\ln\gamma_i^{comb} = \ln\frac{\emptyset_i^{vol}}{x_i} + 1 - \frac{\emptyset_i^{vol}}{x_i} \tag{2}$$

The volume fraction of component *i* is calculated from equation (3):

$$\emptyset_i^{vol} = \frac{x_i V_i}{\sum_j x_i V_i} \tag{3}$$

Where V_i is the molar volume of the component *i*

x_i is the mole fraction of the component *i*

For the original and new UNIFAC the combinatorial term used in that study is represented in equation (4). The residual term for both original and new UNIFAC was taken from the linear temperature dependence group parameter table. (Kontogeorgis *et al.*, 1995).

$$\ln\gamma_{\mathrm{i}}^{\mathrm{comb}} = \ln\frac{\emptyset_{\mathrm{i}}^{S}}{\mathrm{x_i}} + 1 - \frac{\emptyset_{\mathrm{i}}^{S}}{\mathrm{x_i}} - \frac{z}{2}q_i\left(\ln\frac{\emptyset_i^S}{\theta_i} + 1 - \frac{\emptyset_i^S}{\theta_i}\right) \qquad (4)$$

Where z is the coordination number

The segment area fraction $\emptyset^{s}_{i}$ and surface area fraction θ_i of the component *i* were calculated from equations 5 and 6 (Kontogeorgis *et al.*, 1995).

$$\emptyset_i^S = \frac{\mathrm{x_i r_i}}{\sum_{\mathrm{j}} \mathrm{x_j r_j}} \qquad (5)$$

$$\theta_i = \frac{\mathrm{x_i q_i}}{\sum_{\mathrm{j}} \mathrm{x_j q_j}} \qquad (6)$$

In this case the original and new UNIFAC did not predicted the LCST curve due to the combinatorial term. The combinatorial term in these two cases do not account the free volume difference between polymer and solvent that is significant at higher temperatures. Therefore the Entropic-FV model was the able to predict both UCST and LCST critical points most accurately. For Entropic-FV model the combinatorial and free volume term is combined in equation (7). The free volume fraction is presented in equation (8). (Kontogeorgis *et al.*, 1995)

$$\ln\gamma_{\mathrm{i}}^{\mathrm{comb-fv}} = \ln\frac{\emptyset_{\mathrm{i}}^{\mathrm{fv}}}{\mathrm{x_i}} + 1 - \frac{\emptyset_{\mathrm{i}}^{\mathrm{fv}}}{\mathrm{x_i}} \qquad (7)$$

$$\emptyset_{\mathrm{i}}^{\mathrm{vol}} = \frac{\mathrm{x_i V_{f_i}}}{\sum_j \mathrm{x_i V_{f_j}}} = \frac{x_i(V_i - V_{w_i})}{\sum_j \mathrm{x_j}(\mathrm{V_j} - V_{w_i})} \qquad (8)$$

Where V_f is the free volume of component

V_w is the van der Waals volume of component *i*

4.3 Equation of state models

Equations of state (EOS) models such as Sanchez-Lacombe, polymer-SRK, SAFT (and its modifications), perturbed hard sphere chain (PHSC) are typically used for estimating thermodynamic properties of polymer systems (Song *et al.*, 1995; Pedrosa *et al.*, 2006; Folie *et al.*, 1996). Both LCST and UCST boundaries can be predicted properly by using these models (Song *et al.*, 1995).

4.3.1 The Sanchez-Lacombe EOS

The Sanchez-Lacombe EOS is a lattice fluid model (Sanchez *et al.,* 1978). It is actually an extension of the Flory-Huggins theory and the free volume concept is included to this compressible lattice model (Koak *et al.*, 1999; Sanchez *et al.*, 1978; Song *et al.*, 1993). In contrary to the Flory-Huggins model the vacant sites are occupied by additional component (Song *et al.*, 1993). It is one of the simplest models for qualitative prediction of polyethylene-solvent systems (Gauter *et al.*, 2001). Gauter *et al.* used the Sanchez-Lacombe for modeling polyethylene + ethylene and polyethylene + n-hexane systems. This model fit well with the experimental cloud point data. Moreover Khare *et al.,* 2002 developed steady-state and dynamic models for slurry HDPE process. They stated that the Sanchez-Lacombe EOS gave accurate prediction of the phase behavior and thermodynamic properties of the polymer mixtures (Khare *et al.*, 2002).

The Sanchez-Lacombe EOS uses three pure component parameters in following type of equation 9 (Sanchez *et al.*, 1978, Khare *et al.*, 2002, Orbey *et al.*, 1998). For mixtures different combining rules is used.

$$\tilde{\rho}^2 + \tilde{P} + \tilde{T}\left[\ln(1-\tilde{\rho}) + \left(1-\frac{1}{r}\right)\tilde{\rho}\right] = 0 \qquad (9)$$

Where $\tilde{\rho}$, $\tilde{P}$ and $\tilde{T}$ are dimensioless reduced, density, pressure and temperature

r is the number of lattice sites occupied by a molecule.

Reduced values can be calculated from equation (10) (Orbey *et al.*, 1998):

$$\tilde{T} = \frac{T}{T^*},\ \tilde{P} = \frac{P}{P^*},\quad \tilde{\rho} = \frac{\rho}{\rho^*} \tag{10}$$

The pure component molecular parameters are defined in equation (11). Equation (11) represents the relationship of three pure component molecular parameters (ϵ^*, v^*, r) and three equation of state scaling parameters (T*, P*, ρ*) (Sanchez *et al.*, 1978, Orbey et al., 1998).

$$T^* = \frac{\epsilon^*}{k},\quad P^* = \frac{kT^*}{v^*},\ \rho^* = \frac{MP^*}{rkT^*} \tag{11}$$

Where M is the molecular weight (g/mol)
k is the Boltzmann constant (J/K)
r is the number of lattice sides occupied by a molecule
ϵ^* is the pair interaction energy
v^* is the volume occupied by one segment

For mixtures a mixing rule is used as in equations (12) to (17), and they are dependent on the composition (Orbey *et al.*, 1998).

$$v^*_{mix} = \sum_i \sum_j \emptyset_i \emptyset_j v^*_{ij} \tag{12}$$

$$\epsilon^*_{mix} = \frac{1}{v^*_{mix}} \sum_i \sum_j \emptyset_i \emptyset_j \epsilon^*_{ij} v^*_{ij} \tag{13}$$

$$\frac{1}{r_{mix}} = \sum_j \frac{\emptyset_j}{r_j} \tag{14}$$

The segment fraction of component *i* is calculated with equation (15) (Orbey *et al.*, 1998):

$$\emptyset_i = \frac{\frac{w_i}{\rho^*_i v^*_i}}{\sum_j \left(\frac{w_j}{\rho^*_j v^*_j}\right)} \tag{15}$$

Where w is the weight fraction

The cross parameters are calculated from equation (16) and (17) (Orbey et al., 1998):

$$v_{ij}^{*} = \frac{1}{2}\left[v_{ii}^{*} + v_{jj}^{*}\right]\left(1 - l_{ij}\right) \quad (16)$$

$$\epsilon_{ij}^{*} = \sqrt{\epsilon_{ii}^{*}\epsilon_{jj}^{*}}\left(1 - k_{ij}\right) \quad (17)$$

Where k_{ij} and l_{ij} are binary interaction parameters

One area of interest is the modeling of polymer-solvent systems with supercritical gases and quite resent publications have been made on this topic. For example Haruki *et al.,* 2008 and Nagy *et al.*, 2006 utilized the Sanchez-Lacombe EOS for predicting these phase equilibrium systems and they were somewhat successful.. Even though the Sanchez-Lacombe EOS is one of the widely used model, it still has it challenges when predicting ternary and multicomponent systems (Haruki *et al.*, 2008). This difficulty of correlating ternary and multicomponent mixtures is due to the need of fitting the binary parameters from two component data to the experimental multicomponent data (Haruki *et al.*, 2008). In many cases though the Sanchez-Lacombe model can be better than for example SAFT due to its simplicity (Kikic *et al.*, 2009)

One challenge for modeling supercritical systems is the lack of ternary data of polymer-solvent-supercritical fluid (Kikic *et al.*, 2009). Binary behavior is typically well known, however understanding of these ternary systems is very important. Ternary systems are generally difficult to study experimentally and therefore simulation studies are helpful (Kikic *et al.*, 2009). For example Nagy *et al.*, 2006 used a modified Sanchez-Lacombe model and could predict the ternary systems with parameters obtained from the binary data.

4.3.2 Cubic equation of state

Some cubic equation of state models have also been applied to polymer solution mixtures (Goodwin et al., 2010). Sako-Wu-Prausnitz (SWP) is one cubic equation of state model that has been used for modeling polymer systems (Tork *et al.*,

1999a). It is based on Soave-Redlich-Kwong (SRK) equation of state model. The SWP equation is presented in equation (18):

$$P = \frac{RT(V_m - b(1-c))}{V_m(V_m - b)} - \frac{a(T)}{V_m(V_m + b)} \quad (18)$$

Where P is the pressure
R is the gas constant
V_m is the molar volume
a, b and c are the pure component parameters

The pure component parameters can be calculated from equations (19-21) and they are dependent on segment based parameters. The segment based parameter â is a temperature dependent parameter. In addition, parameter â and $\hat{b}$ are calculated from physical properties that are molar polarization (A), van der Waals volume (V_w) and first ionization potential (I). A (m^3/mol), I (J/mol) and V_w (m^3/mol) are calculated from the physical properties of the saturated monomer of the polymer, and for polyethylene it is ethane, but not ethylene. The r indicates that each molecule is built of equally sixed segments of r. The parameters r and ĉ are determined from vapor-pressure data. For spherical molecules such as nitrogen and methane the ĉ is set equal to 1. (Tork *et al.*, 1999a)

$$a = r^2\hat{a} \quad (19)$$

$$b = r\hat{b} = r\beta\hat{V}_w \quad (20)$$

$$c = r\hat{c} \quad (21)$$

Where a, b and c are the pure-component parameters
r is the segment number that is determined from experimental pure component data
β = 1.3768
â, $\hat{b}$ and ĉ are the EOS parameters that are correlated with physical properties

The parameter a, describes the attractive forces between the molecules in the system. The parameter b is dependent on the molecular size and is not temperature dependent. The parameter c is needed when the modeling is done for large molecules such as polymers. This parameter c represents the rotational and vibrational degrees of freedom of a molecule. If the c is set as equal to one the equation reduces to normal SRK equation of state model. (Tork *et al.*, 1999b)

SWP equation of state model is applicable to for example high-pressure polyethylene technology where low-density polyethylene is formed at relatively high temperatures and at high pressures. The low pressure solution polymerization is typically correlated with activity coefficient models that do not include the pressure effect and there for cannot be used for high pressure system modeling. (Goodwin *et al.*, 2010)

Tork *et al.* modeled the high pressure non-polar system of ethylene-HDPE and ethylene-poly(ethylene-co-propylene). The copolymer system modeling with SWP was compared to SAFT modeling. The two EOS could predict UCST, LCST and U-LCST curves. The prediction of SWP was similar to the SAFT model prediction. However SAFT can describe also polar systems that SWP cannot predict. One problem in the SWP model is that it does not include the density changes in the system. This is due to the van der Waals' type EOS which does not account the density changes. Moreover both original SAFT and SWP does not include the structure of the polymer such as branching. (Tork *et al.*, 1999b)

4.3.3 Perturbation theory models

One group for EOS models are ones that have been derived from the thermodynamic perturbation theory (Folie *et al.*, 1995). Typically lattice based models ignore the continuous nature of polymer molecules. Therefore these off-lattice (continuous) models have been developed (Song *et al.*, 1993). These models typically can be used in a wide range of densities and molecular sizes.

PHSC and SAFT are both hard-sphere models and are based on theoretical statistical mechanics (Chen *et al.*, 2002). PHSC utilizes a reference fluid that consists of hard spheres in chains (Koak *et al.*, 1996). PHSC model was further

developed by Song *et al.*1993 based on the Chiew EOS model for athermal hard-sphere chains and the van der Waals type perturbation term. When comparing the PHSC theory to other theories, it has a few advantages, such as all the segments diameters in a chain molecule of the components do not have to be equal. Due to this the PHSC can model the UCST and LCST behavior for binary mixtures that contains copolymers where the spheres have different diameters (Song *et al.*, 1993; Song *et al.*, 1995). PHSC is very similar to SAFT model because it includes a hard sphere term as a perturbation expansion for dispersion interactions (Economou, 2002). Even though the mathematical base is different the two models give quite similar results (Economou, 2002).

SAFT model utilizes the so called cluster integral approximation and it is more complicated algebraically than the PHSC model (Koak *et al.*, 1996). Unlike the traditional EOS models the SAFT model includes particularly the intermolecular association, the chain length and branching along with the repulsion and dispersion forces (Blas *et al.,* 1997; Folie *et al.*, 1995). The SAFT model is classified as a continuum model and in this model the molecules are viewed as a chain of tangentially connected spheres (Jog *et al.*, 2002). In SAFT the molecules are a sum of different terms that are the reference term, the chain term and the association term (Pedrosa *et al.*, 2006). Therefore the Helmholtz free energy is written in this case as a perturbation series shown in equation 22. The segment free equation is a sum of hard sphere and dispersion contribution shown in equation 23 (Jog *et al.*, 2002):

$$A = A_{seg} + A_{chain} + A_{assoc} \tag{22}$$

$$A_{seg} = A_{hs} + A_{disp} \tag{23}$$

The SAFT is applicable to chain like molecules due to the included chain term that is derived from statistical mechanics (Chen *et al.*, 1992a). The association term is added if the molecules can for example form hydrogen bonds (Pedrosa *et al.*, 2006). SAFT accounts the nonspecific (repulsive, dispersion) and specific (hydrogen bonding) interactions between molecules (Chen *et al.*, 1992a). Figure 10 presents schematically the physical basis of the SAFT model.

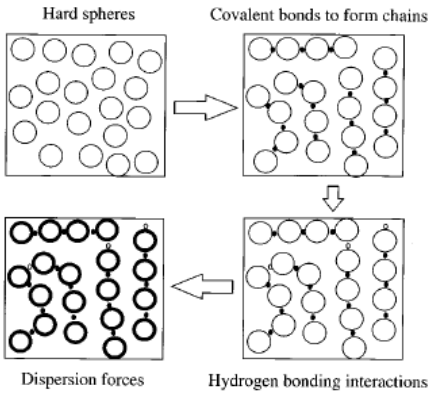

Figure 10. Simple presentation of the physical basis of the SAFT model. The reference fluids consists of hard spheres that are connected through covalent bonds. Also hydrogen bonding between terminal sites and the weak dispersion forces are taken into account (Economou, 2002)

The SAFT model has many different modifications such as polar-SAFT, SAFT-HS, simplified SAFT, SAFT-LJ, copolymer SAFT, soft-SAFT, SAFT-VR, SAFT1, SAFT-BACK, crossover SAFT and PC-SAFT. (Economou, 2002). They mostly differ by the used reference term (Pedrosa *et al.*, 2006). These SAFT models are currently accepted in academia and in industry and are the leading models for polymer solution modeling. Still these models need much work. (Economou, 2002). There are typically two problems with SAFT types of models (Pedrosa *et al.*, 2006). One problem is the difficulty to obtain the polymer pure component molecular parameter. This is due to the lack of vapor pressure data from polymer melts as polymers do not have measurable vapor pressure. The second problem is the large asymmetry of polymer-solvent or polymer-gas systems. Usually the parameters gained from the pure polymer density data give poor results for the mixtures behavior. One solution for this problem is to use polymer binary data for fitting the parameter. However in this case these parameters do not necessarily fit to other systems, where for example the solvent is different and the polymer is the same (Pedrosa *et al.*, 2006).

PC-SAFT was developed by Gross and Sadowski and in their work they derived a new dispersion term (Gross *et al.* 2001). In PC-SAFT the reference term is a hard chain fluid instead of hard sphere fluid (Gross *et al.* 2001; Pedrosa *et al*., 2006). This leads to a dispersion term that is dependent on the chain length of the polymer molecule. PC-SAFT proved to be an improved version of the SAFT for example in

a study performed by Pedrosa *et al.*, 2006. It predicted the polyethylene-pentane mixture behavior well when comparing to the experimental data and the original SAFT model.

Later Gross *et al.*, 2003 extended the PC-SAFT EOS to copolymers. In this modification the model allows different types of segments to be included to the molecular chain as represented in figure 11. One additional parameter had to be included to the model which described the interactions between different types of segments. In this study the PC-SAFT model could successfully model different copolymer systems such as poly(ethylene-*co*-propylene) and poly(ethylene-*co*-1-butene) (Gross *et al.*, 2003).

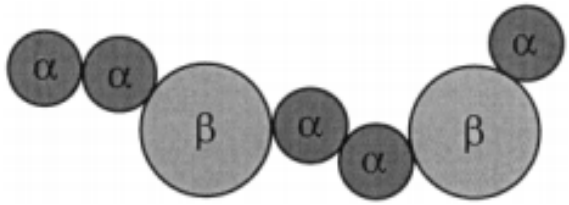

Figure 11. Molecular presentation for a copolymer poly(α-co-β) with different segments (Gross *et al.*, 2003).

Tumakaka *et al.* 2005 investigated also the modeling of complex polymer systems with PC-SAFT. They studied systems that contained non-polar, associating and polar substances, gases, solvents, homopolymers and copolymers. The PC-SAFT showed good capabilities to predict these complex systems over wide range of conditions. Still the model has some limitations and more development is needed (Tumakaka *et al*., 2005).

Modified SAFT, called soft-SAFT, was created by *Blas et al.* (Blas *et al.*, 1997). In this model a soft reference fluid is used and this gives a possibility to locate the associating sites inside the repulsion potential area (Blas *et al.*, 1997). The use of this model to polymer systems has been very limited. Nevertheless Pedrosa *et al.* compared the performance of the widely used PC-SAFT and soft-SAFT (Pedrosa *et al.*, 2006). The models were tested for various solvents with polyethylene. Both models gave quite similar results and the soft-SAFT was in some cases even more accurate. The usual problem for these models is the difficulty to find the pure

polymer parameters and this was solved by two different ways. They used pure component parameter correlation equations for both models and calculated the length of the chain segment m, the size of each segment σ and the energy of the segment ϵ with the polymer molecular weight. In addition they derived a new correlation for the energy parameter instead of fitting the parameters to the polymer mixture. Due to this new energy correlation, the model fitted better to the experimental data with various solvents (Pedrosa *et al.*, 2006).

Experimental part

5. Variable volume cell measurement apparatus

The measurement apparatus utilized in this work was designed and constructed at chemical engineering research group of Aalto University. The same apparatus was used in the Thesis work of Tom Cameron previously (Cameron, 2016). A simplified diagram of the apparatus is in Figure 12. In this work the cloud and bubble points could be determined visually. Pressure of the cell could be changed by altering the volume of the cell and, this was done by moving a piston inside the cell.

The cell (item 1 in Figure 12) consists of a cylindrical shaped sapphire glass that is sealed from both ends with polymer graphite seals and titanium caps. The titanium caps of the cell is supported by three titanium rods. The solution is mixed with a small magnetically driven mixer (item 3). The pressure of the cylinder can be changed by moving a piston inside the cell. Movement of the piston occurs by pressurizing hydraulic oil in to the lower side of the piston. Hydraulic oil is pressurized to the lower part of the cell by a positive displacement pump (items 4 and 5 in figure 12). The piston is sealed from the measurement solution and therefore the measurement solution and hydraulic oil cannot be mixed together

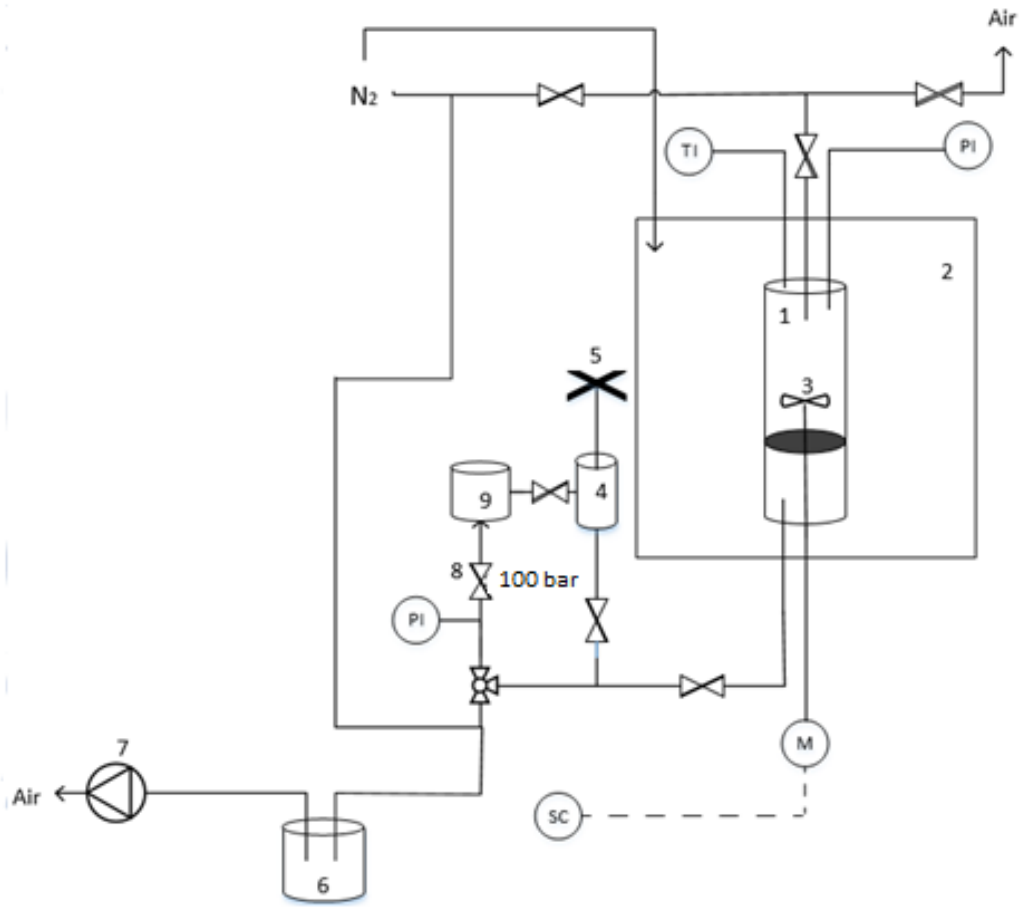

Figure 12. A simplified diagram of the measurement apparatus. 1=cell, 2=oven, 3= magnetic stirrer, 4=positive displacement pump oil cell, 5=manually adjustable pressure regulator, 6=trap cooled with liquid nitrogen, 7=vacuum pump, 8=safety valve (opening pressure 100 bar), 9=hydraulic oil reservoir.

The cell has two valves and lines: one in the upper and second in the lower side of the cell. The upper line is used for gas and liquid additions. The lower line is used for changing the pressure in the cell by pressurizing hydraulic oil to the lower part of the piston. The pressure is raised by rotating a positive displacement pump by hand. Then the hydraulic oil is pressurized through the lines to the measurement cell. When the pressure in the system rises above 100 bar a safety valve (item 8) opens and leaked the hydraulic oil in to a hydraulic oil reservoir (item 9).

The measurement cell is placed in a type 5890 Series II plus Gas Chromatograph oven (item 2). Nitrogen gas is added from a gas cylinder to the oven atmosphere during the tests for safety reasons. The maximum temperature for this apparatus is 250 °C. The temperature is measured with a Pt 100 Ω 0 °C thermometer

(Automatic System laboratories F200 Tempcontrol) that was calibrated previously at MIKES (22.10.2015). The thermometer is placed in the upper cap of the cell. The pressure is measured from inside of the cell with a Kulite Semiconductor XTEH pressure transducer and Omrom K3GN-PDC-FLK DC24V digital panel meter. Picture of the apparatus is presented in Figure 13.

Figure 13. Picture of the measurement system. 1=cell, 2=oven, 3= magnetic stirrer, 4=positive displacement pump oil cell, 5=manually adjustable pressure regulator, 8=safety valve (opening pressure 100 bar), 9=hydraulic oil reservoir.

A vacuum pump (item 7) is used for evacuating both upper and lower lines of the measurement apparatus and also the cell itself. The evacuation of the lines and cell was always done before adding the solvents and gases in to the system. Between the vacuum pump and the vacuumed lines is a trap (item 6) that is cooled

with liquid nitrogen. Trap is needed so that light components would not end in the pump.

The cell contains different sized O-rings. Two smallest size O-rings in the piston sealed the cell system from atmosphere. These O-rings had to be changed when a hydraulic oil leak was observed due to the erosion of the seal. The erosion of one of these seals is presented in Figure 14. The piston also has copper seal that needed to be annealed occasionally for maintaining the sealing capability. Moreover the upper and lower seals of the caps had to be changed approximately after two test runs. The O-ring that was placed on the piston for sealing the measurement system and hydraulic oil system from each other, was changed when some erosion was detected or the pressure test failed.

Figure 14. A new O-ring on the left side and a used O-ring on the right side.

6. Calibrations

The temperature and pressure measurement instruments needed to be calibrated before conducting the tests. The temperature sensor was previously calibrated at MIKES. The pressure sensor thus was calibrated in this work at various temperatures. This was due to the temperature dependence of the pressure sensor.

The temperature sensor calibration results are in Appendix 1. A function was built for determining the actual temperature of the system and is tested in Table 1. The temperature calibration function is presented in formula (24). This calibration function was used for correcting the temperatures in the pressure tests and in the actual tests.

$$T_{calib.func.} = 0.9995 \cdot T_{disp} + 0.0357 \quad (24)$$

An example for testing the calibration formula (24) at display temperature 50 °C which was used in the calibration at MIKES:

$$T_{calib.func.} = 0.9995 \cdot 50{,}000 + 0.0357 = 50.010\,°C$$

As in Table 1 when the display of the F200 tempcontrol of the cell was 50.000 °C the calibrated value at MIKES was 49.997 °C. Then the difference of the calibrated temperature at MIKES and the calibration function is:

$$T_{difference} = 49.997 - 50.010 = -0.013\,°C$$

Table 1. The difference of the calibrated value ta MIKES and calibration function.

Display of F200 T (°C)	Calibration temperature at MIKES T (°C)	Calibration function T (°C)	Difference T (°C)
50.000	49.997	50.010	-0.013
100.241	100.225	100.226	-0.001
150.250	150.230	150.209	0.021
200.051	199.998	199.985	0.013

The pressure sensor of the apparatus was calibrated before initiating the experiments. The calibration pressure sensor was manufactured by Beamex (external pressure module and MC2-PE output indicator) and had range of 0 to 600 bar with maximum pressure 900 bar. The calibration in this work was conducted up to pressure of 100 bar (opening pressure of the safety valve) at several temperatures. The temperature was raised from room temperature to around 50 °C and after that 50 °C at the time to the temperature of 200 °C. The pressure was first set to near 100 bar and then gradually lowered about 10 bar at the time to near atmospheric pressure. Nitrogen gas was used as a pressure calibration gas.

The results for the pressure calibration is presented also in Appendix 1. A slope and intercept was calculated at each calibrated temperature. The slope (a) and the intercept (b) was calculated from functions of p(display, bar)=f(p(calibrated, bar)) at constant temperature Then polynomial function for temperature dependence slope (a=f(T(°C)) and intercept (b=f(T°C)) was formed. By determining the value of slope and intercept from the temperature dependence functions a pressure calibration equation could be formed for each temperature. Therefore the pressure of the system could be determined between the calibration points.

The temperature dependence of the slope and the intercept are presented in equations (25) and (26). By utilizing these values a pressure calibration line could be generated and this pressure calibration equation is shown in equation (27):

$$a_{slope} = -9 \cdot 10^{-7} \cdot T^2 + 0.0004 \cdot T + 0.9559 \quad (25)$$

$$b_{intercept} = -7 \cdot 10^{-5} \cdot T^2 + 0.0012 \cdot T + 2.9877 \quad (26)$$

$$p_{calibrated} = a_{slope} \cdot p_{display} + b_{intercept} \quad (27)$$

Where a_{slope} is the temperature dependence slope
$b_{intercept}$ is the temperature dependence intercept
T is the calibrated temperature of the system (°C)
$p_{calibrated}$ is the calibrated value of the pressure (bar)
$p_{display}$ is the display pressure (bar)

For example if the F200 tempcontrol display value is 175 °C then the calibrated temperature is calculated from equation (24):

$$T_{calib.func.} = 0.9995 \cdot 175 + 0.0357 = 174.947\ °\mathrm{C}$$

Next the temperature dependence slope and intercept for the pressure calibration is calculated from equations (25) and (26):

$$\mathrm{a_{slope}} = -9 \cdot 10^{-7} \cdot (174.947)^2 + 0.0004 \cdot 174.947 + 0.9559 = 0.998$$

$$\mathrm{b_{intercept}} = -7 \cdot 10^{-5} \cdot (174.947)^2 + 0.0012 \cdot 174.947 + 2.9877 = 1.055$$

If the systems display pressure is for example 50 bar then the calibrated pressure at display temperature of 175 °C is calculated form equation (27):

$$\mathrm{p_{calibrated}} = 0.998 \cdot 50 + 1.055 = 50.972\ \mathrm{bar}$$

7. Experimental procedure

Typically the components in the measurement system were polyethylene granules, liquid solvents, monomer and co-monomers. The polyethylene in this study were five different types of LLDPE. The solvent was a mixture of four different hydrocarbons. The monomer in this work was ethylene and the co-monomer was 1-octene. In this work, to some systems also nitrogen was added and it acted as an antisolvent. Used reagents and their purities are listed in Appendix 2.

In this work the solid polymer granules, the liquid mixture and gases were added to the cell to form mixtures. First the polymer granules were weighted directly to the cell with a scale balance (Mettler Toledo XP 2004S Comparator, max 2300 g, d=0.1 mg). Next a pressure test was conducted with nitrogen gas for ensuring that the cell does not leak. The liquid solution was prepared by weighting the right amounts of liquids with a scale (Precisa 410AM-FR; balance with resolution and accuracy of 0.0001 and ±0.002 g respectively). Before adding the liquid mixture to the cell, the mixture had to be evacuated for 10 minutes. The solution evacuation was performed with an air tight flask that was placed in an ice batch. The evacuated liquid was typically 20 times the needed mass for the measurements for minimizing the concentration changes. The concentration of the liquid solution was occasionally measured before and after evacuation with gas chromatography (GC Hawlett Packard HP 6850 series GC system). This was done to ensure that the concentration of the solution was not changed significantly during the evacuation procedure.

The cell was evacuated after the pressure test. Next the evacuated cell was weighted. Then the liquid solution was added through the upper line of the cell. The liquid addition could be determined by weighting (Mettler Toledo, XP 2004S Comparator, max 2300 g, d=0.1 mg). The liquid addition was facilitated by warming the liquid solution flask with warm air. The light warming generated a higher vapor pressure inside the flask and therefore the vapor pressure pushed the liquid to the cell through the lines. The liquid addition is presented in Figure 15. After the liquid addition, the cell was again weighted for determining the mass of the liquid mixture in the cell.

Figure 15. Addition of the liquid solution to the cell.

After the solid and liquid additions, the gases could be added. The cell was once more weighted with the same Mettler Toledo balance, and the gases were added through the upper valve of the cell directly from the gas cylinder. The gas line was flushed three times to remove air before the addition. The aim was to remove all the other gases in the lines, and to ensure that only the desired gases were added to the system. Now the cell was connected to the apparatus again and the lower lines were evacuated for ensuring that there were no gases in the hydraulic oil lines.

When conducting the test, a small nitrogen flow was directed into the oven in case of a leakage. The inert nitrogen addition minimized the risk of explosion and fire. The oven temperature was raised gradually 50 °C at the time to the temperature of 150 °C and simultaneously the pressure was raised slowly. The first measurement point was typically at 150 ° C, and then the temperature was raised usually 10 °C. When the temperature was raised the system was let to stabilize at one phase region 15-30 minutes so that the solution was homogeneous. The pressure could be lowered slowly after obtaining a homogenous solution and a stabile temperature.

When determining the cloud and bubble points the temperature was kept at constant level and the pressure of the system was changed. The temperature and

the pressure of the system was recorded when a cloud (LL) or bubble (VL, VLL) point was found. Also a picture was taken from the solution through a viewing window at the side of the oven. The bubble point was considered to be the pressure and temperature condition where small bubble formation was detected. The cloud point in this work was the point where the solution showed significant change in cloudiness. Small cloudiness could be present before the actual cloud point due to the polydispersity of the polymer, and due to the difficulties of detecting the small change by visually. Cameron, 2016 measured two cloud points, one where small cloudiness already could be detected and a second where the system was completely cloudy. In this work the cloud points are the first detected cloud points so called higher pressure cloud points.

The different stages for measuring the phase equilibria of polymer solutions in this work is represented in Figure 16. In the beginning (1) the cell was loaded with all the components (such as monomer, co-monomer, polymer granules and liquid solvents). The cell was first at room temperature and was not pressurized. The piston was in the lowest position and the volume of the cell was at its maximum. At this moment the polymer granules could be seen in the cell. Next (2) the cell was heated gradually. First from room temperature to 50 °C and then to 100 °C and 150 °C and so on. Moreover the pressure was raised in the cell by moving the piston up. When the piston was in the upper maximum position (3) all the gases were dissolved and only one liquid phase was present. The solution was clear at this stage and therefore the pressure was over the cloud and bubble point pressures.

When a clear solution was reached the pressure was lowered slowly until a bubble point (4) or a cloud point (5) was detected. Typically only bubble point can be determined at lower temperatures and a clear cloud point is visible at higher temperatures. Nevertheless a bubble point can be seen at temperatures where a cloud point is also present. The bubble points are challenging to determine from a cloudy solution. Therefore these bubble (VLL) points were seldom determined in this work because the main focus was in finding the cloud points.

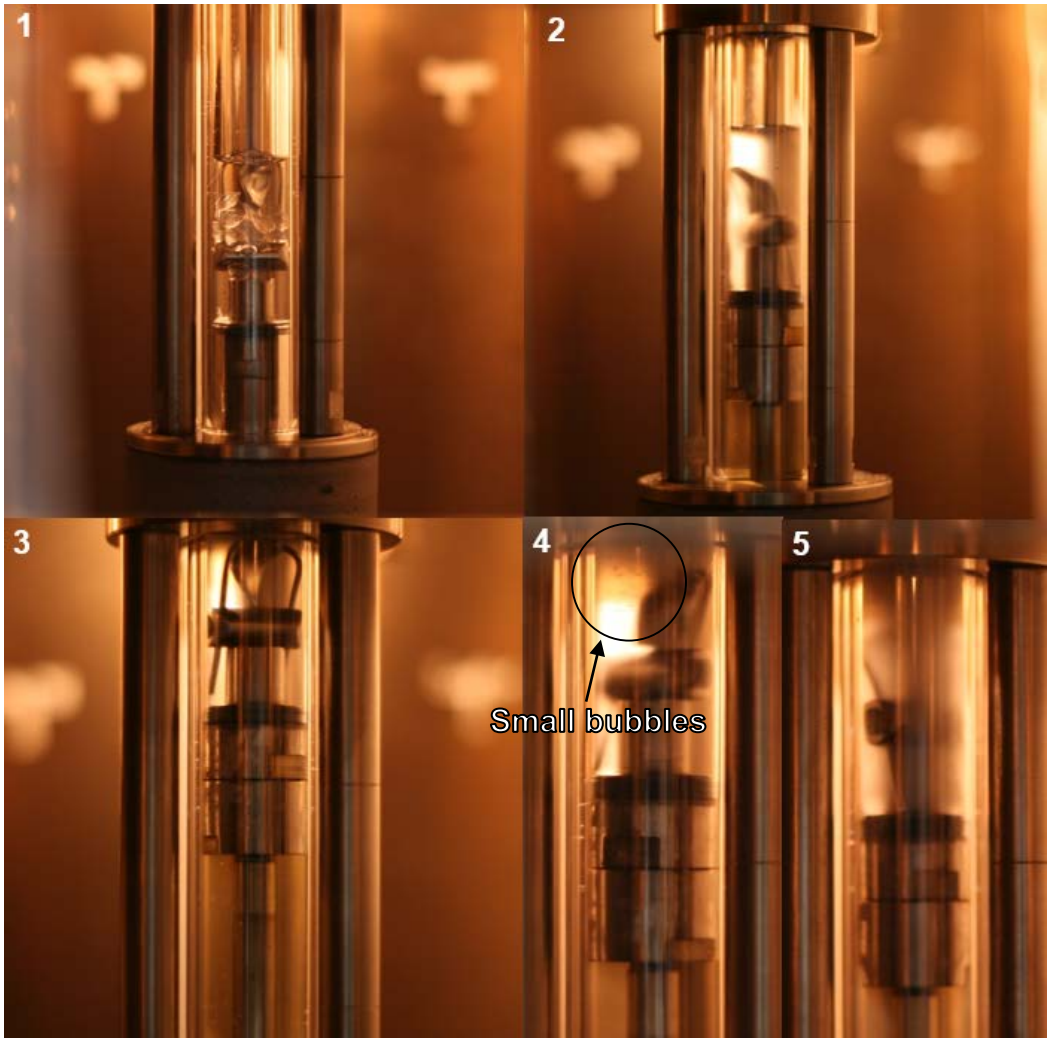

Figure 16. Different stages of polymer solution phase equilibria measurements. 1.The cell not heated or pressurized, 2.Cell heated to 150 °C (polymer melted) and partially pressurized (some of the gases dissolved to the solution, 3. Solution is clear and the pressure and temperature is above cloud point, 4. Bubble point, 5. Cloud point.

The measured polymer systems studied in this work were mixtures of LLDPE polymers, monomer, co-monomer, solvents, and in some cases also nitrogen was added. Five different polymer types were used in this study. Four of them were used for investigating how the polymer weight fraction in the system influences the phase equilibria. The polymers used in this study had different densities and melt flow indexes. The solvent was a mixture of four different components. The aim was to mimic the real process conditions.

8. Results

The cloud and bubble point data obtained in this work is presented in the following chapters. Moreover a polynomial model was fitted based on the measurements of this work. In this work 5 different polymers were investigated. These polymers are named as PE A, B, C, D and E. First the effect of small addition of nitrogen to the phase equilibria was studied. Next the influence of component weight fraction changes to the cloud and bubble points was studied. The concentrations of the measurement systems and the results for the cloud and bubble point measurements are presented in Appendix 3. In Appendix 3 the temperatures and pressures are the calibrated values.

8.1 The Influence of Nitrogen

Small amount of nitrogen was added to the polymer systems. The polymer systems in this work were multicomponent systems. The multicomponent systems consisted of polymer, ethylene, 1-octene and four different solvents. The added nitrogen amounts were relatively different. The nitrogen addition varied from 0.127 w% to 0.986 w% for different polymer systems. This was due to the difficulties in the gas addition procedure. The gas addition was small and the gases were added directly from the gas cylinder. Therefore it caused variations in the added gas amounts. The compositions of nitrogen added systems is collected to Table 2. The reference system is the non-nitrogen system and those compositions are collected to Table 3.

Table 2. The measured concentrations for the nitrogen addition experiments. Value x in the table is not publish.

Components	PE A (Exp. 3)	PE B (Exp. 5)	PE C (Exp. 9)	PE D (Exp. 13)	PE D (Exp. 14)	PE E (Exp. 18)
	w%	w%	w%	w%	w%	w%
Polymer	22.184	24.418	x	x	x	26.361
Ethylene	0.916	2.354	x	x	x	1.940
1-octene	x	x	x	x	x	x
Hexane mix solvent	x	x	x	x	x	x
Nitrogen	0.995	0.140	0.128	0.798	0.175	0.289

Table 3. The reference non-nitrogen system. Value x in the table is not publish.

Components	PE A (Exp. 2)	PE B (Exp. 4)	PE C (Exp. 8)	PE D (Exp. 12)	PE E (Exp. 18)
	w%	w%	w%	w%	w%
PE	19.789	23.903	x	x	23.237
Ethylene	0.909	1.987	x	x	1.715
1-octene	x	x	x	x	x
Hexane mix solvent	x	x	x	x	x

For PE A system the added nitrogen amount was 0.986 w%. The impact of the nitrogen addition to the cloud points of this system can be seen in Figure 17.

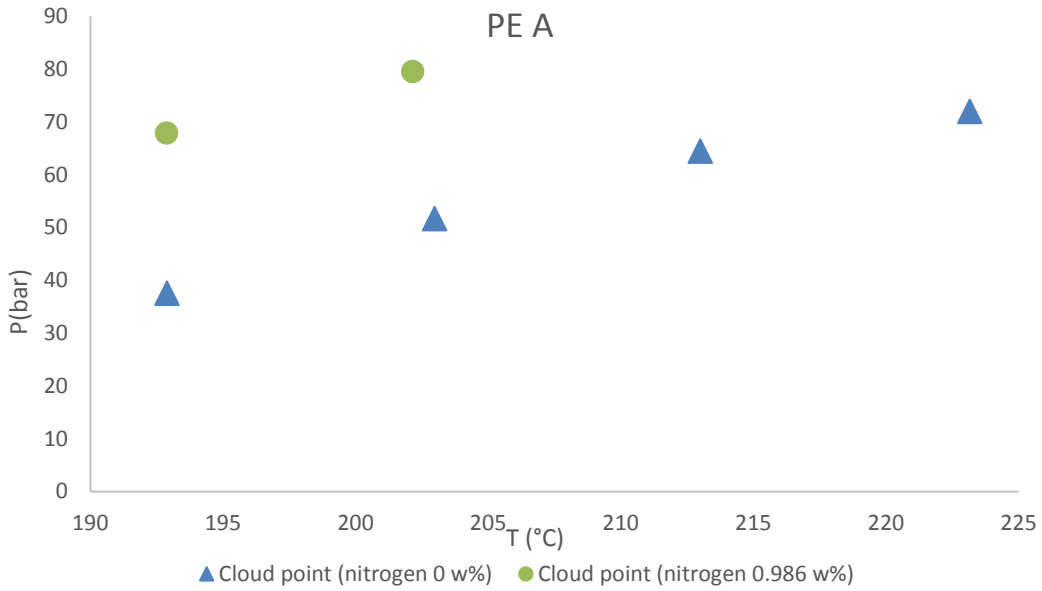

Figure 17. The influence of nitrogen to the cloud points for system of polymer A, monomer, co-monomer and solvents.

For PE B to E the influence of nitrogen addition to the cloud and bubble points are represented in Figures 18-21. For PE D two different nitrogen systems were studied, first with relatively same addition that was done for polymer B, C and E and second with a remarkably higher nitrogen addition.

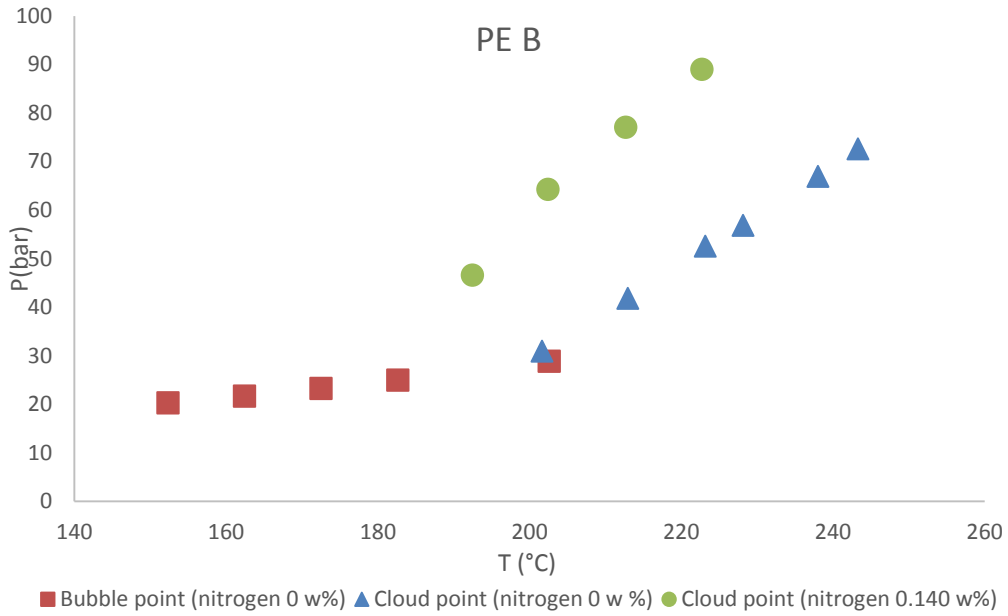

Figure 18.The influence of nitrogen to the cloud points for system of polymer B, monomer, co-monomer, solvents.

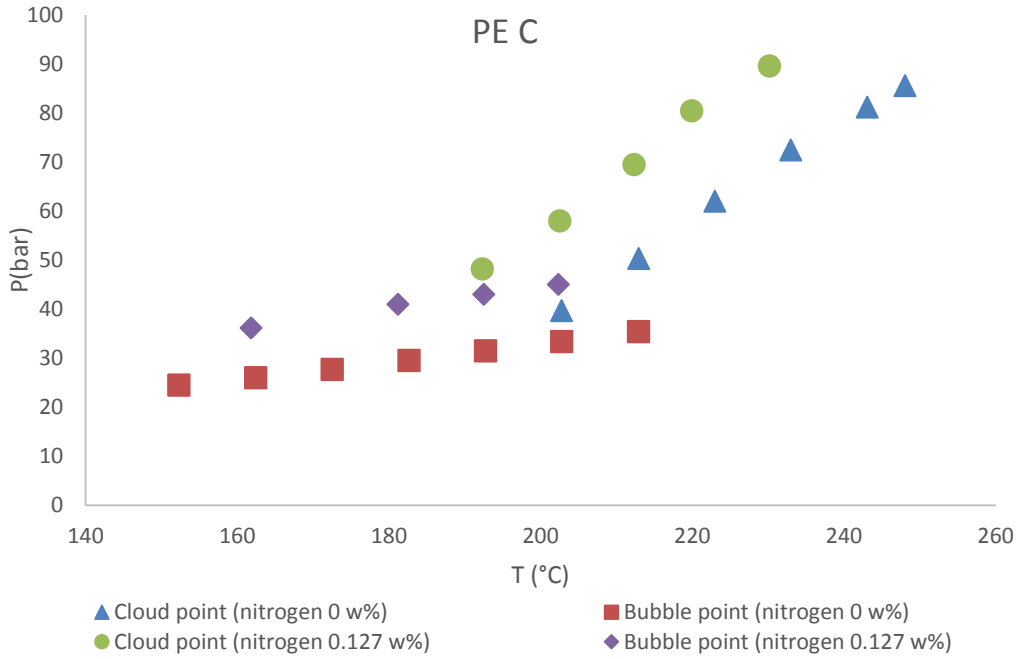

Figure 19. The influence of nitrogen to the cloud and bubble points for system of polymer C, monomer, co-monomer and solvents.

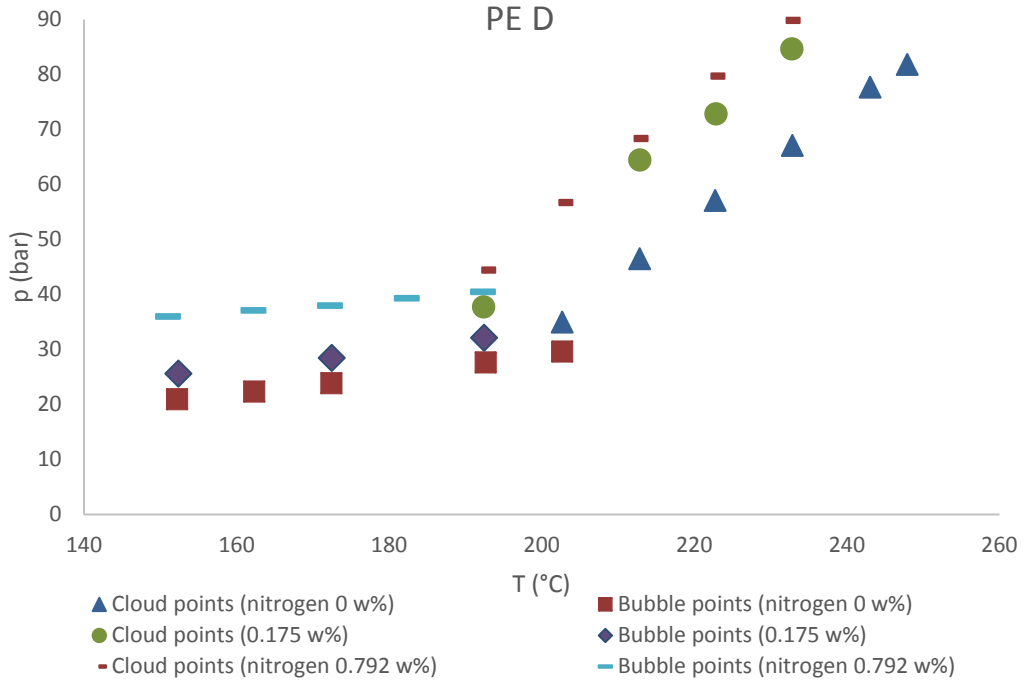

Figure 20. The influence of nitrogen to the cloud and bubble points for a system of polymer D, monomer, co-monomer, solvents.

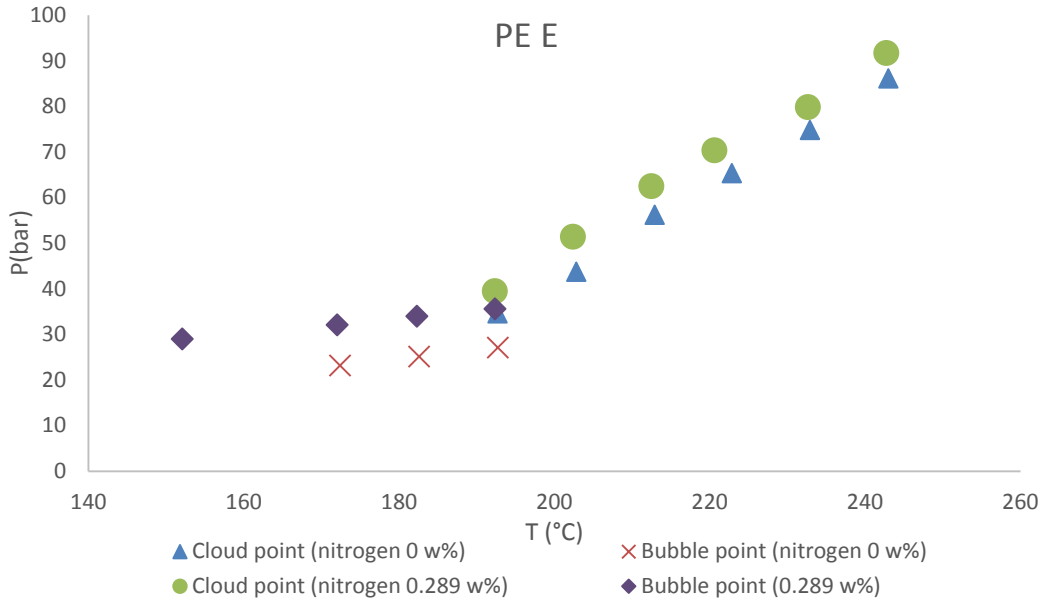

Figure 21. The influence of nitrogen to the cloud and bubble points for systems of polymer E, monomer, co-monomer and solvents.

The slope and intercept values for the trend lines in Figures 17-21 are collected to Table 4

Table 4. The slope and intercept values for the nitrogen addition experiments.

PE	N_2 (w-%)	Cloud point pressure form the measurements: $p_{CP}(bar)= a_{1c}\cdot T_{CP}(°C)+b_{1c}$		Bubble point pressure from the measurements $p_{BP}(bar)= a_{1b}\cdot T_{BP}(°C) +b_{1b}$	
		Slope (a_{1c})	Intercept (b_{1c})	Slope (a_{1b})	Intercept (a_{1b})
A (22.184 w%)	0.995	1.2565	-174.4091	-	-
B (24.418 w%)	0.140	1.3855	-218.2372	-	-
C (x w%)	0.128	1.1266	-168.9566	0.2186	1.0135
D (x w%)	0.175	1.1507	-182.6552	0.1847	-3.3922
D (x w%)	0.798	1.1395	-173.9441	0.1083	19.5270
E (26.361 w%)	0.289	1.0083	-153.0742	0.1643	4.0328

By comparing Figures 17-21 it can be see that nitrogen has different effects on different systems. The increases of bubble (150-200 °C) and cloud point pressures (200-250 °C) caused by nitrogen are calculated in Appendix 4. The increases of pressures are calculated with the slope and intercept values represented in Table 4 and 9 (presented in next chapter). The cloud or bubble point for specific polymer system can be calculated with equation (28) and with values in Table 4 and 9:

$$p = a_{1c,b} \cdot T + b_{1c,b} \quad (28)$$

Where p is the cloud or bubble point pressure depending on the table used (bar).
T is the temperature (°C)
$a_{1c,b}$ is the slope value dependent on the polymer amount (w%) and type (c=cloud point, b=bubble point).
$b_{1c,b}$ is the intercept value dependent on the polymer amount (w%) and type (c=cloud point, b=bubble point).

For example the cloud point for 23.9 w% of PE B and 0 w% of N_2 at 200 °C with Table 9 and equation 28:

$$p = 0.998 \ldots \cdot 200\ °C - 170.51 \ldots = 29.2\ bar$$

The cloud point for 24.418 w% of PE B and 0.140 w% of N_2 at 200 °C with Table 4 and equation 28:

$$\mathrm{p} = 1.386 \ldots 200\ ℃ - 218.23 \ldots = 58.9\ \mathrm{bar}$$

Therefore the pressure increase is 29.6 bar at temperature of 200 °C when 0.140 w% nitrogen is added to PE B system. The same way the increases are calculated for temperatures of 210, 220, 230, 240 and 250 °C for each polymer in Appendix 4. Also the average pressure increases are calculated, and for PE B it is 39.4 bar. The averages pressure increases are also collected to Table 5. The average cloud point temperature decreases are also shown in Table 6, and in this case the average temperatures decreases are calculated at pressures of 50, 60, 70, 80, 90,100 bar.

Table 5. The average increase of cloud and bubble point pressures with different nitrogen additions.

Polymers	Nitrogen addition (w-%)	Cloud point increase (bar)	Bubble point increase (bar)
PE A	0.986	32.3	-
PE B	0.140	39.4	-
PE C	0.127	21.4	10.9
PE D	0.175	17.4	4.3
PE D	0.792	23.6	13.8
PE E	0.289	6.3	9.1

Table 6. The average decrease of cloud point temperatures with different nitrogen additions.

Polymers	Nitrogen addition (w-%)	Cloud point decrease (°C)
PE A	0.986	25.4
PE B	0.140	34.3
PE C	0.127	20.1
PE D	0.175	16.8
PE D	0.792	22.2
PE E	0.289	6.1

The average cloud and bubble point increases with different nitrogen additions are collected to Table 5. For example it can be seen from Table 5 that in some cases even though relatively large amount of nitrogen was added, it had quite small effect

on the location of the cloud point line. The nitrogen addition for polymer A was 0.986 w% and the cloud point increase was approximately 32.3 bar. However for polymer B a nitrogen addition of only 0.140 w% increased the cloud point by 39.4 bar. When nitrogen was added to polymer systems C (nitrogen 0.127 w%) and D (nitrogen 0.175 w%) it had somewhat smaller effect than for polymer B. Only 21.4 bar and 17.4 bar rise as in Table 5. In addition the added nitrogen had only a relatively small effect to polymer E. By adding nitrogen of 0.289 w% the cloud points increased on average only 6.3 bar.

These differences can be explained by the different properties of the polymers. For example polymer E had probably lowest molar mass. Therefore it can be concluded that for low molar weight polymers the nitrogen effect is lower. It can also be detected from figures 19-21 that the nitrogen addition also rises the bubble point pressure.

For polymer D two amount nitrogen additions were made. The cloud points shifted to higher pressures, as expected, for the higher nitrogen amount. The difference of 0.175 w% and 0.792 w% nitrogen systems was however small. The difference in cloud point pressure of these two nitrogen systems was in average only approximately 5 bar as presented in Table 5. This small difference can indicate that the there was some errors in the determination of the added nitrogen of 0.792 w% and maybe a re-run of this experiment would be needed. This indicates that the multicomponent cloud point measurements are quite challenging to perform, and some repetition experiments are needed for ensuring that the cloud points are correct at least when adding small amount of gases.

Also other factors influence the cloud and bubble point values. For example all the other component weight fractions were not maintained constant from run to run. The polymer, monomer, co-monomer and solvent weight fractions changed when conducting these tests. The nitrogen addition was also very small and therefore the weighting of the nitrogen amount was quite difficult. However it is clear that the added nitrogen has a clear effect on the phase behavior of polymer systems.

8.2 The Effect of Component weight fraction

The effect of component weight fraction changes to the cloud and bubble point lines were studied for polymers B, C, D and E. The multicomponent polymer systems consisted of polymer, ethylene, 1-octene and four component solvent system. Typically three different weight fraction systems were studied for each polymer sample. The aim was to mimic the real process compositions. When the polymer amount was increased, the co-monomer and monomer weight fraction also increased. Therefore for higher polymer weight fraction systems the solvent weight fraction was lower than in low polymer weight fraction system. Still all the results are still represented with respect to the polymer amount in the figures. The compositions for lowest polymer amount systems are collected to Table 7 and for the highest polymer amount systems to Table 8. The third polymer amount systems are in previously shown Table 3.

Table 7. The compositions for the low polymer amount systems. Value x is not publish.

Components	PE B (Exp. 6) w%	PE C (Exp. 10) w%	PE D (Exp. 15) w%	PE E (Exp. 19) w%	PE E (Exp. 20) w%
PE	17.761	x	x	14.371	15.914
Ethylene	1.637	x	x	0.928	1.932
1-octene	x	x	x	x	x
Hexane mix solvent	x	x	x	x	x

Table 8. The compositions for the high polymer amount systems. Value x is not publish.

Components	PE B (Exp. 7) w%	PE D (Exp. 16) w%	PE E (Exp. 21) w%
PE	30.621	x	37.595
Ethylene	2.620	x	1.923
1-octene	x	x	x
Hexane mix solvent	x	x	x

For PE B system the influence of component weight fraction changes are presented in Figure 22. When the polymer, monomer and co-monmoer weight

fractions increase, the cloud point lines shifts to higher temperatures and lower pressures. However the bubble point lines do not shift significantly when the compositions were changed in the system. Therefore the bubble point line does not strongly depend on the polymer, co-monomer, and ethylene and probably is depended on the other factors, such as if there is any antisolvent gases present. When comparing the nitrogen addition test and the component weight fraction variation tests a difference can be seen. In Figures 19, 20 and 21 also the bubble point lines move significantly when nitrogen is added. In the non-nitrogen systems this effect could not be seen even though the other components weight fractions were changed.

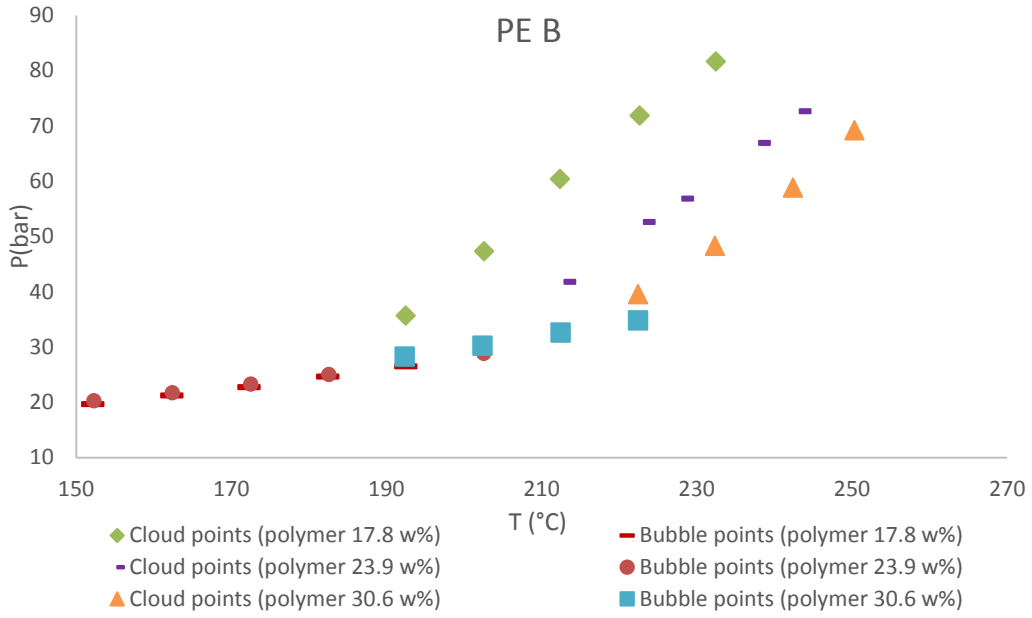

Figure 22. Cloud and bubble point pressures as a function of temperature for polymer B.

For PE C the viscosity was higher than for the other polymers due to the higher molecular weight. This caused mixing problems in high polymer amount experiments. Therefore the cloud and bubble points were measured with only two different polymer, co-monomer, ethylene and solvent weight fractions. The high polymer weight fraction experiments were done twice and both of them were unsuccessful. Even though the polymer amount was only 29 w% the experiment failed. For polymer C the effect of weight fraction changes are represented in

Figure 23. Figure 24 shows the effect of weight fraction changes for PE D solution system.

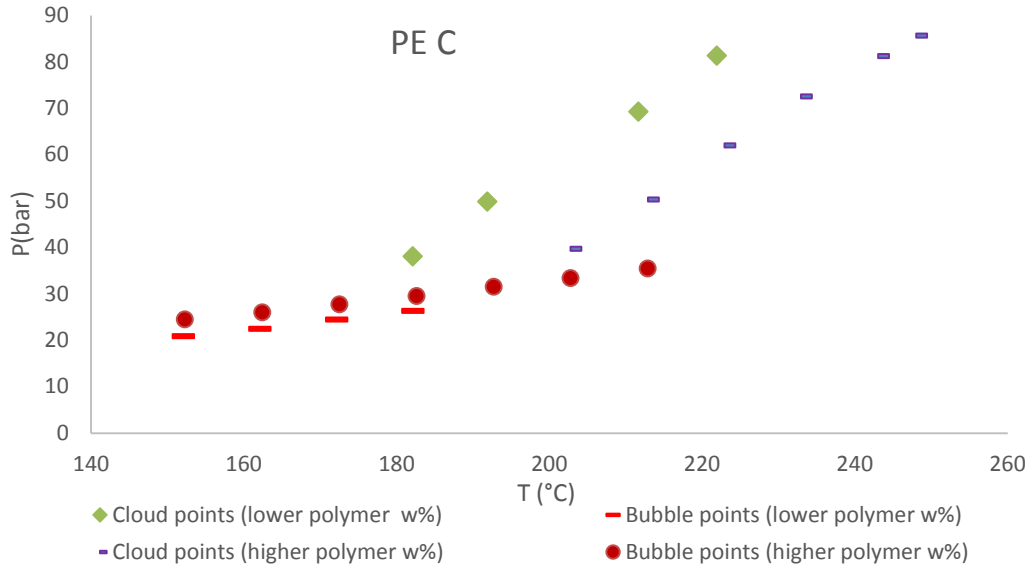

Figure 23. Cloud and bubble point pressures as a function of temperature for polymer C.

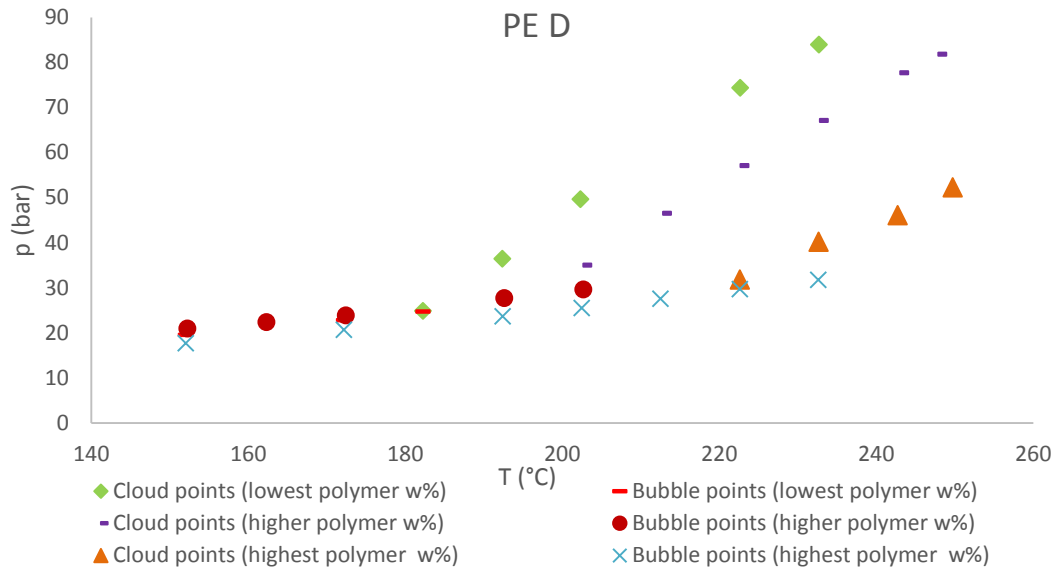

Figure 24. Cloud and bubble point pressures as a function of temperature for polymer D.

For PE E four different polymer weight fraction systems were measured. Two of them had similar polymer amounts (14.4 w% and 15.9 w%) and their cloud point

lines are relatively well aligned. Figure 25 shows the effect of weight fraction changes for PE E solution system. The slope and intercept values for the trend lines in figures 22-25 are collected to Table 9.

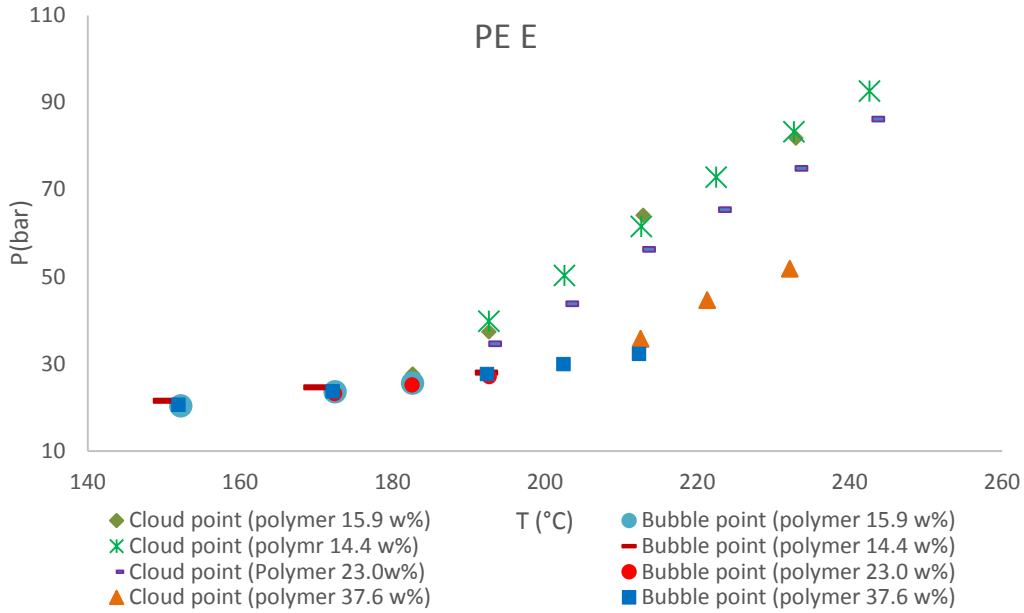

Figure 25. Cloud and bubble point pressures as a function of temperature for polymer E.

Table 9.The slope and intercept values for trend lines in figures 22-25.

	(w%)	(w%)	Cloud point pressure from measurements p(bar)=f(T(°C) (Figures 22-25): p_{CP}(bar)> p_{BP}(bar) T_{CP}(°C) < 250 °C		Bubble point pressure from the measurements (Figures 22-25): p(bar)=f(T(°C) 150 °C < T_{BP} < 250 °C	
			Slope (a_{1c})	Intercept (b_{1c})	Slope (a_{1b})	Intercept (a_{1b})
B	17.761	1.637	1.165	-188.054	0.169	-6.231
B	23.903	1.987	0.998	-170.51	0.171	-5.944
B	30.621	2.620	1.056	-196.096	0.221	-14.247
C	x	x	1.066	-155.5	0.183	-7.066
C	x	x	1.021	-166.65	0.181	-3.302
D	x	x	1.191	-192.114	0.169	-6.231
D	x	x	1.035	-174.105	0.173	-5.685
D	x	x	0.734	-131.21	0.168	-8.269
E	14.371	0.928	1.069	-165.952	0.152	-1.342
E	15.914	1.932	1.105	-174.043	0.169	-5.313
E	23.237	1.715	1.024	-162.952	0.193	-10.021
E	37.595	1.923	0.814	-136.591	0.193	-9.004

9. Modeling

With cloud point data obtained from the previously mentioned measurements a polynomial model was developed for interpolating and extrapolating the cloud points at different component weight fractions and temperatures. The use for this model for wide extrapolation is not recommended. Due to the previously presented multicomponent measurements the model cannot separate the effect of different component compositions to the cloud points. As told previously the performed measurements were done so that when the polymer weight fraction increased also the 1-octene (co-monomer) and ethylene (monomer) weight fractions increased. The cloud point pressures therefore can be presented in relation of polymer, monomer or co-monomer at given temperature, but then the cloud point pressure change is not due to the individual component weight fraction change, because the whole system compositions are changed.

First an example of the model performance is presented. In this example the cloud point pressure could be calculated at given polymer weight fraction and temperature. Also some estimation of the influence of the nitrogen addition was done with a so called nitrogen addition factor. Using these models it was possible to calculate the cloud point pressures with different component compositions and temperatures. The model was done for polymer B, C, D and E.

The model calculates the slope and intercept values that are dependent on the component composition and the polymer in the system. With these slope and intercept values it is possible to calculate the cloud point pressure at given temperature. The temperature dependence cloud point and bubble point pressure can be calculated with equation (28). By using the equations (29) and (30) the slope ($a_{1c,b}$) and intercept ($b_{1c,b}$) values can be calculated with the slope ($a_{S2c,b}$, $a_{l2c,b}$) and intercept ($b_{S2c,b}$, $b_{l2c,b}$) values in Table 10 and 11. The component amount can be therefore changed by implementing the component composition dependence equations (29) and (30) to temperature dependence equation (28).

The slope and intercept values in equation (28) can be calculated with values in Table 9 and 10 ($a_{S2c,b}$, $a_{l2c,b}$, $b_{S2c,b}$, $b_{l2c,b}$) and with the component amount as in equation (29) and (30):

$$a_{1c,b} = a_{S2c,b} \cdot \text{Component}(w\%) + b_{S2c,b} \quad (29)$$

$$b_{1c,b} = a_{I2c,b} \cdot \text{Component}(w\%) + b_{I2c,b} \quad (30)$$

Table 10. The cloud point model parameters for different polymers when polymer composition is changed.

PE	Cloud point pressure from model: p_{CP} (bar)=a_{1c}·T(°C)+b_{1c}			
	Slope (a_{1c}) a_{1c}= a_{S2c}·PE(w%)+b_{S2c}		Intercept (b_{1c}) b_{1c}= a_{I2c}·PE(w%)+b_{I2c}	
	a_{S2c}	b_{S2c}	a_{I2c}	b_{I2c}
B	-0.008	1.271	-0.675	-168.623
C	-0.005	1.145	-1.244	-135.976
D	-0.028	1.652	3.712	-254.096
E	-0.012	1.276	1.457	-193.082

Table 11. The Bubble point model parameters for different polymers when polymer composition is changed.

PE	Bubble point pressure from the model: P_{BP} (bar)=a_{1b}·T(°C)+b_{1b}			
	Slope (a_{1b}) a_{1b}= a_{S2b}·PE(w%)+b_{S2b}		Intercept (b_{1b}) b_{1b}= a_{I2b}·PE(w%)+b_{I2b}	
	a_{S2b} 10^{-3}	b_{S2b}	a_{I2b}	b_{I2b}
B	4.097	0.088	-0.633	6.442
C	-0.231	0.187	0.42	-13.657
D	-0.034	0.171	-0.117	-3.949
E	-1.509	0.142	-0.267	-0.331

The model performance is presented for the PE B system next. For example it would be desired to know the cloud point pressure for 10.0 w% polymer system at temperature of 250 °C and no measurements were done in these condition. First the equations (29) and (30) are used and values in Table 10:

$$a_{2c} = -0.008 \cdot 10.0w\% + 1.271 = 1.189$$

$$b_{2c} = -0.675 \cdot 10.0\ \text{w\%} - 168.623 = -175.373$$

Next the cloud point pressure at temperature of 250 °C is calculated with equation (28) and with the previously calculated values:

$$p_{cloud} = 1.189 \cdot 250\ °C - 175.373 = 121.804 \approx 121.8\ \text{bar}$$

The bubble point pressure at these conditions can be calculated with the same equations 28-30. The values for equation (29) and (30) are taken in this case from Table 11. The bubble point pressure is then 32.4 bar and is lower than the cloud point pressure.

The same calculation can be also done with relation of ethylene monomer or C8 co-monomer composition. Then the slope and intercept values are different than in Table 10 and 11, and these slope and intercept values for ethylene and co-monomer are collected to Appendix 5. The same equations (28), (29) and (30) can be also used for calculating the cloud or bubble point pressure at certain temperature and with some ethylene or co-monomer composition. Here again it has to be taken into account that when one component composition is changed also the other compositions change. The systems measured where always multicomponent systems, and due to this there cannot be separated the effect of individual component to the cloud points.

The previously shown calculation does not take into account the nitrogen addition. If it is desired to know approximately how the nitrogen effects to the cloud and bubble points Table 12 can be used. For PE D only the nitrogen addition of 0.175 w% was accounted to the Table 12.The nitrogen addition factor K_{CP} and K_{BP} are calculated with the values from Table 5. The nitrogen addition factor is calculated with equation (31):

$$K_{CP,BP} = \frac{\Delta p_{CP,BP}}{\Delta N_2} \tag{31}$$

Where $K_{CP,BP}$ is the nitrogen addition factor for either cloud points (CP) or bubble points (BP).

$\Delta p_{CP,BP}$ is the average cloud or bubble point increase with specific nitrogen addition and for specific polymer (bar).

ΔN_2 is the added nitrogen amount (w %).

Next for the PE B the nitrogen addition factor is calculated with the values in Table 5 and equation (31). The calculated nitrogen addition factors for all the polymers are also collected to Table 12.

$$K_{CP,BP} = \frac{39.4 \text{ bar}}{0.140 \text{ w\%}} = 281.429 \frac{\text{bar}}{N_2 \text{w\%}}$$

Table 12. Nitrogen addition factor for the cloud and bubble point pressures.

PE	Cloud point: K_{CP} (bar/N_2(w%))	Bubble point: K_{BP} (bar/N_2(w%))
B	281.429	-
C	168.504	85.827
D	99.429	24.571
E	21.799	31.488

Now the cloud/bubble point pressure with nitrogen addition can be estimated with equation (32):

$$p_{N2} = K_{CP,BP} \cdot N_2(w\%) + p_{CP,BP} \quad (32)$$

Where p_{N2} is the cloud or bubble point pressure with nitrogen (bar).

$K_{CP,BP}$ is the nitrogen addition factor.

$p_{CP,BP}$ is the cloud or bubble point pressure without nitrogen (bar).

Next and example is presented. If to the same PE B (10 w%, 250 °C, 121.8 bar) system presented previously, a nitrogen addition of 0.1 w% is done. Then the new cloud point pressure would be with equation (32):

$$p_{N2} = 281.429 \frac{\text{bar}}{N_2 w\%} \cdot 0.1\ w\% + 121.8\ \text{bar} = 149.9\ \text{bar}$$

Therefore for this PE B system the cloud point pressure rose from 121.8 bar to 149.9 bar with nitrogen addition of 0.1 w%.

This calculation does not take into account the temperature. It can be seen in Appendix 4 that at lower temperatures the same nitrogen additions has a smaller effect to the cloud and bubble point pressures. Table 12 is created with the average values. Note that Table 12 is only valid within narrow range of PE concentrations. The nitrogen additions where done only for systems where the polymer amount was between of 22.105 to 26.361 w% as can be seen in Appendix 3 and Table 2. Also this calculations are most likely valid to maximum nitrogen addition of 0.2 w%. Next presented figures and results are only for non-nitrogen systems.

The performance of the polymer composition model was evaluated by comparing the cloud point pressures of the model to the measured cloud point pressures. The difference of the measured and calculated pressure is presented as a function of temperature in Figures 26 to 29. The absolute average deviation (AAD, equation 33) and the relative absolute average deviation (RAAD, equation 34) for each polymer type and weight present are presented in Table 13. The detailed calculation results with equations (33) and (34) are also collected to Appendix 6.

$$\text{AAD (bar)} = \frac{1}{n}\sum_i^n \left| p_{\text{measured,i}} - p_{\text{model,i}} \right| \quad (33)$$

$$\text{RAAD (\%)} = \frac{1}{n}\sum_i^n \left(\frac{\left| p_{\text{measured,i}} - p_{\text{model,i}} \right|}{p_{\text{measured,i}}} \right) . 100\% \quad (34)$$

Where $p_{measured}$ is the measured pressure (bar)

p_{model} is the pressure calculated with the model at the experiment conditions (bar)

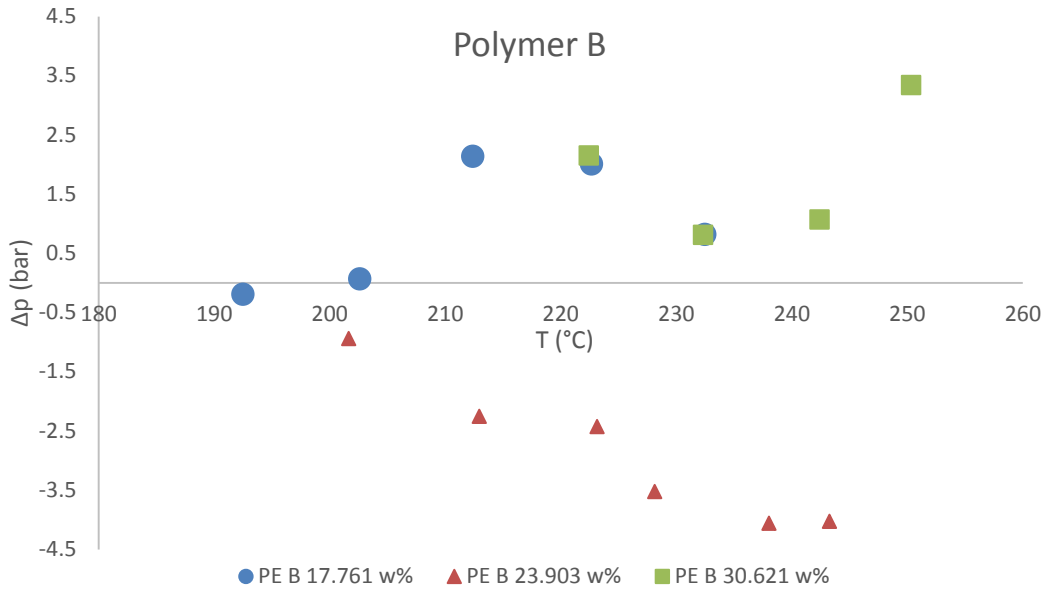

Figure 26. The difference of the measured cloud point pressure and calculated cloud point pressure as a function of temperature for polymer B system. $\Delta p = p_{measured} - p_{model}$.

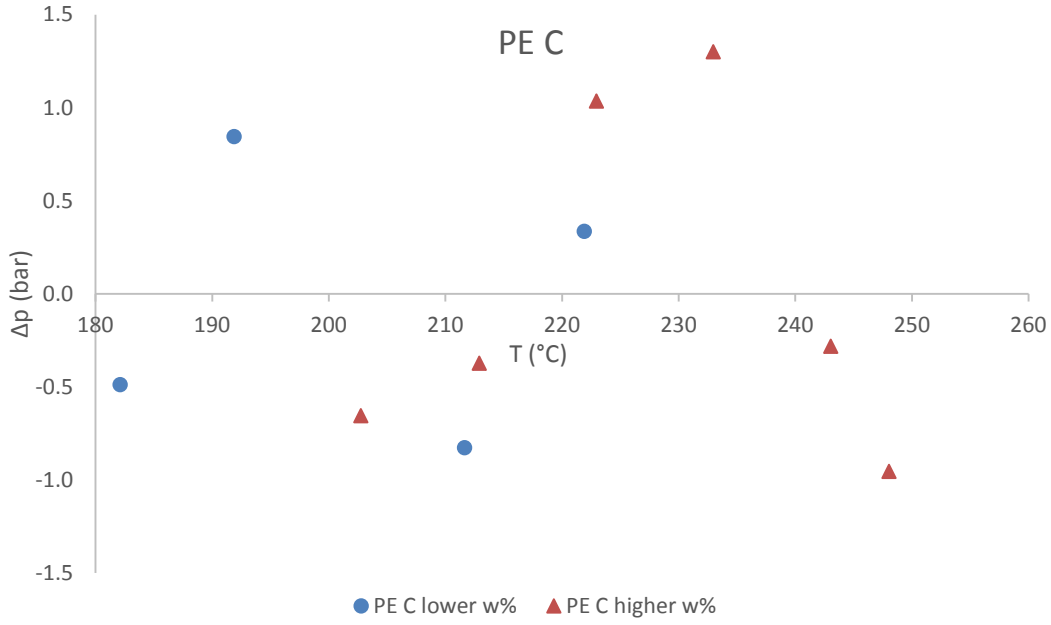

Figure 27. The difference of the measured cloud point pressure and calculated cloud point pressure as a function of temperature for polymer C system. $\Delta p = p_{measured} - p_{model}$.

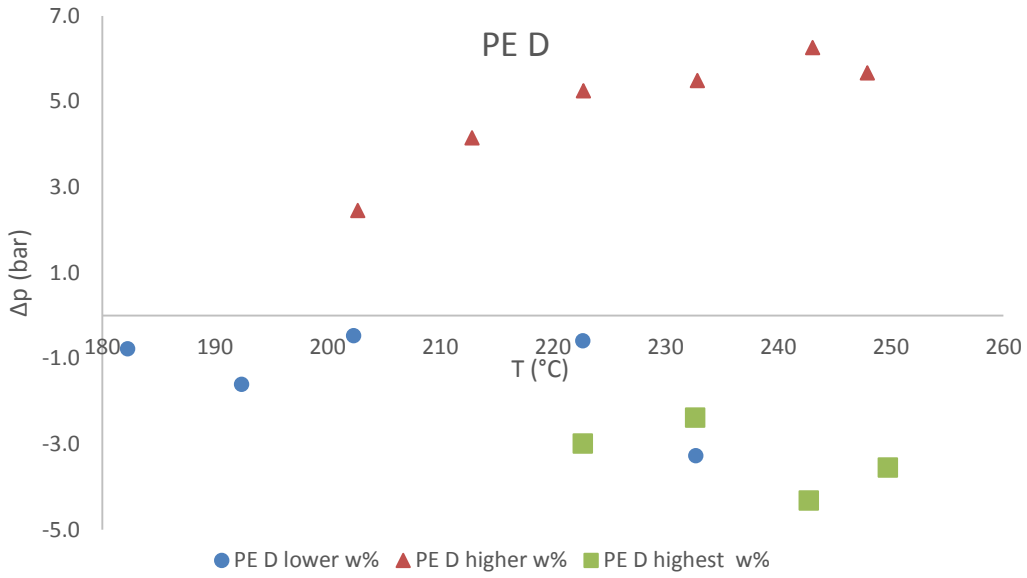

Figure 28. The difference of the measured cloud point pressure and calculated cloud point pressure as a function of temperature for polymer D system. $\Delta p = p_{measured} - p_{model}$.

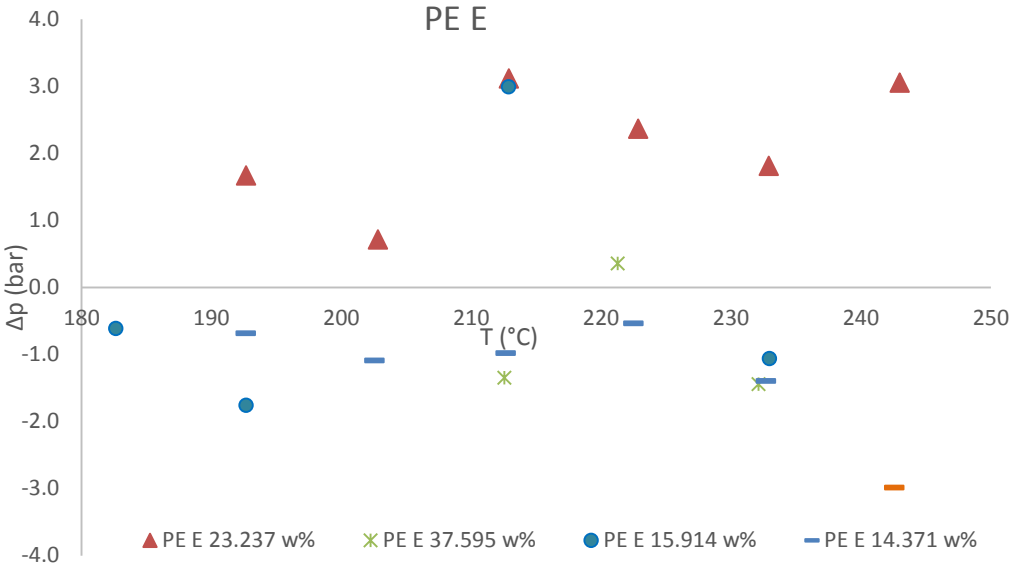

Figure 29. The difference of the measured cloud point pressure and calculated cloud point pressure as a function of temperature for polymer E system. $\Delta p = p_{measured} - p_{model}$.

Table 13. The accuracy of the polymer weight fraction model. The calculated absolute average deviation and the relative absolute average deviation for each polymer type and weight present.

Measurements	Cloud point pressure (bar)		Bubble point Pressure (bar)	
	Absolute average deviation (bar)	Relative absolute average deviation (%)	Absolute average deviation (bar)	Relative absolute average deviation (%)
PE B 23.903 w%	2.872	5.1	-	-
PE B 17.761 w%	1.046	1.6	-	-
PE B 30.6121 w%	1.844	3.4	-	-
PE C low w%	0.767	1.2	0.113	0.4
PE C higher w%	0.624	1.1	0.085	0.4
PE D higher w%	4.336	8.3	1.638	7.4
PE D low w%	0.859	2.3	0.645	2.9
PE D highest w%	3.310	7.9	0.803	3.4
Test 17, PE E 22.237 w%	2.122	3.6	0.664	2.7
Test 19, PE E 14.371 w%	1.277	1.8	0.881	3.7
Test 20, PE E 15.914 w%	1.604	3.2	0.279	1.2
Test 21, PE E 37.595 w%	1.049	2.4	0.401	1.8

The measured points and their equivalent models are presented by graphs in Appendix 7. The model presents quite well the behavior of the measured points. The difference is probably a result of the assumption that the cloud point lines are linear. However the cloud and bubble points have truly a somewhat curved shape. Also even if the measured results are quite consistent there are still some small deviations in the measurement points and this causes also errors to the model. The isothermal cloud point behavior of the polymers B, C, D and E is also presented in Appendix 7. The figures show that by increasing the composition amounts at constant temperature the cloud point pressure increases. Also the isothermal cloud point lines move to higher cloud point pressures when increasing the temperature.

10. Discussion

10.1 Comparison to the literature

The measured LLDPE polymers were unknown and no actual comparison of the measurement results to the literature values can be done. However similar behavior of the polymer systems is found also in this work as in the literature. First in this work a clear shift of the cloud and bubble point behavior was observed when nitrogen was added as shown previously in Figures 17-21. Tork et al., 1999b, modeled the behavior of HDPE + n-hexane + nitrogen system and the results are shown in Figure 30. This figure also shows significant influence of the nitrogen addition to the cloud and bubble points. Nitrogen therefore acts as a strong antisolvent even if used in small amounts. For example in this work for PE C the average increase of cloud point pressure at constant temperature was 21.4 bar when 0.127 w% of nitrogen was added. For bubble points the increase was 10.9 bar (Table 5).

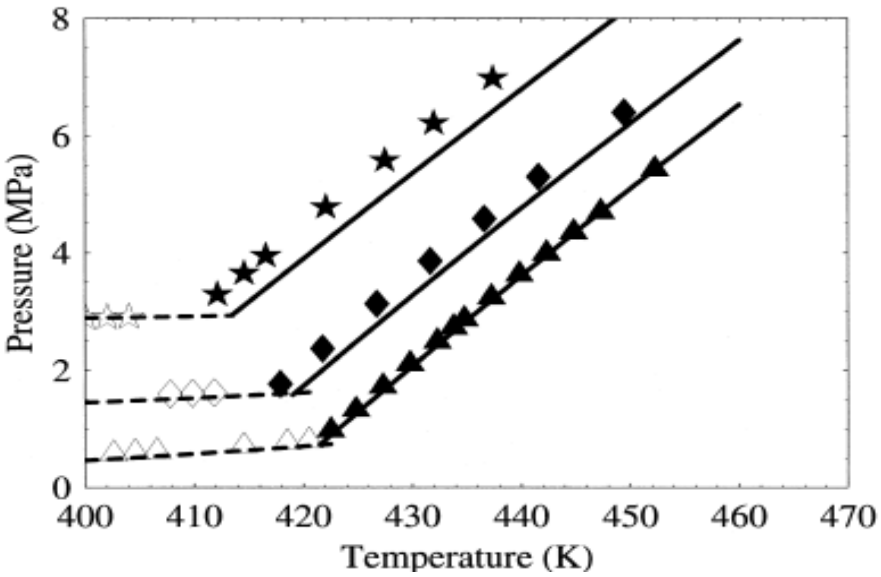

Figure 30. HDPE + n-hexane + nitrogen system. Lowest line (▲) is the 0 w % nitrogen system, the second (♦) is 0.5 w % nitrogen system and the highest line (marked as star) is the 1.2 w % nitrogen system. Lines are the SWP EOS prediction. The unfilled marks are the VLE points and the filled marks are the LCST points. (Tork *et al.*, 1999b)

The influence of the polymer weight fraction to the phase equilibria has been shown also by de Loos *et al.*, 1996 and Nagy et al., 2006. Next in Figures 31 and 32 is the LLDPE + n-hexane system behavior is illustrated when the polymer mass fraction changes. From these figures it can be seen that by increasing the polymer amount the cloud point pressure is decreased at isothermal conditions. The same phenomenon was also observed in this work and the same trend is illustrated in Figures 31 and 32. In this work the polymer weight fractions were always more than 10 w%, therefore the cloud point behavior was dissimilar in comparison to Figure 31. In Figure 31 at polymer weight fraction of lower than 5 w% the cloud point line curves strongly. Above 5 w% the cloud point line is quite linear. Therefore in this work the assumption of linear behavior of the phase transition is valid.

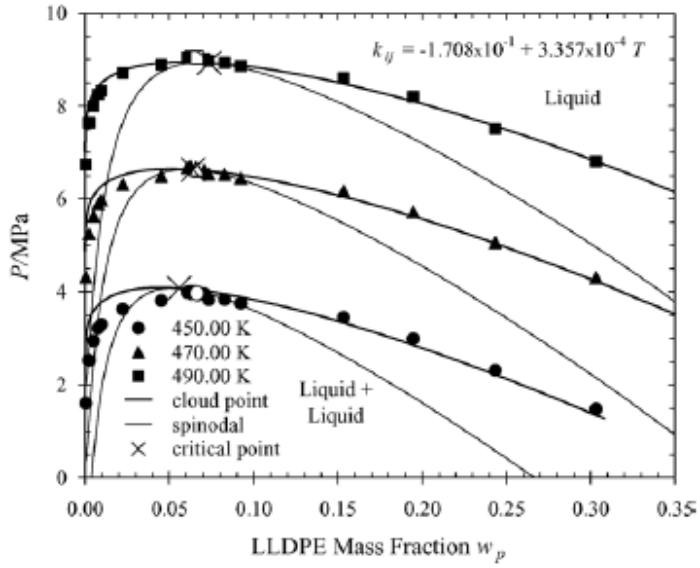

Figure 31. The isothermal behavior of LLDPE + n-hexane system. Measurement points and a modified Sanchez-Lacombe fit. (Nagy *et al.*, 2006).

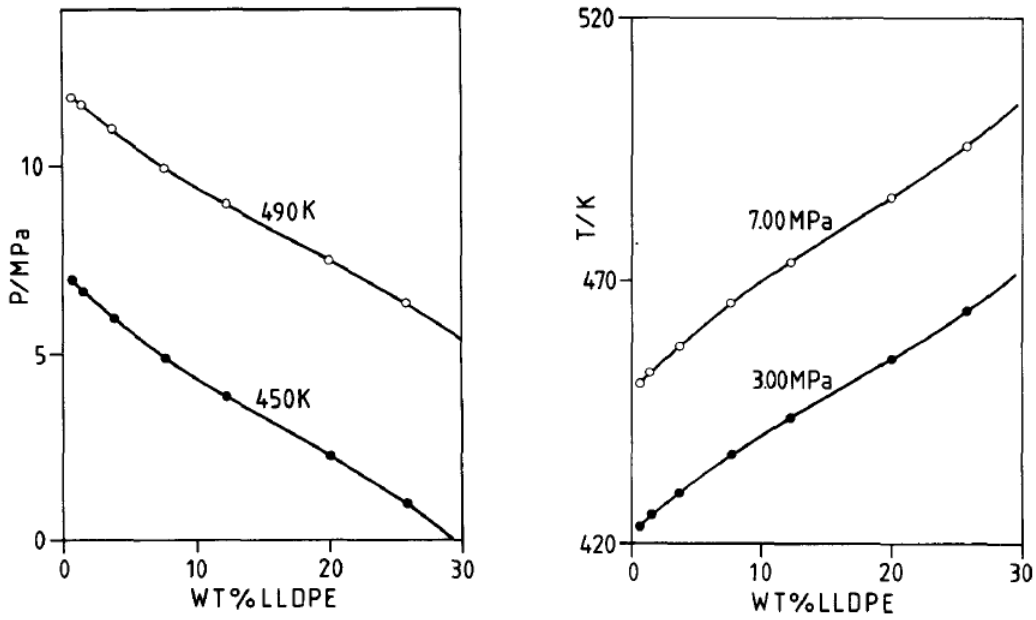

Figure 32. The isothermal and isobaric behavior of LLDPE + n-hexane system (de Loos et al., 1996).

In the beginning of this study one binary PE A + n-hexane system was measured (Appendix 3, experiment 1). Cameron, 2016 also made several of these binary system measurements with the same polymers. In Figure 33 is illustrated how the measurement results obtained in this work correlates with the earlier data points by Cameron. Figure 33 also shows the influence of the polymer weight fraction to the cloud points at isothermal conditions. The points in this figure are plotted with the calculated slope and intercept values from the measurements. Figure 33 shows that the binary system studied in this work fits relatively well with the earlier data points.

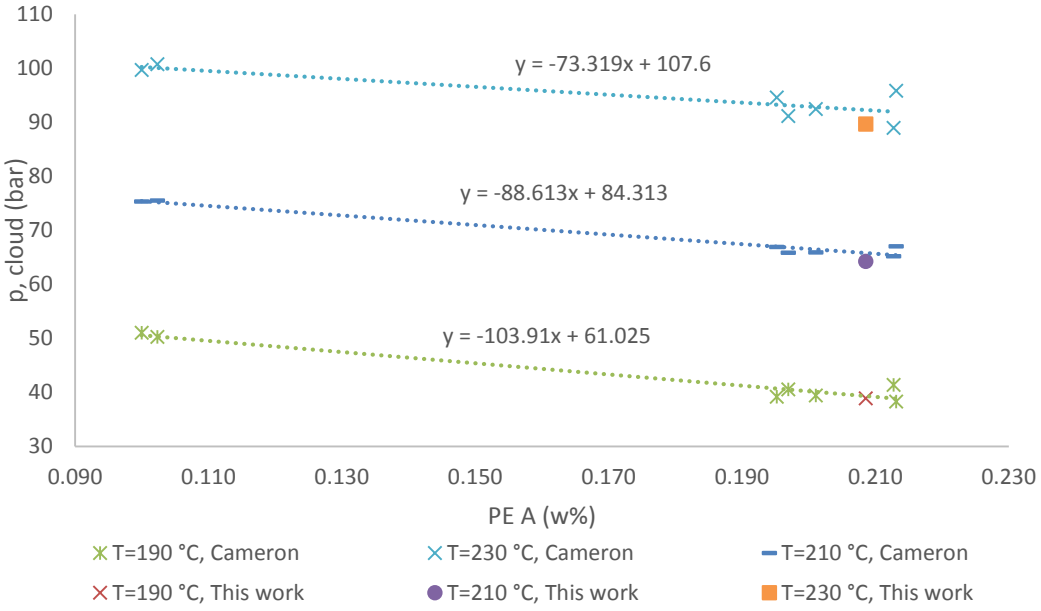

Figure 33. Comparison of the measurement points obtained in this work related to the previously made measurement with the same system PE A + n-hexane system by Cameron, 2016.

Cameron also investigated the multicomponent polymer phase behavior for system of polymer, ethylene, butane/1-butene and hexane mix solvent. The mixtures were quite similar as in this work but the used co-monomer was different. Cameron used butane/1-butene as comonomers and in this work the co-monomer was a 1-octene. Next the effect of the co-monomer is investigated in figures 34 and 35 for polymers D and E. The polymer amount for 1-octene system was set as equal as in the work of Cameron with the polynomial model. The C4 data presented in figures 34 and 35 is obtained from the thesis work of Cameron, 2016. The co-monomer influence comparison is not done for polymers B and C. This is due to the difference with the repetition tests of Cameron for PE B and C. Therefore it was difficult to select data set for this comparison.

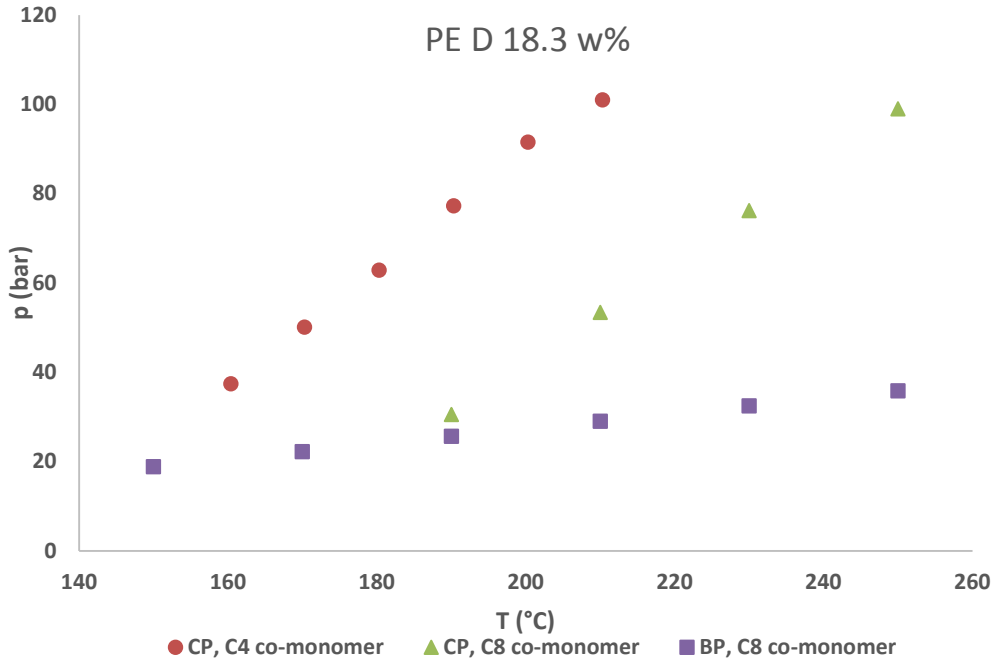

Figure 34. The effect of co-monomers to the phase equilibria to the polymer PE D system.

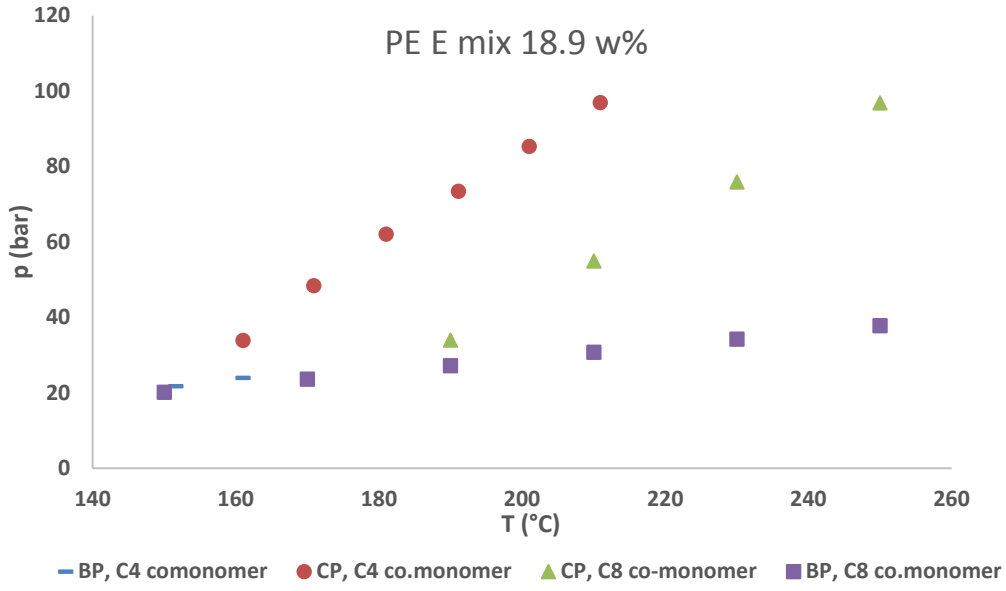

Figure 35. The effect of co-monomers to the phase equilibria to the polymer PE E system.

The slope and intercept values from figures 34 and 35 are collected to Table 14.

Table 14. The slope and intercept values for the PE D and Polymers with different co-monomers.

Polymer	Co-monomer	Cloud point		Bubble point	
		Slope	Intercept	Slope	Intercept
PE D	butane/1-butene (C4)	1.306	-171.968	-	-
PE D	1-octene (C8)	1.141	-186.226	0.170	-6.086
PE E	butane/1-butene (C4)	1.251	-166.035	0.242	-14.983
PE E	1-octene (C8)	1.075	-177.832	0.160	-3.904

For PE D solution, the switch of co-monomer changes the cloud point pressure, depending on the temperature, 45-55 bar (190-250 °C). For polymer E the change is, depending on the temperature, 37-50 bar (190-250 °C). These values can be calculated with the slope and intercept values from Table 14. According to the Figures 34 and 35 the change of 1-octene to butane/1-butene shifts the cloud points to higher pressures and lower temperatures. Bubble point line does not shift according to Figure 35. The same type of observation was done for example also by de Loos *et al*., 1996 as in Figure 36 for binary systems.

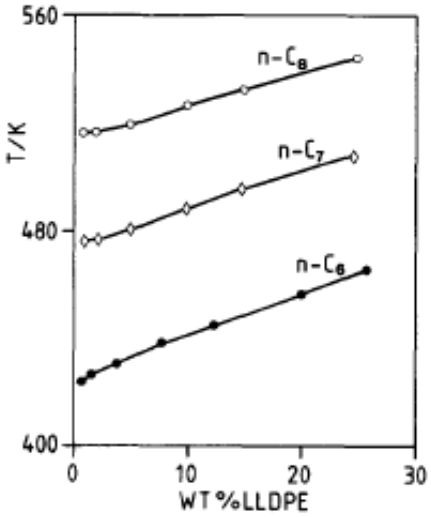

Figure 36. The isobaric cloud point curve for LLDPE + n-alkanes. Pressure is 30 bar.

10.2 Source of errors and challenges in the measurements

The most significant source of error in this work was considered to be the determination of the cloud and bubble points visually. The phase transitions were

observed through a window at the side of the oven. The window caused some visual difficulties. However the foremost problem was the lightning in the oven. Only one simple oven lamp was inside the roof of the oven, and the lightning properties of the lamp were quite poor. Also the lamp was placed to the opposite side of the viewing window, behind the cell.

The visual determination depends also on the person conducting the measurements. The cloud points were quite difficult to determine due to the constant increase of cloudiness in the solution when the pressure decreased. Some solutions were already originally quite clouded and the pressure addition did not improve the situation. One possibility is that some air could have remained in the cell and caused this problem. Again the high polymer weight fraction measurements were also quite clouded, and then the high polymer amount caused this.

The high polymer amount test caused some problems in the mixing of the solution. For PE C it was not possible to do any high polymer amount tests. Even when the polymer amount was lowered to 29 w% the test failed. The magnetic stirrer could not move due to the poorly dissolved polymer. The PE C had probably a very high molecular weight compared to the other polymers, and therefore was highly viscous. This probably caused these mixing problems. For the other polymers the high polymer amount did not cause so several problems, but the mixing was not as good as in the lower polymer amount tests. The stirring rate was kept at lower rate in these tests due to the viscosity of the solution, and due to the magnetic coupling of the stirrer.

Other sources of errors in this work came from the pressure and temperature measurements. The pressure was measured directly inside the cell. The pressure instrument was temperature dependent and therefore a pressure calibration function was generated. Previously in Table 1 the pressure calibration function was tested. The maximum difference of the calibrated pressure to the real pressure value was calculated to be 0.021 bar. Therefore probably only minor errors come from the pressure measurements. However the temperature measurement was done from the cap of the cell and not directly from the measurement solution.

Therefore some temperature differences between the cap and the measurement solution might have been present.

One problem with these multicomponent mixture measurements was the changing component masses. It was impossible to repeat the measurements with similar weight fractions due to the many variables. The polymers were added directly to the cell and simultaneously weighted. However the liquid additions had to be assessed first visually and after that the addition was determined by weighting. The liquid addition was therefore seldomly exactly as planned. Some variations occurred also with the liquid solution weighting, and also the evacuation procedure changed the liquid solutions weight fractions in a small degree. For some of the solutions a gas chromatography analysis was performed. Table 15 presents the composition weight fraction changes caused by evacuating of the six component liquid solution. Table 15 shows that the weight fraction of the light components decrease and the weight fraction of the heavy component increase. The calculations were done with equation 35:

$$\Delta(\mathrm{w}\%) = \mathrm{A}_{\mathrm{evacuated}}(\%) - \mathrm{A}_{\mathrm{Not\_evacuated}}(\%) \qquad (35)$$

Where $A_{evacuated}$ is the area of the gas chromatography peak(%) measured from evacuated solution.

$A_{not\_evacuated}$ is the area of the gas chromatography peak (%) measured from not evacuated solution.

Table 15. The gas chromatography analysis. Difference of the evacuated and not evacuated solution.

GC, solution	Test 2	Test 3	Test 5	Test 8	Test 12	Average
	Δ(w%)	Δ(w%)	Δ(w%)	Δ(w%)	Δ(w%)	Δ(w%)
Solvent component 1	-0.976	-1.014	-0.999	-1.264	-1.118	-1.074
Solvent component 2	-0.720	-0.622	-0.786	-1.001	-0.821	-0.790
n-Hexane	0.268	0.268	-0.984	-1.384	-0.736	-0.514
Solvent component 3	0.233	0.231	-0.276	-0.382	-0.164	-0.072
1-Octene	0.613	0.576	2.130	2.716	1.688	1.545

The most significant challenge though was the addition of the gases. Especially the nitrogen addition was so small that the error in weighting was probably very

high. The nitrogen addition varied from 0.016-0.00189 g and the scales accuracy was informed to be 0.0001 g. Moreover the display reading of the scale varied during the weighting process of ±0.0005 g. In the future it would be recommended that the gas addition process would be changed to some volume based method, especially if the gas additions are really small. This way the repetition of the tests would improve. The addition directly from the gas cylinder was quite difficult. The operator has to practically guess the outlet pressure of the pressure reduction valve and then determine the added gas by weighting. If too much gas went to the cell nothing could be done. The operator learns approximately the right pressures to certain mass additions by experience.

There were several problems with the measurement apparatus. At least eight tests had to be aborted due to hydraulic oil leakages. The oil leakages were the main problems in the beginning. Typically this caused loosing of two work days. The two seals inside the piston had to be changed by a workshop technician. Another problem was the wearing of threads in the upper part of the cell. The three pillars had to be changed so that the cap could be installed. The material for the pillars had to be ordered and the shipping took some time.

In the end the most significant problems were caused by the valve and the upper line. The upper line of the cell was blocked at least three times and the whole line was changed. The valve had some leaking problems that were found during the pressure tests. The valve was opened couple of times and cleaned by a technician. In addition three tests failed due to the mixing problems with PE C mentioned previously.

11. Summary and recommendations for the future

The aim of this work was to measure the cloud and bubble points of LLDPE, monomer, co-monomer and solvent systems. Five different polymers were under investigation. Moreover the influence of nitrogen addition to systems was investigated. A polynomial model was formed based on the composition weight fraction results. The objective was to imitate the polymer systems that are processed in industry, and to obtain information on these systems for process operation.

The literature part of this thesis was focused on different polyethylene processes, and why the understanding of these processes is important. The phase separation of polymer systems can happen in two ways which are the UCST and LCST curves (Kontogeorgis *et al.*, 1995). In this work the LCST points were measured. LCST phase separation occurred then by heating at high temperatures (Kontogeorgis *et al.*, 1995).

The LLDPE process is typically carried out by solution polymerization (de Loos *et al.,* 1996). In solution polymerization it is important to keep the solution in the one phase region. This is important to achieve successful polymerization and also for kinetic reasons (de Loos *et al.*, 1996). The polymerization can be controlled better in the one phase region (Folie *et al.*, 1996). The formation of the second phase can cause film formation to the inner walls of the reactor. This reduces the heat transfer efficiency and a purification of the reactor is needed (Folie *et al.*, 1996).

The phase equilibria of polymer systems are typically measured with variable volume optical batch cell by varying the pressure at constant temperature and composition (Folie *et al.*, 1996). The phase boundaries are detected either by the light scattering method or visually (Folie *et al.*, 1996). In this work the phase transitions were detected only visually. The visual determination method was found to be quite challenging. Due to the difficulty to measure the phase equilibria of polymer systems in a wide range of temperatures, pressures and compositions different thermodynamic models have been created (Liu *et al.*, 1980). In this work some of these models were represented and it was concluded that the most

interesting models today are those based on theoretical statistical mechanic such as SAFT and PHSC models.

In the experimental part the measurement apparatus and the experimental procedure was presented. The aim was to study the effect of nitrogen and varying polymer compositions to the phase transitions. It was found that nitrogen gas has a clear effect on the cloud and bubble points of the systems studied. The effect was different for each polymer system and the reason for this was the different properties of the polymer and varying compositions in the systems. Nevertheless in all systems the cloud points shifted to higher pressures and lower temperatures when nitrogen was added. Also the bubble point line shifted significantly to higher pressures by nitrogen addition.

The effect of component concentrations were studied for four different polymers. It was detected that the component amount in the systems had a clear influence on the cloud points pressures and temperatures. By increasing the component amount in the system the cloud point lines shifted to lower pressures and higher temperatures. However in these studies the bubble points did not shift as much as the cloud points by changing the component amount.

In the polynomial model the cloud and bubble point pressures could be calculated with different temperatures and component compositions. The difference of the measurement results and the model was illustrated with several graphs. The major drawback with the model is that it assumes that the cloud point lines are linear. Also in the measurements there were challenges to keep the compositions as desired due to the composition adding procedure. It would be recommended to improve the addition procedure to some volumetric based system.

In this work a thermodynamic model such as PC-SAFT could not be utilized due to the unknown polymers. Also for determining the influence of the different individual components to the phase boundaries, additional experiments should be made. In this work the systems were always multicomponent systems, and the measurements were done so that when the polymer composition increased also the monomer and co-monomer composition also increased. For example if it would be desired to know only the influence ethylene composition changes, then the co-

monomer and polymer compositions should be maintained constant in the measurements. The influence of co-monomer should be studied with a systems where the polymer and ethylene amounts are constant and co-monomer and solvent compositions are changed.

There could probably be found that ethylene and 1-octene has opposite influences. The literature results presented in this work (de loos *et al.*, 1996, Chen *et al.* 1992a. Nagy *et al.*, 2006) indicate that the ethylene shifts the cloud points to higher pressures and lower temperatures and C8 hydrogarbons (such as 1-octene) would shift the cloud points to lower pressures and higher temperatures. By these measurements the influence of ethylene and 1-octene cloud also be included in the polynomial model. Now the model follows the compositions in the reactor.

Nevertheless the effect of nitrogen addition and polymer composition changes are in line with the literature results. According to literature nitrogen acts as a strong antisolvent. Also by increasing the polymer amount the polymer solubility to the liquid phase increases. Also there was a clear shift of the cloud points when the co-monomer was changed. No quantitative comparison to the literature could not be done. This was due to the unknown polymer and also no similar multicomponent system studies could not be found in literature. Typically the phase equilibria measurements are done in literature for maximum of three component. Still the behavior of the systems were quite consistent with literature.

12. References

Brydson, J., *Plastics Materials (7th Edition),* Butterworth-Heineman, Oxford 1999, ss. 206-212.

Bergstra, M.F., *Catalytic Ethylene Polymerization,* The Netherlands 2004, ss. 3-4 http://doc.utwente.nl/48232/1/Thesis_Bergstra.pdf.

Anonymous 1, Polyethylene, http://www.essentialchemicalindustry.org/polymers/polyethene.html, 28.3.2016.

Anonymous 2, IUPAC GOLD BOOK, doi:10.1351/goldbook.UT07280, 22.4.2016.

Blas, F.J., Vega, L.F., Thermodynamic behavior of homonuclear and heteronuclear Lennard-Jones chains with association sites from simulation and theory, *Molecular Physics*, **92** (1997) 135-150.

Cameron, T., Master's Thesis; Phase equilibrium of polyethylene and n-hexane systems at different operating conditions, 2016

Chen, C., Mathias, P.M., Applied Thermodynamics for Process Modeling, *AIChE Journal*, **48** (2002) 194-200.

Chen, S., Economous, I.G., Radosz, M., Density-Tuned Polyolefin Phase Equilibria. 2. Multicomponent Solutions of Alternating Poly(ethylene-propylene) in Subcritical and Supercritical Olefins. Experiment and SAFT Model, *Macromolecules* **25** (1992a) 4987-4995.

Chen, S., Radosz, M., Density-Tuned Polyolefin Phase Equilibria. 1. Binary Solutions of Alternating Poly(ethylene-propylene) in Subcritical and Supercritical Propylene, 1-Butene, and 1-Hexene. Experiment and Flory-Patterson Model, *Macromolecules* **25** (1992b) 3089-3096.

Chen, X., Sato, Y., Takishima, S., Masuoka, H., Liquid–liquid equilibria of solvent + polymer solutions with a chain-referenced perturbed hard-sphere-chain equation

of state chain-referenced perturbed hard-sphere-chain equation of state, *Fluid Phase Equilibria* **237** (2005) 162–169.

de Loos T.W., de Graaf, L.J., de Swaan Arons, J., Liquid-Liquid phase separation in linear low density polyethylene-solvent systems, *Fluid Phase Equilibria* **117** (1996) 40-47.

de Loos, T.W., Poot, W., Diepen, G.A.M., Fluid Phase Equilibria in the System Polyethylene + Ethylene. 1. Systems of Linear Polyethylene + Ethylene at High Pressure, *Macromolecules* **16** (1983) 111-117.

de Loos, T.W., van der Kool, H.J., Ott, P.L., Vapor-Liquid Critical Curve of the System Ethane + 2-Methylprapane, *J. Chem. Eng. Data* **31** (1986) 166-168.

Economou, I.G., Statistical Associating Fluid Theory: A Successful Model for the Calculation of Thermodynamic and Phase Equilibrium Properties of Complex Fluid Mixtures, *Ind. Eng. Chem. Res.* **41** (2002) 953-962.

Elbro, H.S., Fredenslund, A., Rasmussen, P., A New Simple Equation for the Prediction of Solvent Activities in Polymer Solutions, *Macromolecules* **23** (1990) 4707-4714.

Flory, P.J., Thermodynamics of Heterogeneous Polymers and Their Solutions, *Journal of Chemical Physics,* **12** (1944) 425-438.

Folie, B., Radosz, M., Phase Equilibria in High-pressure Polyethylene Technology, *Ind. Eng. Chem. Res.* **34** (1996) 1501-1516.

Fredenslund, A., UNIFAC and related group-contribution models for phase equilibria, *Fluid Phase Equilibria* **52** (1989) 135-150.

Gauter, K., Heidemann, R.A., Modeling polyethylene-solvent mixtures with the Sanchez–Lacombe equation, *Fluid Phase Equilibria* **183–184** (2001) 87–97.

Goodwin, A.R.H., Sengers, J.V., Peters, C.J., *Applied Thermodynamics of Fluids,* The Royal Society of Chemistry, Cambridge 2010, ss. 74-77.

Gross, J., Sadowski, G., Perturbed-Chain SAFT: An Equation of State Based on a Perturbation Theory for Chain Molecules, *Ind. Eng. Chem. Res.* **40** (2001) 1244-1260.

Gross, J., Spuhl, O., Tumakaka, F., Sadowski, G., Modeling Copolymer Systems Using the Perturbed-Chain SAFT Equation of State, *Ind. Eng. Chem. Res.* **42** (2003) 1266-1274.

Hansen, H. K.; Coto, B.; Kuhlmann, B. UNIFAC with Lineary Temperature-Dependent Group-Interaction Parameters; Technical Report (No. 9212), TVC-SEP Research Engineering Center, Institut for Kemiteknik, The Technical University of Denmark Lyngby, 1992.

Haruki, M., Takakura, Y., Sugiura, H., Kihara, S., Takishima, S., Phase behavior for the supercritical ethylene + hexane + polyethylene systems, *J. of Supercritical Fluids* **44** (2008) 284–293.

Jog, P.K., Chapman, W.G., Gupta, S.K., Swindoll, R.D., Modeling of Liquid-Liquid-Phase Separation in Linear Low-Density Polyethylene-Solvent Systems Using the Statistical Associating Fluid Theory Equation of State, *Ind. Eng. Chem. Res.* **41** (2002) 887-891.

Khare, N.P., Seavey, K.C., Liu, Y.A., Ramanathan, S., Lingard, S., Chen, C., Steady-State and Dynamic Modeling of Commercial Slurry High-Density Polyethylene (HDPE) Processes, *Ind. Eng. Chem. Res.* **41** (2002) 5601-5618.

Kikic, I., Polymer-supercritical fluid interactions, *J. of Supercritical fluids* **47** (2009) 458-465.

Koak, N., Heidemann, R.A., Polymer-Solvent Phase Behavior near the Solvent Vapor Pressure, *Ind. Eng. Chem. Res.* **35** (1996) 4301-4309.

Koak, N., Visser, R.M., de Loos, T.W., High-pressure phase behavior of the systems polyethylene + ethylene and polybutene + 1-butene, Fluid Phase Equilibria **158–160** (1999) 835–846.

Kontogeorgis, G.M., Saraiva, A., Fredenslund, A., Tassios, D.P., Prediction of Liquid-Liquid Equilibrium for Binary Polymer Solutions with Simple Activity Coefficient Models, *Ind. Eng. Chem. Res.* **34** (1995) 1823-1834.

Krenz, R.A., Hedemann, R.A., Modelling the fluid phase behaviour of polydisperse polyethylene blends in hydrocarbons using the modified Sanchez–Lacombe equation of state, *Fluid Phase Equilibria* **262** (2007) 217–226.

Liu, D.D., Prausnitz, J.M., Calculation of Phase Equilibria for Mixtures of Ethylene andLow-Density Polyethylene at High Pressures, *Ind. Eng. Chem. Process Des. Dev.* **19** (1980) 205-211.

Madden, W.G., Pesci, A.I., Freed, K.F., Phase Equilibria of Lattice Polymer and Solvent: Tests of Theories against Simulations, *Macromolecules* **23** (1990) 1181-1191.

Maloney, D.P., Prausnitz, J.M., Solubility of Ethylene in Liquid, Low-Density Polyethylene at Industrial-Separation Pressures, *Ind. Eng. Chem., Process Des. Dev.,* **15** (1976) 216-220.

Meilchen, M.A., Hasch, B.M., McHugh, M.A., Effect of Copolymer Composition on the Phase Behavior of Mixtures of Poly(ethy1ene-co-methyl acrylate) with Propane and
Chlorodifluoromethane, *Macromolecules* **24** (1991) 4874-4882.

Mecking., S., Olefin Polymerization by Late Transition Metal Complexes
A Root of Ziegler Catalysts Gains New Ground, *Angewandte Chemie International Edition* **40** (2001) 534-540.

Nagy, I., de Loos, T.W., Krenz, R.A., Heidemann, R.A., High pressure phase equilibria in the systems linear low density polyethylene + n-hexane and linear low

density polyethylene + n-hexane + ethylene: Experimental results and modelling with the Sanchez-Lacombe equation of state, *J. of Supercritical Fluids* **37** (2006) 115–124.

Nagy, I., Krenz, R.A., Heidemann, R.A., de Loos, T.W., High-pressure phase equilibria in the system linear low density polyethylene + isohexane: Experimental results and modelling, *J. of Supercritical Fluids* **40** (2007) 125–133.

Orbey, H., Bokis, C.P., Chen, C., Equation of State Modeling of Phase Equilibrium in the Low-Density Polyethylene Process: The Sanchez-Lacombe, Statistical Associating Fluid Theory, and Polymer-Soave-Redlich-Kwong Equations of State, *Ind. Eng. Chem. Res.* **37** (1998) 4481-4491.

Patterson, D., Free Volume and Polymer Solubility. A Qualitative View, *Macromolecules* **2** (1969) 672-677.

Pedrosa, N., Vega, L.F., Coutinho, J.A.P., Marrucho, I.M., Phase Equilibria Calculations of Polyethylene Solutions from SAFT-Type Equations of State, *Macromolecules* **39** (2006) 4240-4246.

Sanchez, I.C., Lacombe, R.H., Statistical Thermodynamics of Polymer Solutions, *Macromolecules* **11** (1978) 1145-1155.

Song, Y., Hino, T., Lambert, S.M., Prausnitz, J.M., Liquid-Liquid Equilibria for Polymer Solutions and Blends, Including Copolymers, *Fluid Phase Equilibria* **117** (1996) 69-76.

Song, Y., Lambert, S.M., Prausnitz, J.M., Liquid-Liquid Phase Diagrams for Binary Polymer Solutions from a Perturbed Hard-Sphere-Chain Equation of State, *Chemical Engineering Science* **47** (1994) 2765-2775.

Szydlowski, J., Rebelo, L.P., Van Hook, W.A., A new apparatus for the detection of phase equilibria in polymer solvent systems by light scattering, *Rev. Sci. Instrum.* **63** (1992) 1717-1725.

ter Horst, M.H., Behme, S., Sadowski, G., de Loos, T.W., The influence of supercritical gases on the phase behavior of polystyrene–cyclohexane and polyethylene–cyclohexane systems: experimental results and modeling with the SAFT-equation of state, *J. of Supercritical Fluid* **23** (2002) 181–194.

Tork, T., Sadowski, G., Arlt. W., de Haan, A., Krooshof, G., Modelling of high-pressure phase equilibria using the Sako–Wu–Prausnitz equation of state I. Pure-components and heavy n-alkane solutions, *Fluid Phase Equilibria* **163** (1999a) 61–77.

Tork, T., Sadowski, G., Arlt. W., de Haan, A., Krooshof, G., Modelling of high-pressure phase equilibria using the Sako–Wu–Prausnitz equation of state II. Vapour–liquid equilibria and liquid–liquid equilibria in polyolefin systems, *Fluid Phase Equilibria* **163** (1999b) 79–98

Tumakaka, F., Gross, J., Sadowski, G., Thermodynamic modeling of complex systems using PC-SAFT, *Fluid Phase Equilibria* **228–229** (2005) 89–98.

Temperature calibration:

M-15T109

Digital thermometer

Type F200

Calibrated at MIKES (22.10.2015)

Calibration temperature (°C)	Channel 1, Sensor T3343.1		Extended uncertainty of the calibration (K=2)
	Display (°C)	Difference of calibration temp. and display temp.	
49.997	50.000	-0.003	0.015
100.225	100.241	-0.016	0.030
150.230	150.250	-0.020	0.030
199.998	200.051	-0.053	0.030
250.192	250.304	-0.112	0.030

Slope 0.99949041 Intercept 0.035724737

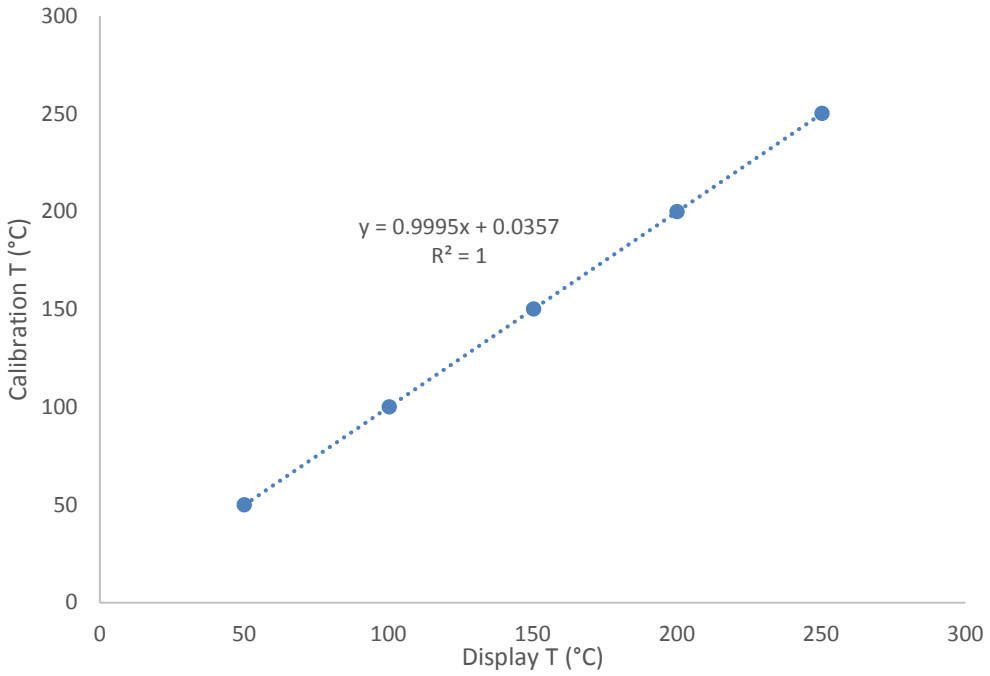

Pressure calibration:

Display T (°C)	Calibrated T (°C)
22.132	22.156

Display (bar)	Calibrated (bar)	Difference
98.46	99.05	-0.59
90.58	90.83	-0.25
78.78	78.58	0.20
72.36	71.94	0.42
61.20	60.38	0.82
50.25	49.03	1.22
42.24	40.73	1.51
32.32	30.45	1.87
21.86	19.60	2.26
12.46	9.84	2.62
3.95	1.02	2.93

slope	**intercept**	**Average error**
0.96	**2.96**	**1.18**

Display T (°C)	Calibrated T (°C)
50.512	50.522

Display (bar)	Calibrated (bar)	Difference
99.41	98.93	0.48
90.71	90.00	0.71
81.11	80.17	0.94
71.37	70.19	1.18
61.59	60.17	1.42
52.13	50.48	1.65
42.60	40.70	1.90
32.37	30.22	2.15
22.05	19.63	2.42
12.63	9.98	2.65
3.88	1.02	2.86

slope	**intercept**	**Average error**
0.98	**2.89**	**1.67**

Display T (°C)	Calibrated T (°C)
100.501	100.486

Display (bar)	Calibrated (bar)	Difference
99.46	98.06	1.40
92.06	90.60	1.46
82.02	80.44	1.58
71.10	70.01	1.09
61.75	59.94	1.81
52.21	50.30	1.91
41.84	39.87	1.97
31.44	29.37	2.07
22.96	20.81	2.15
12.06	9.79	2.27
3.40	1.02	2.38

Slope	**Intercept**	**Average error**
0.99	**2.38**	**1.83**

Display T (°C)	Calibrated T (°C)
150.43	150.389

Display (bar)	Calibrated (bar)	Difference
98.60	97.23	1.37
91.39	90.03	1.36
81.68	80.31	1.37
71.32	69.95	1.37
61.25	59.87	1.38
51.44	50.03	1.41
41.64	40.21	1.43
31.28	29.81	1.47
21.31	19.81	1.50
10.98	9.49	1.49
2.56	1.02	1.54

Slope	**Intercept**	**Average error**
1.00	**1.52**	**1.43**

Display T (°C)	Calibrated T(°C)
200.260	200.194

Display (bar)	Calibrated (bar)	Difference
97.2	96.52	0.68
90.49	89.85	0.64
81.49	80.89	0.60
71.46	70.90	0.56
60.28	59.77	0.51
50.04	49.57	0.47
40.95	40.50	0.45
30.14	29.73	0.41
20.49	20.09	0.40
10.28	9.90	0.38
1.40	1.02	0.38

Slope	**Intercept**	**Average error**
1.00	**0.34**	**0.50**

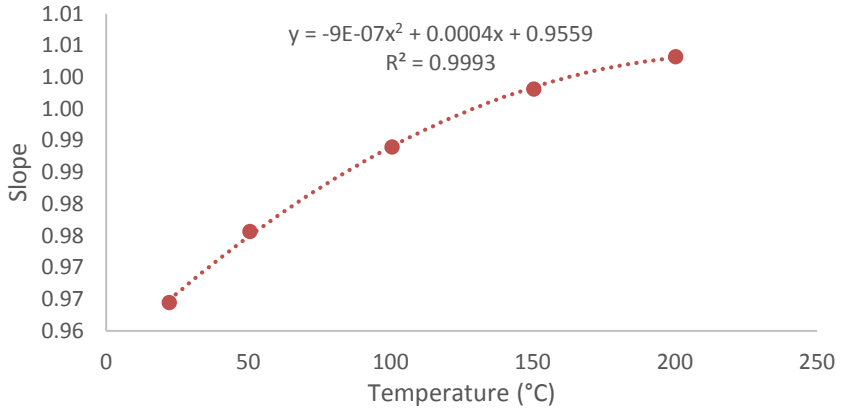

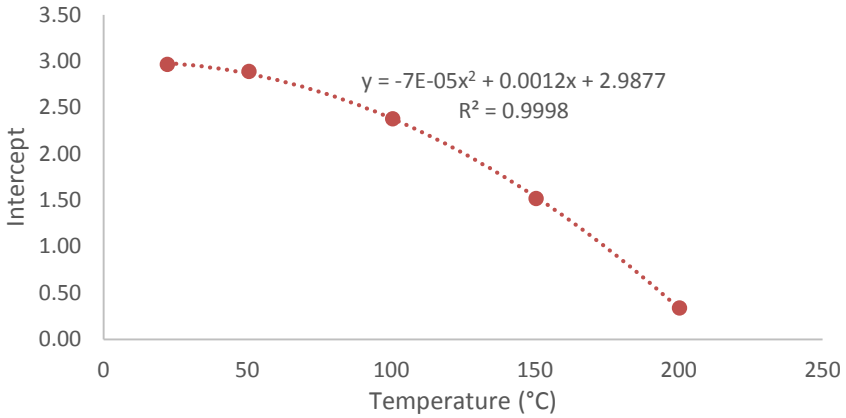

Name	Manufacturer	Purity (%)	Type	Phase
PE A	Borealis Polymers Oy	No information	Polymer LLDPE	Solid, granule
PE B	Borealis Polymers Oy	No information	Polymer LLDPE	Solid, granule
PE C	Borealis Polymers Oy	No information	Polymer LLDPE	Solid, granule
PE D	Borealis Polymers Oy	No information	Polymer LLDPE	Solid, granule
PE E	Borealis Polymers Oy	No information	Polymer LLDPE	Solid, granule
1-Octene	Sigma-Aldrich	98.000	co-monomer	Liquid
n-Hexane	Aldrich	≥ 99.000	Solvent	Liquid
Hexane mix component 1	Aldrich	97.000	Solvent	Liquid
Hexane mix component 2	Aldrich	≥ 99.000	Solvent	Liquid
Hexane mix component 3	Aldrich	≥ 99.000	Solvent	Liquid
Ethylene (Ethen scientific)	HiQ	99.950	Monomer	Gas
Nitrogen (instrument)	Aga	99.999	Antisolvent	Gas

Components	Experiment 1		
	w%	Cloud points	
PE A	20.855	p (bar)	T (°C)
Ethylene	-	41.180	192.346
1-octene	-	49.775	197.481
x	-	54.148	202.558
n-Hexane (pure)	79.145		

Components	Experiment 2		
	w%	Cloud points	
PE A	19.789	p (bar)	T (°C)
Ethylene	0.909	37.609	192.884
1-octene	x	51.738	202.978
x	x	64.525	212.994
Hexane mix solvent	x	71.984	223.161

Components	Experiment 3		
	w%	Cloud points	
PE A	22.184	p (bar)	T (°C)
Ethylene	0.916	67.926	192.862
1-octene	x	79.588	202.144
x	x		
Hexane mix solvent	x		
Nitrogen	0.995		

Components	Experiment 4				
	w%	Cloud points		Bubble points	
PE B	23.903	p (bar)	T (°C)	p (bar)	T (°C)
Ethylene	1.987	30.982	201.643	20.320	152.291
1-octene	x	41.810	212.942	21.747	162.405
x	x	52.598	223.142	23.330	172.482
Hexane mix solvent	x	56.856	228.125	25.037	182.579

Components	Experiment 5		
	w%	Cloud points	
PE B	24.418	p (bar)	T (°C)
Ethylene	2.354	46.676	192.423
1-octene	x	64.313	202.393
x	x	77.108	212.629
Hexane mix solvent	x	89.055	222.667
Nitrogen	0.140		

Components	Experiment 6				
	w%	Cloud points		Bubble points	
PE B	17.761	p (bar)	T (°C)	p (bar)	T (°C)
Ethylene	1.637	35.720	192.465	19.676	152.133
1-octene	x	47.358	202.579	21.221	162.321
x	x	60.431	212.360	22.736	172.258
Hexane mix solvent	x	71.870	222.643	24.632	182.420

Components	Experiment 7				
	w%	Cloud points		Bubble points	
PE B	30.621	p (bar)	T (°C)	p (bar)	T (°C)
Ethylene	2.620	39.596	222.415	28.276	192.328
1-octene	x	48.351	232.319	30.263	202.377
x	x	58.884	242.396	32.642	212.431
Hexane mix solvent	x	69.217	250.306	34.864	222.424

Components	Experiment 8				
	w%	Cloud points		Bubble points	
PE C	x	p (bar)	T (°C)	p (bar)	T (°C)
Ethylene	x	39.70	202.75	24.54	152.25
1-octene	x	50.34	212.90	26.07	162.42
x	x	62.01	222.94	27.79	172.49
Hexane mix solvent	x	72.50	232.95	29.58	182.63

Components	Experiment 9				
	w%	Cloud points		Bubble points	
PE C	x	p (bar)	T (°C)	p (bar)	T (°C)
Ethylene	x	48.29	192.27	36.19	161.79
1-octene	x	58.04	202.49	41.00	181.17
x	x	69.57	212.26	43.06	192.47
Hexane mix solvent	x	80.53	219.87	45.07	202.31
Nitrogen	0.128				

Components	Experiment 10				
	w%	Cloud points		Bubble points	
PE C	x	p (bar)	T (°C)	p (bar)	T (°C)
Ethylene	x	38.14	182.11	20.87	152.07
1-octene	x	49.88	191.87	22.47	162.08
x	x	69.29	211.65	24.49	172.12
Hexane mix solvent	x	81.39	221.90	26.32	182.11

Components	Experiment 11 (Aborted test due to hyd. oil leakage)		
	w%	Bubble point	
PE D	x	p (bar)	T (°C)
Ethylene	x	20.519	152.322
1-octene	x	22.505	162.432
x	x	25.645	182.659
Hexane mix solvent	x		

Components	Experiment 12				
	w%	Cloud points		Bubble points	
PE D	x	p (bar)	T (°C)	p (bar)	T (°C)
Ethylene	x	35.02	202.69	20.97	152.22
1-octene	x	46.49	212.83	22.38	162.30
x	x	57.11	222.71	23.86	172.41
Hexane mix solvent	x	67.11	232.83	27.69	192.63

Components	Experiment 13				
	w%	Cloud points		Bubble points	
PE D	x	p (bar)	T (°C)	p (bar)	T (°C)
Ethylene	x	44.50	192.18	35.99	151.01
1-octene	x	56.77	202.31	37.09	162.21
x	x	68.41	212.17	37.95	172.26
Hexane mix solvent	x	79.73	222.21	39.29	182.31
Nitrogen	0.798				

Components	Experiment 14				
	w%	Cloud points		Bubble points	
PE D	x	p (bar)	T (°C)	p (bar)	T (°C)
Ethylene	x	37.79	192.36	25.60	152.38
1-octene	x	64.48	212.83	28.46	172.46
x	x	72.87	222.79	32.15	192.44
Hexane mix solvent	x	84.69	232.78	2.99	0.04
Nitrogen	0.175				

Components	Experiment 15				
	w%	Cloud points		Bubble points	
PE D	x	p (bar)	T (°C)	p (bar)	T (°C)
Ethylene	x	24.88	182.26	19.54	151.98
1-octene	x	36.41	192.38	22.80	172.14
x	x	49.66	202.31	24.70	182.26
Hexane mix solvent	x	74.40	222.66		

Components	Experiment 16				
	w%	Cloud points		Bubble points	
PE D	x	p (bar)	T (°C)	p (bar)	T (°C)
Ethylene	x	31.84	222.64	17.69	152.03
1-octene	x	40.19	232.64	20.63	172.19
x	x	46.06	242.71	23.66	192.41
Hexane mix solvent	x	52.27	249.73	25.52	202.47

Components	Experiment 17				
	w%	Cloud points		Bubble points	
PE E	23.237	p (bar)	T (°C)	p (bar)	T (°C)
Ethylene	1.715	34.64	192.66	23.22	172.38
1-octene	x	43.79	202.80	25.19	182.55
x	x	56.27	212.90	27.14	192.68
Hexane mix solvent	x	65.43	222.84		

Components	Experiment 18				
	w%	Cloud points		Bubble points	
PE E	26.361	p (bar)	T (°C)	p (bar)	T (°C)
Ethylene	1.940	39.54	192.32	29.08	152.08
1-octene	x	51.44	202.39	32.13	171.99
x	x	62.52	212.49	34.04	182.27
Hexane mix solvent	x	70.39	220.58	35.65	192.32
Nitrogen	0.289				

Components	Experiment 19				
	w%	Cloud points		Bubble points	
PE E	14.371	p (bar)	T (°C)	p (bar)	T (°C)
Ethylene	0.928	39.80	192.63	21.52	150.05
1-octene	x	50.34	202.54	24.64	169.80
x	x	61.59	212.64	27.98	192.30
Hexane mix solvent	x	72.88	222.46	24.68	172.42

Components	Experiment 20				
	w%	Cloud points		Bubble points	
PE E	15.914	p (bar)	T (°C)	p (bar)	T (°C)
Ethylene	1.932	27.69	182.62	20.47	152.20
1-octene	x	37.43	192.65	23.67	172.43
x	x	64.13	212.87	25.67	182.61
Hexane mix solvent	x	81.86	232.94		

Components	Experiment 21				
	w%	Cloud points		Bubble points	
PE E	37.595	p (bar)	T (°C)	p (bar)	T (°C)
Ethylene	1.923	35.79	212.53	20.68	151.91
1-octene	x	44.71	221.27	23.72	172.12
x	x	51.85	232.10	27.71	192.38
Hexane mix solvent	x			29.96	202.42

Cloud point (PE A)			
T (°C)	N_2 0 w% (bar)	N_2 0.986 w% (bar)	Increase (bar)
200	47.3	76.9	29.6
210	58.8	89.5	30.7
220	70.2	102.0	31.8
230	81.7	114.6	32.9
240	93.2	127.2	33.9
250	104.7	139.7	35.0
		Average difference	32.3

Cloud point (PE B)			
T (°C)	N_2 0 w% (bar)	N_2 0.140 w% (bar)	Increase (bar)
200	29.2	58.9	29.7
210	39.1	72.7	33.6
220	49.1	86.6	37.4
230	59.1	100.4	41.3
240	69.1	114.3	45.2
250	79.1	128.1	49.1
		Average difference	39.4

Cloud point (PE C)			
T (°C)	N_2 0 w% (bar)	N_2 0.127 w% (bar)	Increase (bar)
200	37.6	56.4	18.8
210	47.8	67.6	19.9
220	58.0	78.9	20.9
230	68.2	90.2	22.0
240	78.4	101.4	23.0
250	88.6	112.7	24.1
		Average difference	21.4

Bubble point (PE C)			
T (°C)	N_2 0 w% (bar)	N_2 0.127 w% (bar)	Increase (bar)
150	23.9	33.8	9.9
160	25.7	36.0	10.3
170	27.5	38.2	10.7
180	29.3	40.4	11.1
190	31.1	42.5	11.4
200	32.9	44.7	11.8
		Average difference	10.9

Cloud point (PE D)					
T (°C)	N_2 0 w% (bar)	N_2 0.175 w% (bar)	N_2 0.792 w% (bar)	Increase 1 (bar)	Increase 2 (bar)
200	32.9	47.5	54.0	14.6	21.0
210	43.3	59.0	65.4	15.7	22.1
220	53.6	70.5	76.7	16.9	23.1
230	64.0	82.0	88.1	18.0	24.2
240	74.3	93.5	99.5	19.2	25.2
250	84.7	105.0	110.9	20.3	26.3
			Average difference	17.4	23.6

Bubble point (PE D)					
T (°C)	N_2 0 w% (bar)	N_2 0.175 w% (bar)	N_2 0.798 w% (bar)	Increase 1 (bar)	Increase 2 (bar)
150	20.3	24.3	35.8	4.0	15.4
160	22.1	26.2	36.9	4.1	14.8
170	23.8	28.0	37.9	4.2	14.1
180	25.5	29.9	39.0	4.3	13.5
190	27.3	31.7	40.1	4.4	12.8
200	29.0	33.5	41.2	4.6	12.2
			Average difference	4.3	13.8

Cloud point (PE E)			
T (°C)	N_2 0 w% (bar)	N_2 0.289 w% (bar)	Increase (bar)
200	41.9	48.6	6.7
210	52.2	58.7	6.5
220	62.4	68.8	6.3
230	72.7	78.8	6.2
240	82.9	88.9	6.0
250	93.1	99.0	5.9
		Average difference	6.3

Bubble point (PE E)			
T (°C)	N_2 0 w% (bar)	N_2 0.289 w% (bar)	Increase (bar)
150	18.9	28.7	9.8
160	20.8	30.3	9.5
170	22.8	32.0	9.2
180	24.7	33.6	8.9
190	26.6	35.2	8.6
200	28.6	36.9	8.3
		Average difference	9.1

PE	**Cloud point pressure** from model: p_{CP} (bar)=a_{1c}·T(°C)+b_{1c}			
	Slope (a_{1c}) a_{1c}= a_{S2c}·**Ethylene**(w%)+b_{S2c}		Intercept (b_{1c}) b_{1c}= a_{I2c}·**Ethylene**(w%)+b_{I2c}	
	a_{S2c} (10^{-3})	b_{S2c}	a_{I2c}	b_{I2c}
B	-86.529	1.253	-12.058	-159.789
C	-53.444	1.163	-13.242	-131.479
D	1445.190	-1.476	-200.512	175.862
E	-102.103	1.169	9.672	-175.597

PE	**Bubble point pressure** from the model: P_{BP} (bar)=a_{1b}·T(°C)+b_{1b}			
	Slope (a_{1b}) a_{1b}= a_{S2b}·**Ethylene**(w%)+b_{S2b}		Intercept (b_{1b}) b_{1b}= a_{I2b}·**Ethylene**(w%)+b_{I2b}	
	a_{S2b} (10^{-3})	b_{S2b}	a_{I2b}	b_{I2b}
B	56.037	0.070	-8.751	9.407
C	-2.375	0.187	4.470	-15.175
D	15.514	0.144	9.978	-23.730
E	31.282	0.126	-6.343	3.883

PE	**Cloud point pressure** from model: p_{CP} (bar)=a_{1c}·T(°C)+b_{1c}			
	Slope (a_{1c}) a_{1c}= a_{S2c}·**Co-monomer**(w%)+b_{S2c}		Intercept (b_{1c}) b_{1c}= a_{I2c}·**Co-monomer**(w%)+b_{I2c}	
	a_{S2c} (10^{-3})	b_{S2c}	a_{I2c}	b_{I2c}
B	7.485	0.794	-0.925	-150.344
C	2.662	0.945	0.660	-185.397
D	-0.126	0.991	0.121	-170.339
E	-34.971	1.633	4.332	-237.955

PE	**Bubble point pressure** from the model: P_{BP} (bar)=a_{1b}·T(°C)+b_{1b}			
	Slope (a_{1b}) a_{1b}= a_{S2b}·**Co-monomer**(w%)+b_{S2b}		Intercept (b_{1b}) b_{1b}= a_{I2b}·**Co-monomer**(w%)+b_{I2b}	
	a_{S2b} (10^{-3})	b_{S2b}	a_{I2b}	b_{I2b}
B	0.272	0.177	-0.071	-6.142
C	0.118	0.178	-0.223	3.027
D	-0.163	0.176	-0.047	-4.966
E	3.106	0.121	-0.498	2.564

Experiment 4, PE B 23.903 w%				
Cloud point				
p (bar) model	**T (°C)**	**Δp**	**AAD**	**RAAD**
31.924	201.6	-0.941	0.941	3.038
44.066	212.9	-2.255	2.255	5.394
55.026	223.1	-2.428	2.428	4.616
60.381	228.1	-3.525	3.525	6.199
71.997	238.0	-4.061	4.061	6.066
76.648	243.3	-4.025	4.025	5.542
		Average	**2.872**	**5.143**

Experiment 6, PE B 17.761 w%				
Cloud point				
p (bar) model	**T (°C)**	**Δp**	**AAD**	**RAAD**
35.910	192.5	-0.190	0.190	0.532
47.289	202.6	0.069	0.069	0.146
58.292	212.4	2.139	2.139	3.539
69.861	222.6	2.009	2.009	2.796
80.874	232.4	0.821	0.821	1.005
		Average	**1.046**	**1.604**

Experiment 7, PE B 30.6121 w%				
Cloud point				
p (bar) model	**T (°C)**	**Δp**	**AAD**	**RAAD**
37.444	222.4	2.152	2.152	5.435
47.540	232.3	0.811	0.811	1.677
57.812	242.4	1.072	1.072	1.820
65.876	250.3	3.341	3.341	4.826
		Average	**1.844**	**3.440**

Experiment 8, PE C higher w%				
Cloud point				
p (bar) model	**T (°C)**	**Δp**	**AAD**	**RAAD**
40.359	202.8	-0.655	0.655	1.6
50.717	212.9	-0.374	0.374	0.7
60.972	222.9	1.035	1.035	1.7
71.196	233.0	1.300	1.300	1.8
81.484	243.0	-0.283	0.283	0.3
86.582	248.0	-0.955	0.955	1.1
		Average	**0.767**	**1.2**

Experiment 8, PE C higher w%				
Bubble point				
p (bar) model	**T (°C)**	**Δp**	**AAD**	**RAAD**
24.256	152.3	0.288	0.288	1.2
26.096	162.4	-0.021	0.021	0.1
27.919	172.5	-0.128	0.128	0.5
29.754	182.6	-0.172	0.172	0.6
31.578	192.7	-0.032	0.032	0.1
33.397	202.8	0.037	0.037	0.1
		Average	**0.113**	**0.4**

Experiment 10, PE C lower w%				
Cloud point				
p (bar) model	**T (°C)**	**Δp**	**AAD**	**RAAD**
38.632	182.1	-0.488	0.488	1.3
49.033	191.9	0.844	0.844	1.7
70.120	211.7	-0.827	0.827	1.2
81.050	221.9	0.336	0.336	0.4
		Average	**0.624**	**1.1**

Experiment 10, PE C lower w%				
Bubble point				
p (bar) model	**T (°C)**	**Δp**	**AAD**	**RAAD**
20.762	152.1	0.110	0.110	0.5
22.594	162.1	-0.122	0.122	0.5
24.432	172.1	0.054	0.054	0.2
26.261	182.1	0.056	0.056	0.2
		Average	**0.085**	**0.4**

Experiment 12, PE D higher w%				
Cloud point				
p (bar) model	**T (°C)**	**Δp**	**AAD**	**RAAD**
32.563	202.7	2.452	2.452	7.0
42.343	212.8	4.151	4.151	8.9
51.864	222.7	5.249	5.249	9.2
61.617	232.8	5.492	5.492	8.2
71.461	243.0	6.260	6.260	8.1
76.144	247.9	5.669	5.669	6.9
		Average	**4.336**	**8.3**

Experiment 12, PE D higher w%				
Bubble point				
p (bar) model	**T (°C)**	**Δp**	**AAD**	**RAAD**
19.049	152.2	1.920	1.920	9.2
20.762	162.3	1.616	1.616	7.2
22.482	172.4	1.379	1.379	5.8
25.917	192.6	1.773	1.773	6.4
27.626	202.7	1.990	1.990	6.7
		Average	**1.638**	**7.4**

Experiment 15, PE D lowest w%				
Cloud point				
p (bar) model	**T (°C)**	**Δp**	**AAD**	**RAAD**
25.662	182.3	-0.777	0.777	3.1
38.014	192.4	-1.602	1.602	4.4
50.136	202.3	-0.471	0.471	0.9
74.986	222.7	-0.585	0.585	0.8
87.223	232.7	-3.275	3.275	3.9
		Average	**0.859**	**2.3**

Experiment 15, PE D lowest w%				
Bubble point				
p (bar) model	**T (°C)**	**Δp**	**AAD**	**RAAD**
20.130	152.0	-0.590	0.590	3.0
23.563	172.1	-0.764	0.764	3.4
25.286	182.3	-0.581	0.581	2.4
		Average	**0.645**	**2.9**

Experiment 16, PE D highest w%				
Cloud point				
p (bar) model	**T (°C)**	**Δp**	**AAD**	**RAAD**
34.823	222.6	-2.987	2.987	9.4
42.574	232.6	-2.386	2.386	5.9
50.382	242.7	-4.318	4.318	9.4
55.823	249.7	-3.549	3.549	6.8
		Average	**3.310**	**7.9**

Experiment 16, PE D highest w%				
Bubble point				
p (bar) model	**T (°C)**	**Δp**	**AAD**	**RAAD**
18.195	152.0	-0.509	0.509	2.9
21.618	172.2	-0.987	0.987	4.8
25.050	192.4	-1.394	1.394	5.9
26.758	202.5	-1.237	1.237	4.8
28.462	212.5	-0.923	0.923	3.4
30.179	222.6	-0.464	0.464	1.6
31.875	232.6	-0.108	0.108	0.3
		Average	**0.803**	**3.4**

Experiment 17, PE E 22.237 w%				
Cloud point				
p (bar) model	**T (°C)**	**Δp**	**AAD**	**RAAD**
32.964	192.7	1.672	1.672	4.8
43.079	202.8	0.714	0.714	1.6
53.150	212.9	3.115	3.115	5.5
63.065	222.8	2.366	2.366	3.6
73.097	232.9	1.811	1.811	2.4
83.151	243.0	3.052	3.052	3.5
		Average	**2.122**	**3.6**

Experiment 17, PE E 22.237 w%				
Bubble point				
p (bar) model	**T (°C)**	**Δp**	**AAD**	**RAAD**
24.045	172.4	-0.822	0.822	3.5
25.849	182.5	-0.661	0.661	2.6
27.648	192.7	-0.509	0.509	1.9
		Average	**0.664**	**2.7**

Experiment 19, PE E 14.371 w%				
Cloud point				
p (bar) model	**T (°C)**	**Δp**	**AAD**	**RAAD**
40.486	192.6	-0.682	0.682	1.7
51.426	202.5	-1.087	1.087	2.2
62.571	212.6	-0.977	0.977	1.6
73.412	222.5	-0.537	0.537	0.7
84.682	232.7	-1.394	1.394	1.7
95.611	242.6	-2.984	2.984	3.2
		Average	**1.277**	**1.8**

Experiment 19, PE E 14.371 w%				
Bubble point				
p (bar) model	T (°C)	Δp	AAD	RAAD
20.444	150.0	1.081	1.081	5.0
23.684	169.8	0.959	0.959	3.9
27.375	192.3	0.602	0.602	2.2
24.114	172.4	0.565	0.565	2.3
		Average	**0.881**	**3.7**

Experiment 20, PE E 15.914 w%				
Cloud point				
p (bar) model	T (°C)	Δp	AAD	RAAD
28.305	182.6	-0.611	0.611	2.2
39.192	192.7	-1.757	1.757	4.7
61.138	212.9	2.990	2.990	4.7
82.917	232.9	-1.059	1.059	1.3
		Average	**1.604**	**3.2**

Experiment 20, PE E 15.914 w%				
Bubble point				
p (bar) model	T (°C)	Δp	AAD	RAAD
20.740	152.2	-0.268	0.268	1.3
24.105	172.4	-0.434	0.434	1.8
25.799	182.6	-0.133	0.133	0.5
		Average	**0.279**	**1.2**

Experiment 21, PE E 37.595 w%				
Cloud point				
p (bar) model	T (°C)	Δp	AAD	RAAD
37.136	212.5	-1.346	1.346	3.8
44.352	221.3	0.359	0.359	0.8
53.292	232.1	-1.443	1.443	2.8
		Average	**1.049**	**2.4**

Experiment 21, PE E 37.595 w%				
Bubble point				
p (bar) model	T (°C)	Δp	AAD	RAAD
19.866	151.9	0.810	0.810	3.9
23.891	172.1	-0.173	0.173	0.7
27.926	192.4	-0.220	0.220	0.8
29.924	202.4	0.038	0.038	0.1
31.899	212.3	0.416	0.416	1.3
		Average	**0.401**	**1.8**

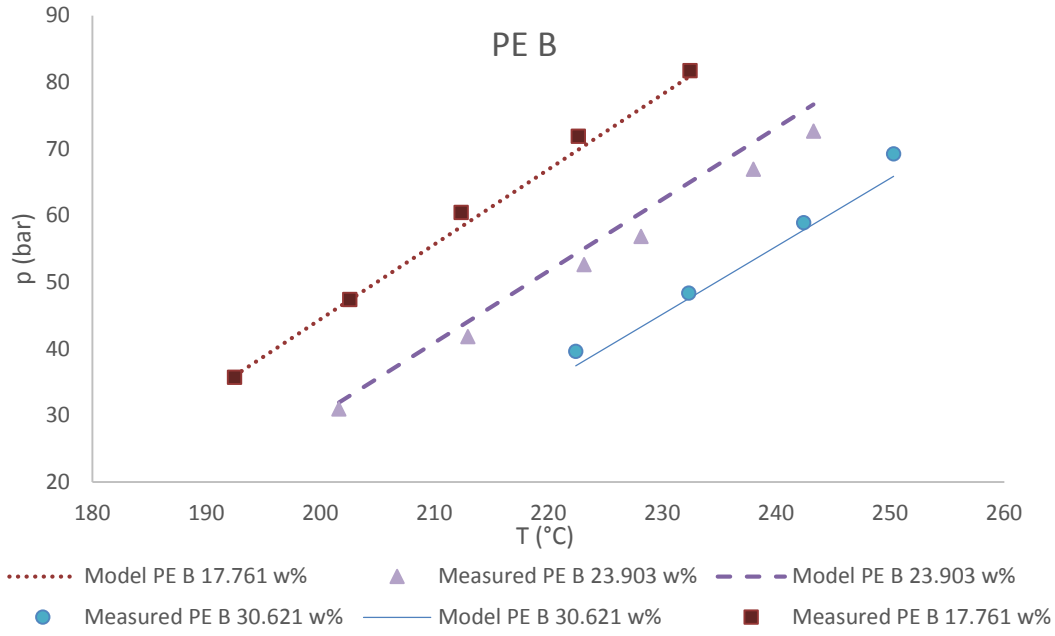

Graph I. Model and measurement points for polymer system B.

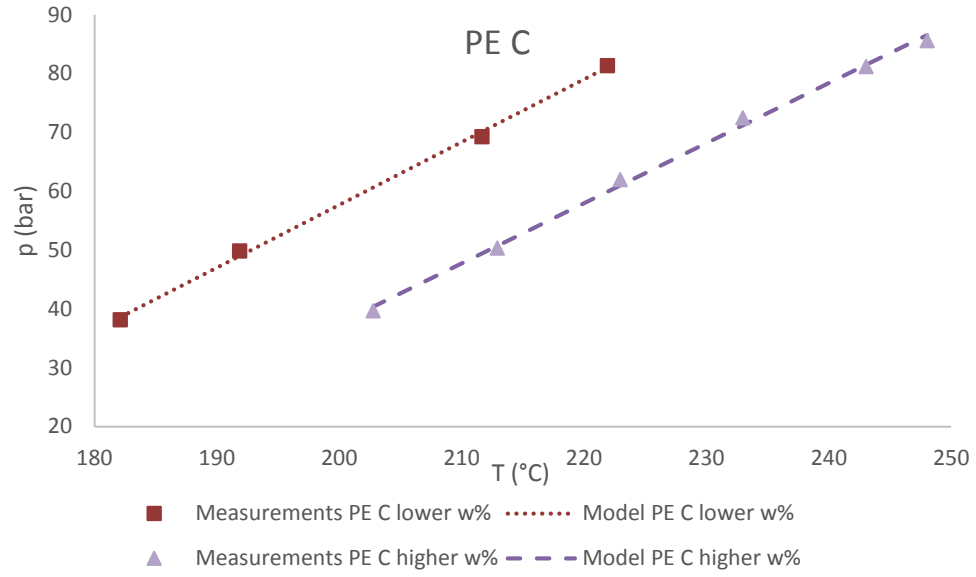

Graph II. Model and measurement points for polymer system C.

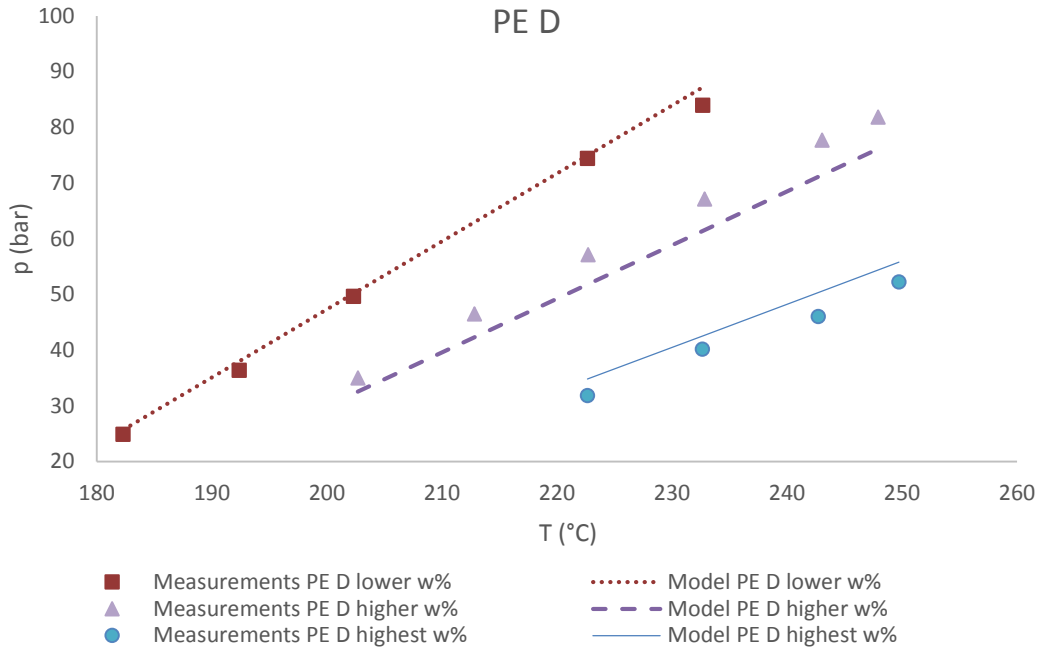

Graph III. Model and measurement points for polymer system D.

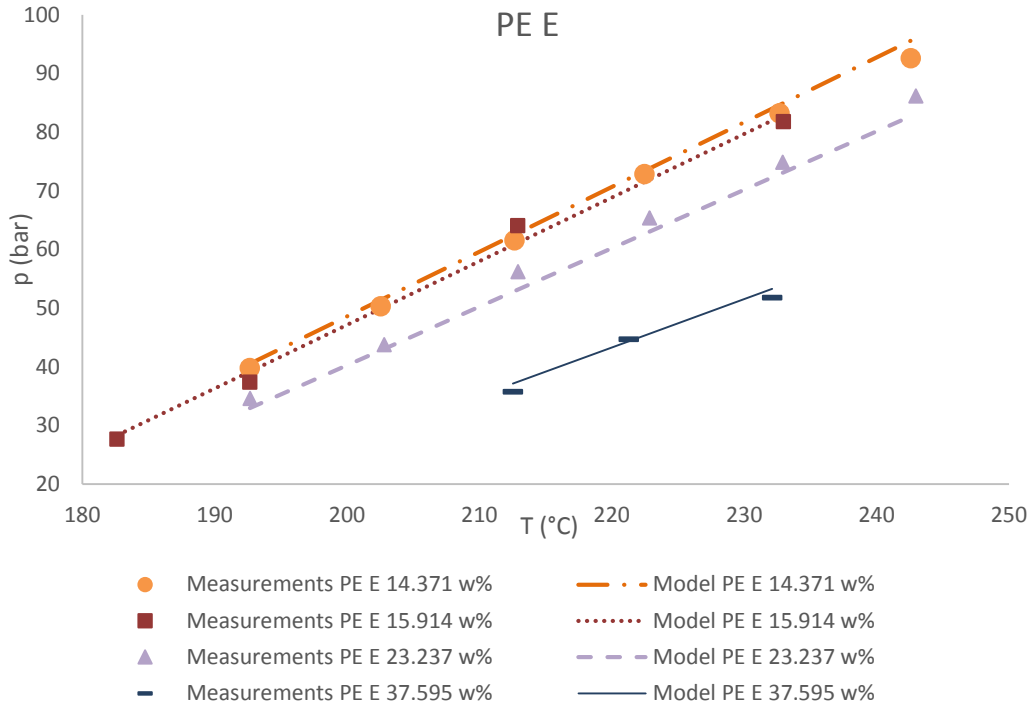

Graph IV. Model and measurement points for polymer system E.

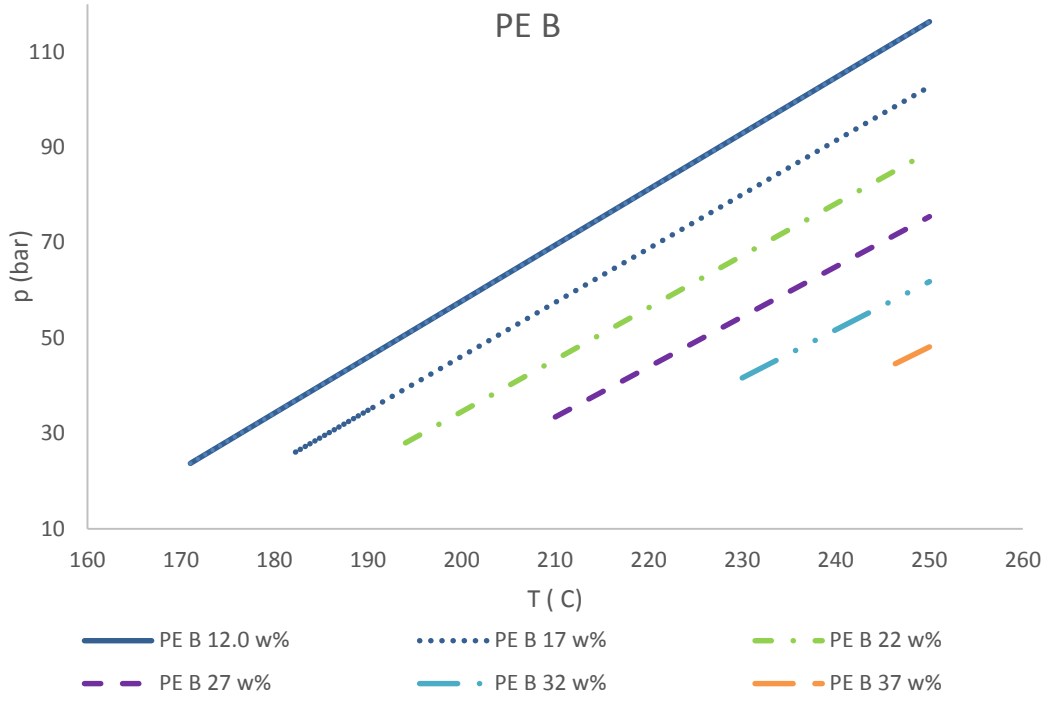

Graph V. The model prediction at different polymer weight percentage for polymer B.

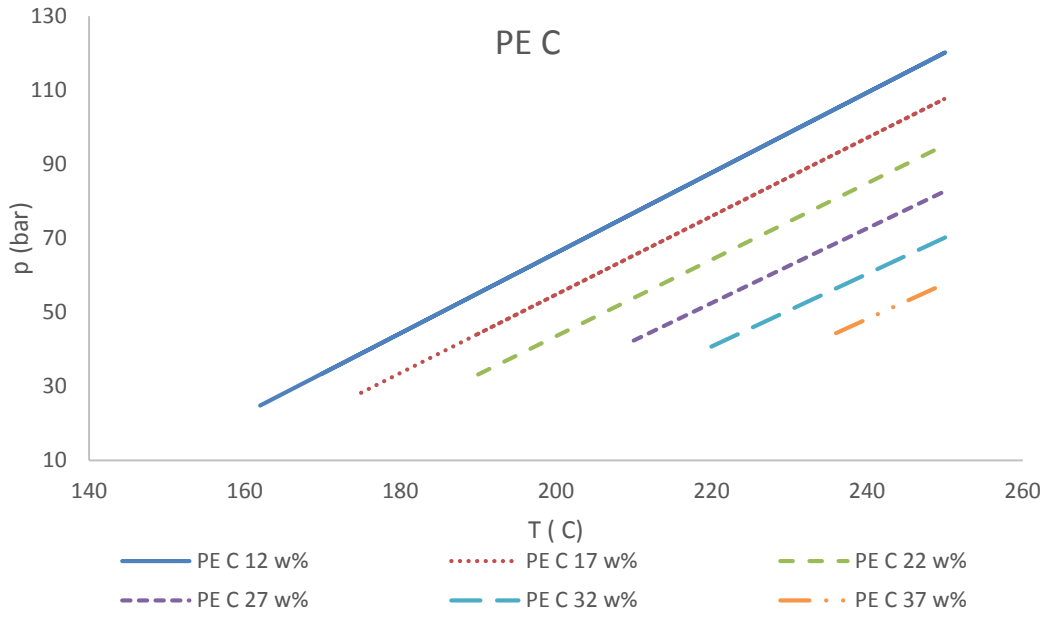

Graph VI. The model prediction at different polymer weight percentage for polymer C.

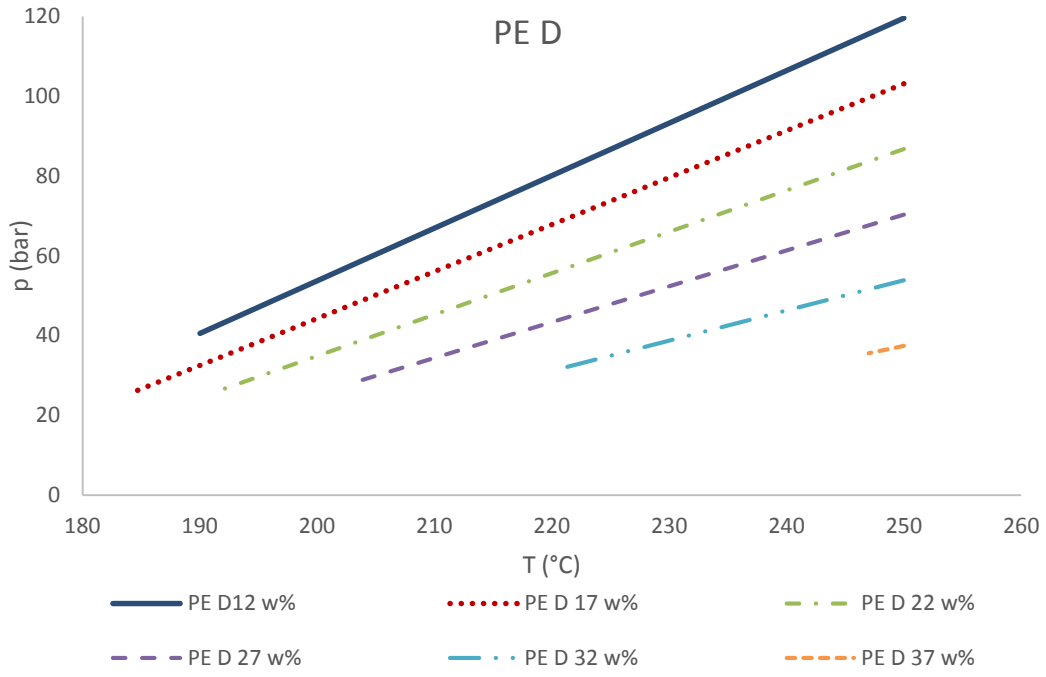

Graph VII. The model prediction at different polymer weight percentage for polymer D.

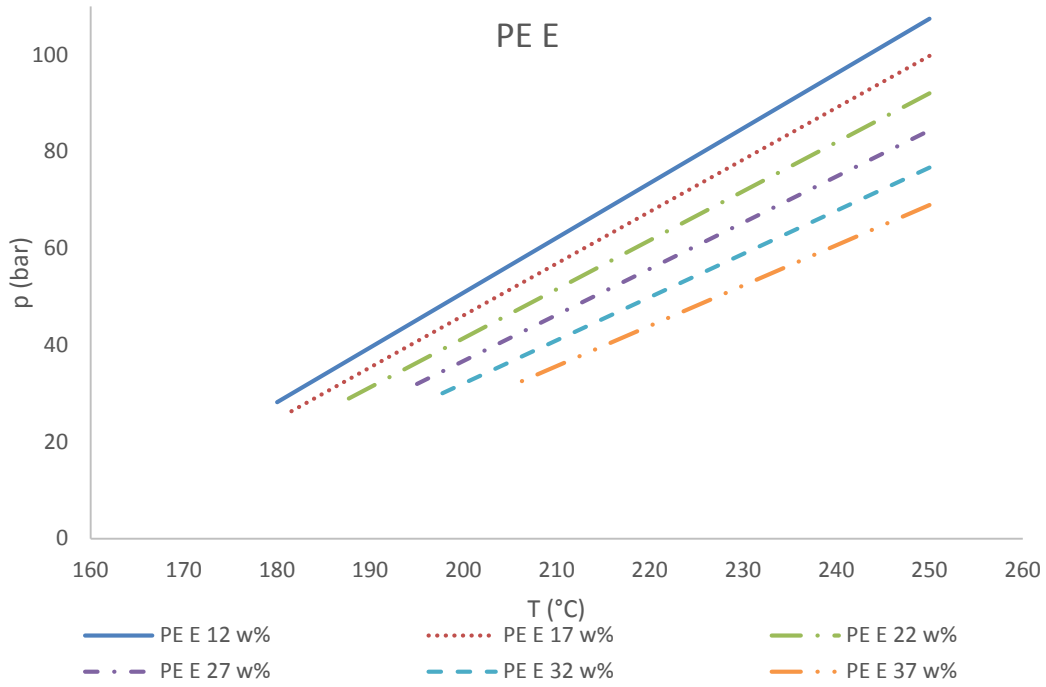

Graph VIII. The model prediction at different polymer weight percentage for polymer E.

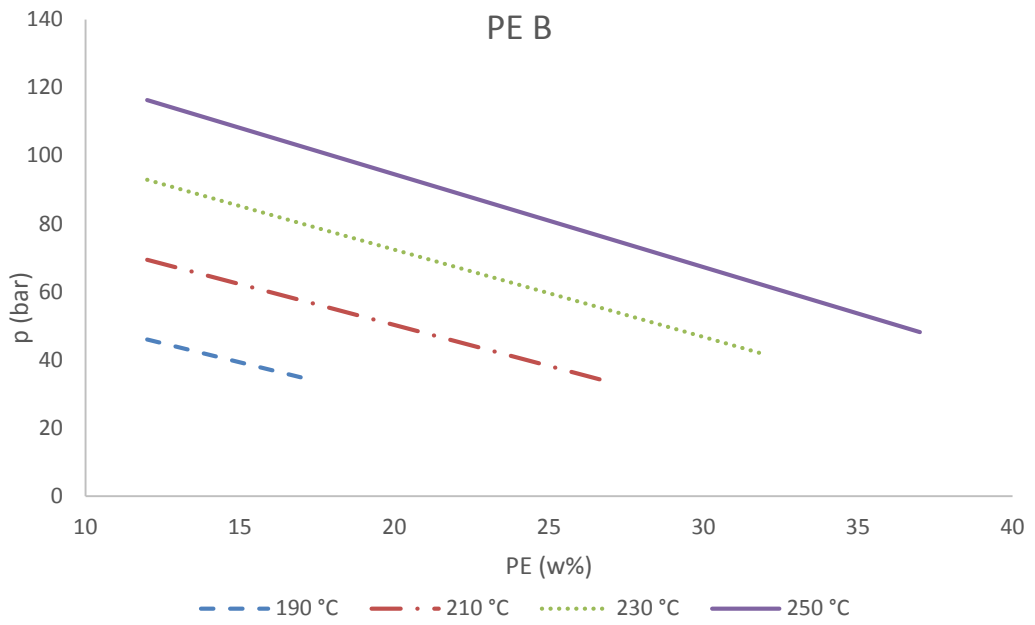

Graph IX. The isothermal behaviour predicted with the model for polymer system B at several temperatures.

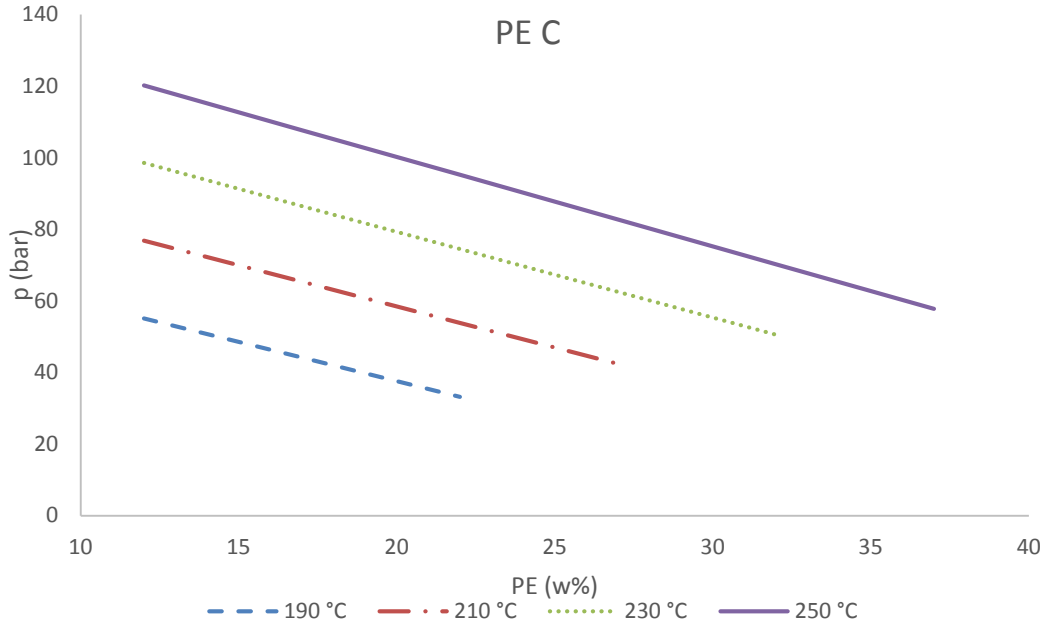

Graph X. The isothermal behaviour predicted with the model for polymer system C at several temperatures.

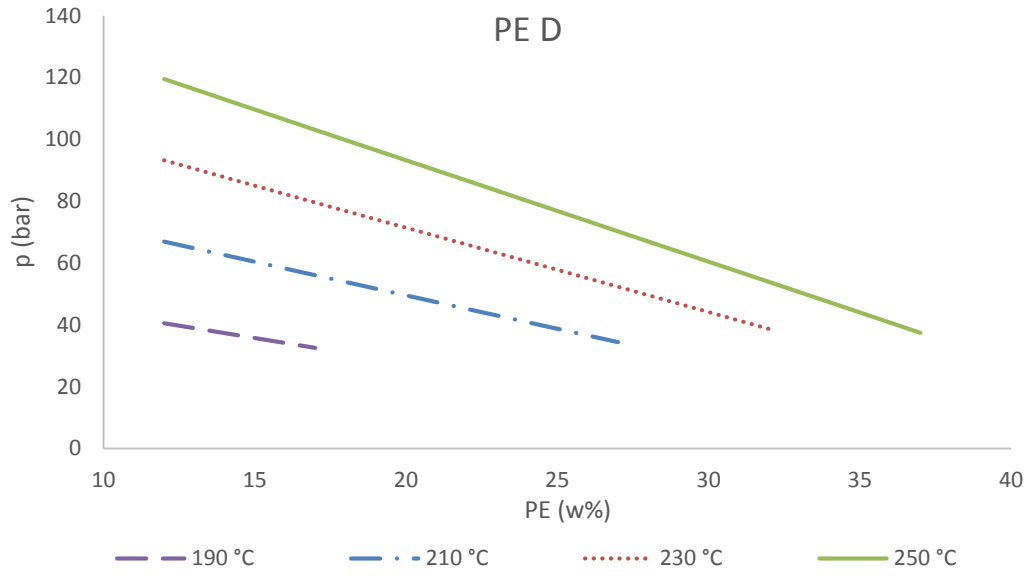

Graph XI. The isothermal behaviour predicted with the model for polymer system D at several temperatures.

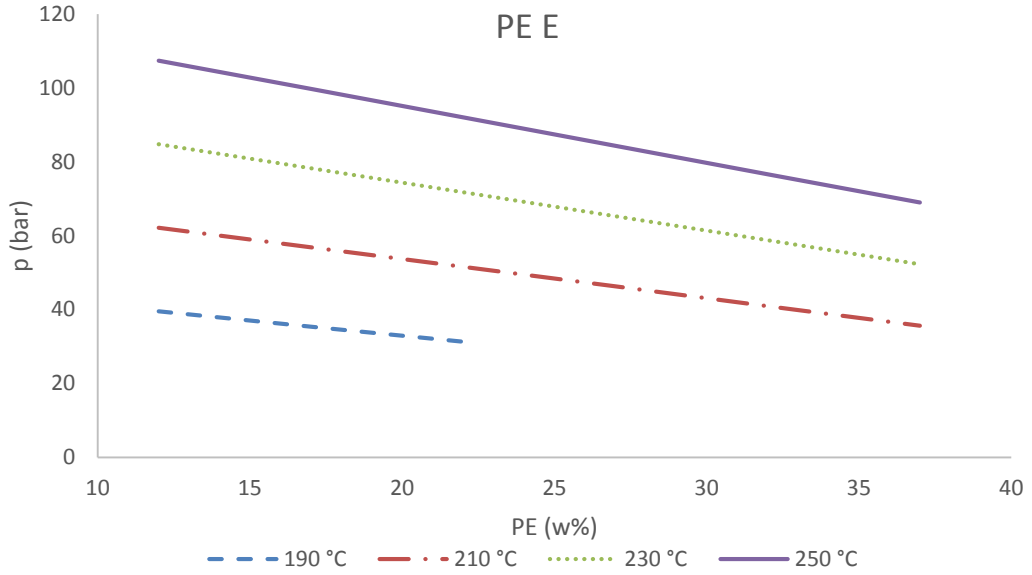

Graph XII. The isothermal behaviour predicted with the model for polymer system E at several temperatures.